The mechanism of myosin replacement in the thick filament of the skeletal muscle

(骨格筋筋原線維内の太いフィラメントにおける ミオシン分子の置換機構)

Graduate School of Agriculture, Hokkaido University
（北海道大学　大学院農学院
生命フロンティアコース　博士後期課程）

UENAKA (ICHIMURA) Emi

上仲 (市村)　恵美

Table of contents

Abstract

Myosin is one of the most abundant proteins in the myofibrils of skeletal muscle. Approximately 300 myosins form a bipolar thick filament with 1.6 μm in length in vivo. We previously have shown that about 50% of eGFP tagged myosin (eGFP-Myh3) is replaced in the myofibrils in 10 hours by fluorescence live imaging technique (Ojima et al., 2015). However, little is known about the mechanism underlying myosin replacement in the thick filament while maintaining its function and structure. To address this, the thesis consists of three chapters: (1) spatiotemporal observation of myosin replacement in the thick filament, (2) muscle-specific ubiquitin ligase in myosin replacement, and (3) potential involvement of post-transcriptional modification in myosin replacement.

First, to investigate how rapidly myosin replacement occurs and whether the myosin exchange rate differs depending on the region of the thick filament, myosin release and insertion rates over a short period were measured in myotubes expressing a photoconvertible fluorescence protein-tagged myosin. About 20% of myosins were replaced within 10 min, while 70% of myosins were exchanged over 10 h with symmetrical and biphasic alteration of myosin release and insertion rates. A fluorescence pulse-chase assay showed that newly synthesized myosin was located the end of the thick-filament rather than the center in the first 7 min of pulse-chase labeling and was observed in the remainder of the thick filament by 30 min. In addition, I observed the thick filament-dissociated myosin was reused for myosin replacement in the thick filament. The recycled myosin also tended to be incorporated faster into the tip of the thick filament than the center of the filament. These results suggest that the myosin replacement rate differs depending on the regions of the thick filament.

Next, to study the involvement of a protein degradation system in the myosin replacement

process, I studied whether the muscle-specific ubiquitin ligase Ozz regulates replacement rate of Myh3. Ozz overexpression significantly decreased the replacement rate of eGFP-Myh3 in the myofibrils, whereas it had no effect on other myosin isoforms. It is likely that ectopic Ozz promoted myosin degradation through increment of ubiquitinated myosin, and decreased myosin supply for replacement, thereby reducing myosin replacement rate. Intriguingly, treatment with a proteasome inhibitor MG132 also decreased myosin replacement rate, although MG132 enhanced the accumulation of ubiquitinated myosin in the cytosol where replaceable myosin is pooled, suggesting that ubiquitinated myosin is not replaced by myosin in the myofibril. Collectively, our findings showed that Myh3 replacement rate was reduced in the presence of overexpressed-Ozz probably through enhanced-ubiquitination and -degradation of Myh3 by Ozz.

Finally, to confirm the intracellular environment was involved in the myosin replacement, myosin replacement was compared between Myh1 and Myh7 expressing the same myotubes. The Myh1 replacement rate was higher and faster than the Myh7. This result showed the myosin replacement rate was different between myosin isoforms in the same myotubes. Then, it was focused on myosin modified post translational modifications that affect protein-protein interaction and localization. Because the different muscle type-specific myosin methylation pattern was detected by western blotting, the methylation site of myosin was identified by mass spectrometry. The methylation sites of myosin were different between isoform and fraction. Moreover, methylation sites differ among ages of derived mice. These results imply that methylation might work as a key factor to regulate myosin replacement.

In this thesis, I showed that thick filament associate-myosin was frequently and ununiformly replaced in the thick filament using both newly synthesized and recycled myosin, which replacement rate was controlled by Ub ligase depending on Myh isoforms. In addition, the myosin

replacement rate was different between myosin isoforms, which may be regulated by the methylation pattern of myosin molecules.

Abbreviations

5% RT	5% recovery time
ACD	assembly competence domain
AcK	Acetyl lysine
CBB-R	coomassie brilliant blue R250
DM	differentiation medium
EDL	Extensor digitorum longus
ELC	essential light chain
FRAP	fluorescence recovery after photobleaching
GM	growth medium
KikGR	Kikume Green-Red
KuO	KusabiraOrange fluorescence protein
LMM	light meromyosin
Lac-K	lacthyl lysine
MAFbx	muscle atrophy F-box
Mettl21	methyltransferase-like 21
Mf	mobile fraction
Murf1	muscle ring finger protein 1
Murf2	muscle ring finger protein 2
Murf3	muscle ring finger protein 3
MybpC	myosin binding protein C
MybpC	myosin binding protein C
Myh	myosin heavy chain
Neurl2	Neuralized E3 ubiquitin protein ligase 2
PTM	post translational modification
RLC	regular light chain
ROI	region of interest

RT-qPCR	reverse transcription quantitative PCR
SDS-PAGE	sodium dodecyl sulfate polyacrylamide gel electrophoresis
SE	standard error
SOL	soleus
TA	tibialis anterior
UMAP	uniform manifold approximation and projection
UPS	ubiquitin-proteasome system
UV	ultraviolet
Ub	ubiquitin
WB	western blotting
dme-K	dimethyl lysine
eGFP	enhanced green fluorescence proteins
$t_{1/2}$	Half-life
tme-K	trimethyl lysine

General Introduction

Meat is a good protein source for humans and contributes to the longevity of the Japanese in modern society. In Japanese people, chicken, pork, and beef are frequently eaten as daily meat. These meats are originated from the skeletal muscles of domestic animals and poultry. In Japan, the full-fledged breeding of livestock has begun after World war, and the livestock production had expanded rapidly thereafter. Domestic meat production has not changed for the past 30 years, however, global meat production has been still expanding because the global demand expansion for meats with the economic growth and population growth of developing countries (H.-W. Windhorst, 2014; OECD-FAO, 2021). However, the situation surrounding the livestock industry is changing from the viewpoint of the food crisis, SDGs, and animal warfare. So, there is necessary to produce meat more efficiently and naturally with the lower environmental and forage resources. Achieving this purpose requires an understanding at the tissue and cellular level of how livestock muscle grows and is maintained.

Skeletal muscle tissue, the origin of the meat, is an organ to play an exercise function and makes up approximately 40–60% of body weight in livestock. Muscle tissue is predominantly composed of muscle fiber. The muscle fiber is a multinuclear cell formed by fusion of the myoblast (Azevedo & Baylies, 2020), resulting in the formation of a long cell that connects to the bone via tendons (Estrella & Naya, 2014; Moyle et al., 2020). The 80% volume of myofibrils is occupied by myofibrils which have a function of contraction. Myofibrils are composed of the regularly repeating minimum contraction unit, the sarcomere, which in turn is made up of more than 20 kinds of myofibrillar proteins (Clark et al., 2002; Henderson et al., 2018). Muscle contraction is induced by the interdigitation between the thin filament and the thick filament in the sarcomere (Burbaum et al., 2021; Huxley, 1969). The main myofibrillar proteins of the thin

filament are sarcomeric-α-actin, tropomyosin, troponin complex, and nebulin (Henderson et al., 2018; Prill & Dawson, 2020). The thin filament spans from the Z-band toward the M-lines with nebulin (Kontrogianni-Konstantopoulos et al., 2009). The thick filament contains myosin and myosin-associated proteins, such as myosin-binding protein C (MybpC), myomesin, and connectin/titin. MybpC bundles polymerized myosin at multiple sites, and myomesin ties the thick filament together at the M-lines (Dennis et al., 1984a; Luther et al., 2008; Luther & Vydyanath, 2011; Obermann et al., 1997). A single polypeptide of a giant protein, connectin/titin, extends from the Z bands to the M-lines and interacts with MybpC and myosin on the thick filaments to maintain the thick filament at the center of the sarcomere (Kontrogianni-Konstantopoulos et al., 2009; Labeit & Kolmerer, 1995; Swist et al., 2020; Tonino et al., 2019a). Thus, the sarcomere structure is made up of extensively organized myofibrillar protein complexes, which precisely control contraction like a machine.

Myosin, which plays a fundamental role in contraction as a motor protein, is one of the most abundant myofibrillar proteins. Approximately 300 myosins are self-assembled under physiological conditions and mainly form the thick filament. The thick filament is bipolar and precisely regulated 1.6 μm length in vivo (Huxley, 1963b). The myosin molecule is a hexamer composed of two myosin heavy chains (Myh), two essential light chains (ELC), and two regular light chains (RLC) (Craig & Woodhead, 2006; Weeds & Lowey, 1971). Myh has a head globular region and long-tail region like a rod (Lowey et al., 1969). The head region of myosin functions as ATPase when it interacts with actin in the thin filament, which is needed in muscle contraction (Rayment et al., 1993). ELC and RLC assist function of Myh as a motor protein (Sitbon et al., 2020). ELC contributes to the regulation of cross-bridge kinetics (Ho & Chisholm, 1997). The N-terminal domain of RLC is phosphorated by myosin light chain kinase-dependent on Ca2+ concentration, modulating force generation during contractions (Szczesna, 2003). The rod region

of two Myhs forms an α-helical coiled-coil rod that has approximately 160 nm in length and 2 nm in width. The rod consists of the S2 domain and light meromyosin (LMM). LMM plays an important function for polymerization under a physiological ionic condition (Cripps, 1999). In particular, the assembly competence domain called ACD located in LMM is known as an essential domain to start filament formation (Sohn et al., 1997). Moreover, skeletal muscle is expressing several Myh isoforms which have different contraction abilities. Main Myh isoforms expressed in adult mice are Myh1, Myh2, Myh4, and Myh7, which contraction velocity ranks in order Myh4 > Myh1 > Myh2 > Myh7 (C. A. Johnson et al., 2019; Resnicow et al., 2010; Walklate et al., 2016). Myofiber expressing each isoform is distinguished as type IIb, IIx, IIa, and I (He et al., 2000). Type IIb, IIx, and IIa myofibers are called fast myofiber and type I is recognized as slow myofiber. In addition to these isoforms, embryonic Myh3 and neonatal Myh8 are expressed during myogenesis and muscle regeneration. Fast type of Myhs gradually becomes predominant a few days after birth in mice, which causes the downregulation of Myh3 and Myh8, resulting in Myh isoform shift in myofibril (Agarwal et al., 2020; Stefano Schiaffino et al., 2015).

The protein turnover process occurs within all living organisms. In the myofibrils of skeletal muscle cells, protein turnover is thought to be necessary for replacing damaged or unnecessary proteins with new ones and for isoform change embryonic type to adult type. The half-life of myosin is approximately 5 days as measured by the radioisotope technique in muscle cells and tissue (Rubinstein et al., 1976; Zak et al., 1977). However, it remains unclear how myosin in myofibrils turnover without effect on sarcomere structure and contraction function. To answer this question, several studies have been reported previously. Using synthesized myosin filament in vitro, myosin exchange is observed between filaments (Saad et al., 1986), and myosin is replaced at the end of the thick filament within 5 min and in the whole filament within 60 min (Saad et al., 1991). In myotube observation using imaging technique, iodoacetamide-fluorescein

labeled myosin was incorporated into the thick filament approximately 6 h after microinjection of labeled myosin (C. S. Johnson et al., n.d.). On replacement of other myofibrillar proteins, it is reported that Z disc constituting proteins are exchanged approximately 30 min (Wang et al., 2005), actin in the thin filament is replaced 2 h (Hasebe-Kishi & Shimada, 2000), and connectin/titin, a giant protein, is also replaced approximately 14 h (da Silva Lopes et al., 2011; Rudolph et al., 2019). These results suggest that myofibrillar proteins containing myosin are exchangeable with maintaining the sarcomere structure. Since the time required for exchange differs among these myofibril proteins, it is considered that the proteins constituting sarcomere are replaced by each protein at an appropriate timing.

Our laboratory has reported previously using live imaging technic that half of eGFP tagged myosin (eGFP-Myh3) in the thick filament is replaced within 3 h using live imaging technic (Ojima et al., 2015). Moreover, replacement patterns were different between myosin and myosin-binding proteins such as myomesin and MybpC (Ojima et al., 2015). This result suggests that the thick filament constituting proteins are also exchanged by each. However, little is known about the mechanism of myosin replacement in the thick filament. Therefore, the purpose of this study was to investigate the mechanism of myosin replacement in the thick filament of the skeletal muscle with conducting the following three studies.

Chapter 1: spatiotemporal observation of myosin replacement in the thick filament

Chapter 2: muscle-specific ubiquitin ligase involvement on myosin replacement

Chapter 3: potential involvement of post-transcriptional modification in myosin replacement

Chapter 1

Introduction

In myofibrils, the regulated 1.6 μm length thick filament is formed by multiple myofibrillar proteins (Huxley, 1963a). Approximately 300 myosin molecules polymerize and predominantly form a bipolar thick filament. M-line associate proteins, such as myomesin and M protein, bundle the middle of the thick filament called the central bare zone (Henderson et al., 2018; Obermann et al., 1997). MybpC bound thick filament at approximately 43 nm intervals (Dennis et al., 1984a), and plays a function to reinforce the structure of the thick filament and help interact between actin in the thin filament and myosin (Luther et al., 2008; Luther & Vydyanath, 2011). Connectin/titin that extends from Z-bands to M-line supports the whole of the thick filament and holds the proper position (Henderson et al., 2018; Labeit & Kolmerer, 1995; Swist et al., 2020; Tonino et al., 2019b). Altogether, the thick filament has the structure regularly arrayed and consisted of multiple proteins.

Myosin, one of the most abundant myofibrillar proteins, is an important component of the thick filament. The myosin molecule is a hexamer composed of two myosin heavy chains (Myh), two essential light chains, and two regular light chains. The head region of myosin functions as ATPase when it interacts with actin in the thin filament (Rall, 2021). The rod region of myosin consists of the α-helical coiled-coil S2 domain and light meromyosin (LMM), the latter of which is responsible for myosin polymerization and incorporation into the thick filament (William F. Harrington, 1984). In the LMM, the assembly competence domain (ACD), 29 amino acid residues near the C-terminal region of sarcomeric Myhs and are conserved among species, is necessary but not sufficient to form the thick filament (Sohn et al., 1997). A cluster of four positive amino acid residues located in the C-terminal region of the ACD is crucial for in vitro myosin filament

assembly in test tubes and incorporation into the thick filament in cultured cardiac cells (Thompson et al., 2012). In vitro, biochemical studies have shown that the length of the myosin filament varies between 0.2 and over 5 μm according to the pH and ionic strength of the polymerization buffer (Kaminer & Bell, 1966; Service, 1982). In contrast, in vivo skeletal muscle cells spontaneously generate a bipolar-shaped thick filaments with 1.6 μm in length (Huxley, 1963b). Thus, muscle cells have an instinctive ability to generate an authentic thick filament. However, the mechanism by which approximately 300 myosin molecules are assembled into the thick filament in the skeletal muscle cells is still not fully understood.

The protein turnover process occurs within all living organisms. In the myofibrils of skeletal muscle cells, damaged or unnecessary proteins are replaced by new ones. Although myofibrils are highly organized protein complexes, each myofibrillar protein in the sarcomere component must be exchanged with another. We have previously used a live imaging technique to study myosin replacement in the thick filament of cultured myotubes, and found that half of the eGFP-tagged myosin (eGFP-Myh3) was exchanged in myofibrils within 10 h (Ojima et al., 2015). However, it remains unclear (1) how rapidly myosin is replaced in the thick filament and (2) whether myosin is uniformly replaced within the thick filament. To address these questions, the present study was examined in the following three experiments. First, I monitored the myosin replacement in the myofibrils over a short interval. Next, I determined the pattern of myosin insertion and release in the thick filament using a fluorescence pulse-chase assay. Finally, I investigated whether myosin once released from the thick filament was re-incorporated into the thick filament.

Material and Methods

1. Experimental animals

All experiments were performed using primary muscle cells from chick embryos. Experimental animals were cared for as outlined in the Hokkaido University and National Agriculture and Food Research Organization (NARO) guidelines for the care and use of laboratory animals. The relevant committees of Hokkaido University and NARO approved this study.

2. Cell culture and transfection

Skeletal muscle cells were obtained from day 11 chick embryo pectoral muscles. Connective tissues were removed from muscles under a stereomicroscope. Minced muscle was incubated in 0.025% trypsin solution (Thermo Fisher Scientific, Tokyo, Japan) for 25 min at 37℃. To stop trypsinization, growth medium [GM: 10% (v/v) horse serum (Thermo Fisher Scientific), 10% (v/v) chick embryo extract, and 1% (v/v) penicillin-streptomycin-glutamine ×100 (Thermo Fisher Scientific) in minimum essential medium (Thermo Fisher Scientific)] was added to the cell suspension. After centrifugation at 600 g for 5 min, the precipitated cell fraction was resuspended in GM and then filtered through 100- and 40-μm cell strainers (CORNING, Tokyo, Japan) to eliminate cellular debris. Cells were cultured on non-coating dishes for 50 min in an incubator to remove contaminated non-muscle cells. Non-adherent cells were collected and seeded at 10,000 cells per cm^2 on glass-bottom dishes (Iwaki, Shizuoka, Japan) for live-imaging assays or on Lab-Tek chamber slides (Thermo Fisher Scientific) for fluorescence pulse-chase assays; both the glass-bottom dishes and chamber slides were coated with poly-L-lysine (Sigma-Aldrich, Tokyo, Japan) and collagen Type I-A (Nitta Gelatin, Osaka, Japan). The GM medium was shifted from

GM to differentiation medium [DM: 11% (v/v) horse serum, 3% (v/v) chick embryo extract, and 1% (v/v) penicillin-streptomycin-glutamine ×100 in minimum essential medium] on the day of transfection or on the day after seeding. Cells were transfected with expression vectors using Lipofectamine® LTX and Plus reagents (Thermo Fisher Scientific). DM was changed every two days.

3. cDNA constructs

Mouse cDNA for *Myh3* (45–5868 in NM_001099635) was cloned into the HaloTag® vector (Promega KK, Tokyo, Japan) or a humanized monomeric Kikume green-red 1 vector (KikGR1; Medical and Biological Laboratories, Nagoya, Japan). Tags were located at the N-terminal region of Myh3: Halo-Myh3 and KikGR-Myh3 were expressed in cells. The inserted sequences of all constructs were verified with a 3730 DNA Analyzer (Applied Biosystems, Tokyo, Japan).

4. Photoconversion assay

Photoconversion assay was performed with a Leica TCS SP5 confocal microscope (Leica Microsystem, Tokyo, Japan) equipped with a microscope incubation system (Tokai Hit, Shizuoka, Japan) to perform live cells imaging. A part of myofibrils was irradiated with a 405 nm wavelength of ultraviolet (UV) light at 15% power of maximum output for 8 sec to convert KikGR fluorescence green to red. Images were obtained every 10 min after photoconversion. The green and red fluorescence of KikGR were detected at excitation wavelengths of 3% 488 nm and 15% 543 nm with 500–540 nm and 600–700 nm band-pass filters. The identical focal plane was selected for the quantification of fluorescence intensity. The green intensity of KikGR-Myh3 at photo-conversion area was normalized with green intensity of non-conversion area to adjust for

photobleaching due to frequent imaging. We adjusted the red intensity of KikGR-Myh3 using a correction value. This value was the slop of the fluorescence intensity from 500 min to 600 min, which showed a linear change during these times. The relative green fluorescence intensity at pre-photoconversion was defined as 1, and the relative green fluorescence intensity just after photoconversion was defined as 0. The relative red fluorescence intensity just after photoconversion was defined as 1, and the relative red fluorescence intensity just after photoconversion in the non-photoconverted area was defined as 0. Normalized fluorescence data were applied to recovery curve-fitting using the following exponential formula by ImageJ 1.52a software (National Institutes of Health, Bethesda, MD, USA): $FI=Mf*(1-e^{(-b*t)})+c$, where FI is the normalized fluorescence intensity, and t is the elapsed time after bleaching. The mobile fraction (Mf) was the maximum change value of fluorescence intensity. The half-life ($t_{1/2}$) was calculated as the time required for the fluorescence intensity change to reach half of Mf. Mf and $t_{1/2}$ were used as indicators of fluorescence recovery (green fluorescence) and fluorescence reduction (red fluorescence) rates of KikGR-Myh3.

5. Fluorescence recovery after photobleaching (FRAP) assay

FRAP assay was performed with a Leica TCS SP5 confocal microscope (Leica Microsystem) or a Leica TCS SP8 confocal microscope (Leica Microsystem) equipped with a microscope incubation system (Tokai Hit) to observe live cells. Red fluorescence recovery of KikGR-Myh3 was observed in live myotubes by a Leica TCS SP8 confocal microscope after bleaching a part of the photoconversion area. Following 30% strength UV light irradiated for 10 sec to KikGR-Myh3 fluorescence conversion from green to red, the center of the photoconverted area (5 μm × 5 μm size) was bleached by 100 % output laser of wavelength 405 and 543 nm. Images were obtained every 10 min after bleaching. The red fluorescence of KikGR-Myh3 was

detected at excitation wavelengths of 543 nm with 600–700 nm band-pass filters. The identical focal plane was selected and some of the sarcomeres were line-scanned by ImageJ to check for recovery of striation pattern of red fluorescence after bleaching.

Red fluorescence recovery of Halo-Myh3 was observed in live myotubes by a Leica TCS SP5 confocal microscope after washing out of TMR ligand (Promega). Myotubes were incubated with TMR ligand at a final concentration of 0.1% in DM to label Halo-Myh3 expressing in myotubes. After overnight incubation, DM containing TMR was removed and washed 3 times with PBS. The medium was shifted to regular DM 1 h before FRAP. The red fluorescence of Halo-Myh3 was bleached by a 100% strength laser of wavelength 488, 514, and 543 nm for 90 sec in part of the myofibrils. The TMR fluorescence was detected at excitation wavelengths of 543 nm with 555–630 nm band-pass filters at 10 min intervals. After FRAP assay, images indicating identical plane were selected, and fluorescence intensity in bleaching area was detected. The relative red fluorescence intensity just after bleaching was defined as 1, and the relative red fluorescence intensity before bleaching in the bleaching area was defined as 0. Normalized fluorescence data were applied to recovery curve-fitting using the following exponential formula by ImageJ: $FI=Mf*(1-e^{(-b*t)}) +c$, where FI is the normalized fluorescence intensity, and t is the elapsed time after bleaching.

6. Fluorescence pulse-chase assay

Day 6 myotubes expressing Halo-Myh3 were labeled with Oregon Green® ligand (green fluorescence; Promega) at a final concentration of 0.3% in DM for 16 h. Following washout, myotubes were reacted with TMR ligand (red fluorescence, Promega) at a final concentration of 0.1% in minimum essential medium to label newly synthesized Halo-Myh3 for 7, 15, and 30 min. Myotubes were fixed with 4% paraformaldehyde in PBS (Nacalai Tesque, Kyoto, Japan), rinsed

with 0.5% Triton X-100 in PBS, and mounted with media containing 4',6-diamidino-2-phenylindole (DAPI; Vector Laboratories, Burlingame, CA, USA). Samples were analyzed using an LSM 700 Confocal Laser Scanning Microscope (Carl Zeiss, Tokyo, Japan) equipped with a Plan-Apochromat ×63 (numerical aperture 1.4) lens. The DAPI, OregonGreen, and TMR fluorescence were detected at excitation wavelengths of 405, 488, and 555 nm with 300–483 nm, 493–550 nm, and 560–800 nm band-pass filters, respectively. Images were processed by using Zen 2012 imaging software (Carl Zeiss).

7. Image analysis

KikGR-Myh3 or Halo-Myh3 images were line-scanned and analyzed with ImageJ by calculating an average line-scanned value from the line-scanned region of the sarcomere. Image data were applied for curve-fitting with a polynomial to extract one peak corresponding to one sarcomere. Two turning points of the green fluorescence curve were defined as the Z-bands. The red fluorescence curve was also extracted at the exact position of green fluorescence. The baseline was defined as a line between two turning points. The fluorescence intensity of green and red was normalized as a max value of 1. The horizontal axis (x-axis) indicates that the normalized distance from the center of the sarcomere (M-line) is 0.0, whereas the Z-bands are located at 1.0 and -1.0. For image analysis of KikGR-Myh3, the average fluorescence intensities were calculated from unprocessed fluorescence intensities. Average waveforms at each time point were curve fitted with a polynomial. In normalized line-scanned data, green fluorescence intensities were subtracted from the red fluorescence intensities to compare the waveforms of green and red fluorescence.

For image analysis of the fluorescence pulse-chase assay using Halo-Myh3, the red waveform containing a peak was compared with the green waveform during a pulse-chase assay

and categorized into six patterns based on the red peak position: both sides, right side, left side, center, random fashion, and no incorporation. The red fluorescence peak shift was evaluated as the distance between the red fluorescence intensity peak and the center of the thick filament using graphs categorized into three patterns: both sides, right side, and left side.

For image analysis for FRAP assay using Halo-Myh3, 8–14 sarcomeres in the bleaching area per one myotube were line-scanned by Image J. The fluorescence waveforms of TMR were extracted containing one peak and the x-axis was normalized in the manner described above. The extracted waveforms were averaged to obtain average data per myotube. Total average data was calculated using average data in each myotube. The average data of unprocessed fluorescence intensity were normalized as a max value 1.0. The same calculation was performed with images at each time point. To detect fluorescence distribution change during 0–300 min, the subtraction results were obtained using unprocessed or normalized fluorescence intensity data.

All waveform analysis and graph drawing were conducted with a home-built program written in Collaboratory (Google Research, Tokyo, Japan).

8. Statistics

All data are expressed as the mean ± standard error (SE). Student's *t-test* was used to compare differences between two groups. The Tukey test was used for multiple comparisons. Statistical significance was set at $p < 0.05$. All statistical tests were performed using EZR on R commander ver. 1.54.

Results

1. Simultaneous myosin incorporation and release were observed in the myofibrils.

To understand how fast myosin is replaced in the thick filament, I investigated the myosin replacement rate in cultured myotubes expressing a photoconvertible fluorescence protein, Kikume Green-Red fused Myh3 (KikGR-Myh3), whose fluorescence color irreversibly shifts from green to red with exposure to UV light (Tsutsui et al., 2005). The green fluorescence signal of KikGR-Myh3 was observed in the myofibrils, whereas red fluorescence was not detected at pre-conversion (Fig.1A). After exposure of the myotubes to UV light, green fluorescence was photoconverted to red fluorescence (post-conversion in Fig. 1A). Since the reduction of red fluorescence intensity and the increment of green fluorescence intensity reflect the myosin release and myosin incorporation, it was able to clarify the dynamics of myosin incorporation and release. The identical focal plane of the myofibrils was selected to monitor green and red fluorescence signal intensities at 10 min intervals (Fig. 1B). Green fluorescence increased to ~10% of signal intensity in 10 min and ~20% in 60 min, while red fluorescence decreased by ~20% of signal intensity in 10 min and by ~30% in 60 min (Fig. 2A). The fluorescence intensities of green and red were symmetrically changed in 10 h after photoconversion. The fluorescence intensity of each color also showed a biphasic alteration, i.e., the fluorescence intensity was changed drastically at the early phase of the FRAP experiment, then changed more gradually, and finally reached a plateau. Consequently, some myosin in the myofibrils was replaced within 10 min. Importantly, Mf and $t_{1/2}$ were not significantly different between red and green fluorescence (Fig. 2B–C).

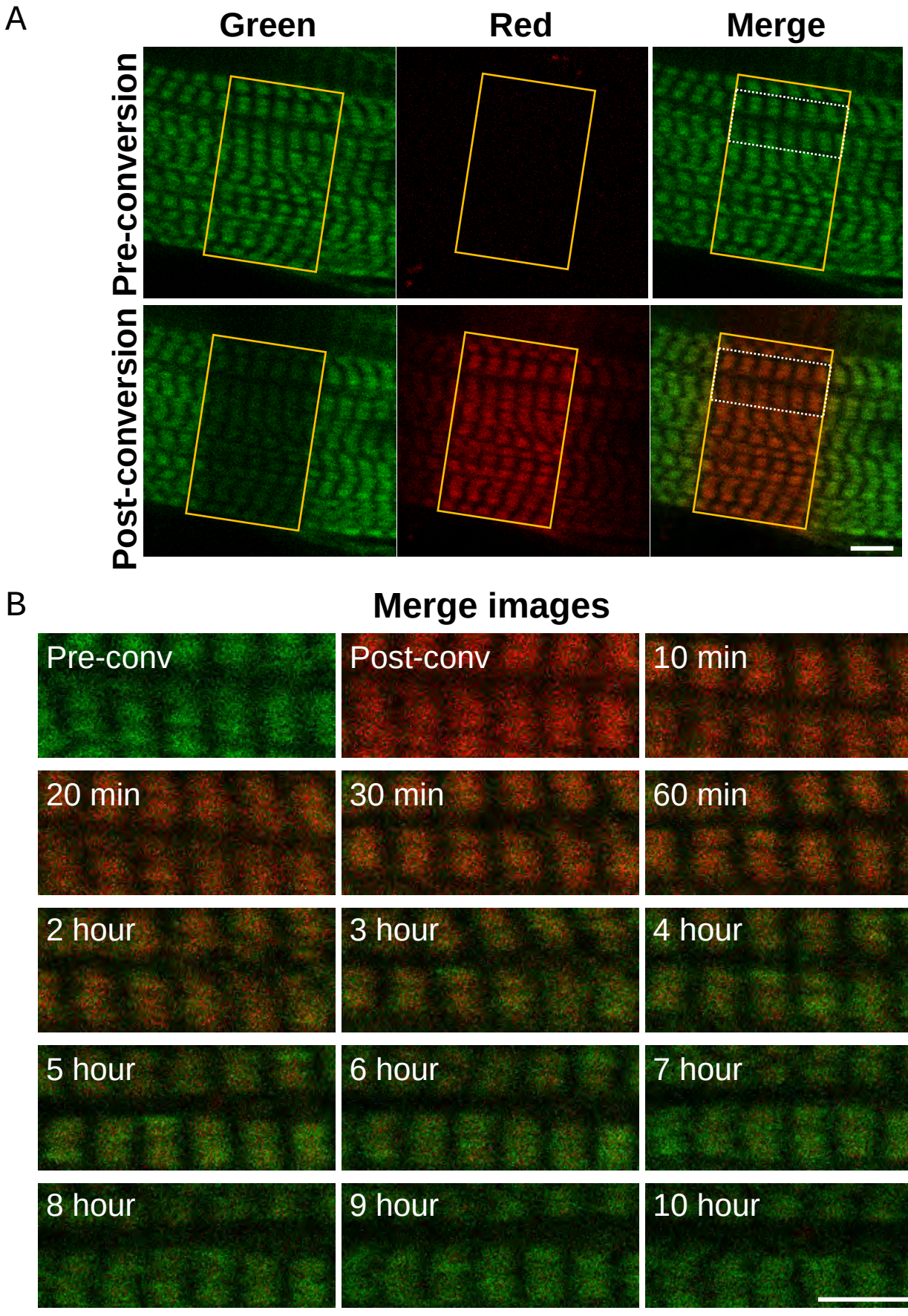

Fig.1 Localization of photoconvertible KikGR-Myh3 in the myofibrils

A. Green fluorescence signal of KikGR-Myh3 was detected in the thick filament of myofibril at pre-conversion. The fluorescence color of KIkGR-Myh3 shifted from green to red with exposure to UV light (yellow rectangles). Bar, 5 μm.

B. Alternation of KikGR-Myh3 fluorescence signals was monitored at 10 minutes intervals up to 10 hours after photoconversion. Merged images with green and red fluorescence signals were indicated in dashed rectangles in A. Bar, 5 μm.

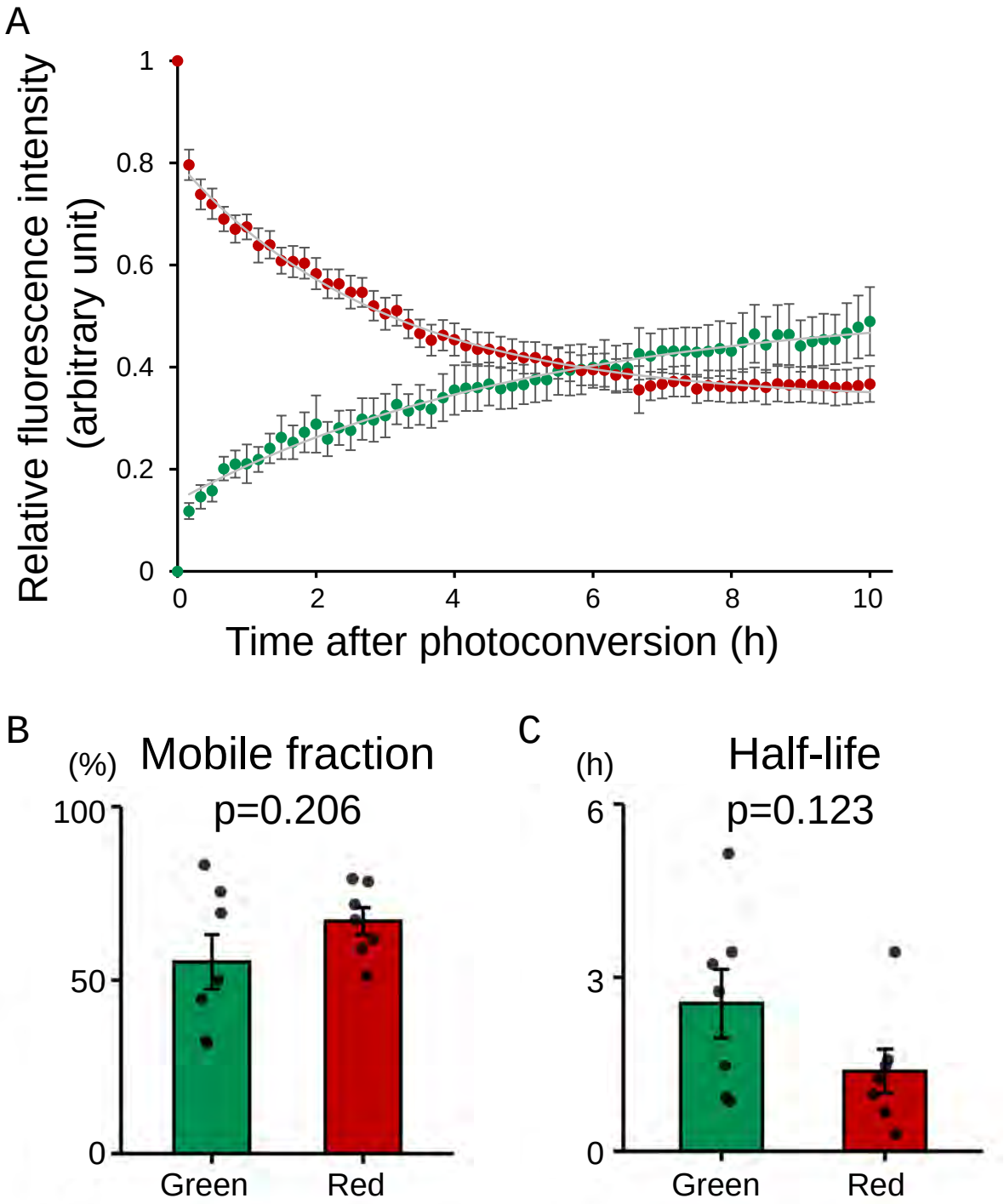

Fig. 2. Symmetrical and biphasic changes of KikGR-Myh3 fluorescence intensities in the myofibrils

A. Green and red fluorescence signals of KikGR-Myh3 were measured in the myofibrils at indicated time point.

B–C. Mobile fractions (%) were 55.24±7.86% in Green and 66.98±3.90% in Red (B). $t_{1/2}$ (h) were 2.55±0.59 in Green and 1.38±0.38 in Red (C). Values represent the mean ± SE. n = 7 for each group.

2. Red fluorescence of KikGR-Myh3 was released faster at the tip of the thick filament.

The present results showed that myosin release and insertion occur concurrently in the myofibrils, based on the measurement of the ratio of fluorescence signals in selected myofibrils. The next question was which regions within the thick filament were favored for myosin exchange. To answer question, I analyzed the patterns of myosin release and insertion at the thick filament level. The green and red fluorescence signals of each sarcomere were line-scanned to draw fluorescence waveforms during the photoconversion experiments (Fig. 3A–C). Normalized green fluorescence signals were subtracted from normalized red fluorescence signals to calculate the difference of two fluorescence waveforms on the thick filaments during photoconversion experiments (Fig. 3D). The red fluorescence intensity was observed to more significant than the green fluorescence intensity in the middle part of the thick filament after 60 min post-photoconversion (Fig. 3D). By contrast, green fluorescence signal intensities were dominant in the region indicated by around -0.75 and 0.75 at the X-axis in Fig.3D, corresponding to the tip of the thick filaments.

3. Newly synthesized myosin tends to be incorporated into the tip of the thick filament

After KikGR-Myh3 experiments, it suggested a trend in which the thick filament-associated myosin is released more frequently from the tip of the thick filaments than the middle of the thick filaments. The advantage of a fluorescence pulse-chase assay technique was taken to determine the myosin-specific incorporation region in the thick filament of myotubes expressing Halo-Myh3, which irreversibly binds to the fluorescence-conjugated cell membrane permeable ligand. The

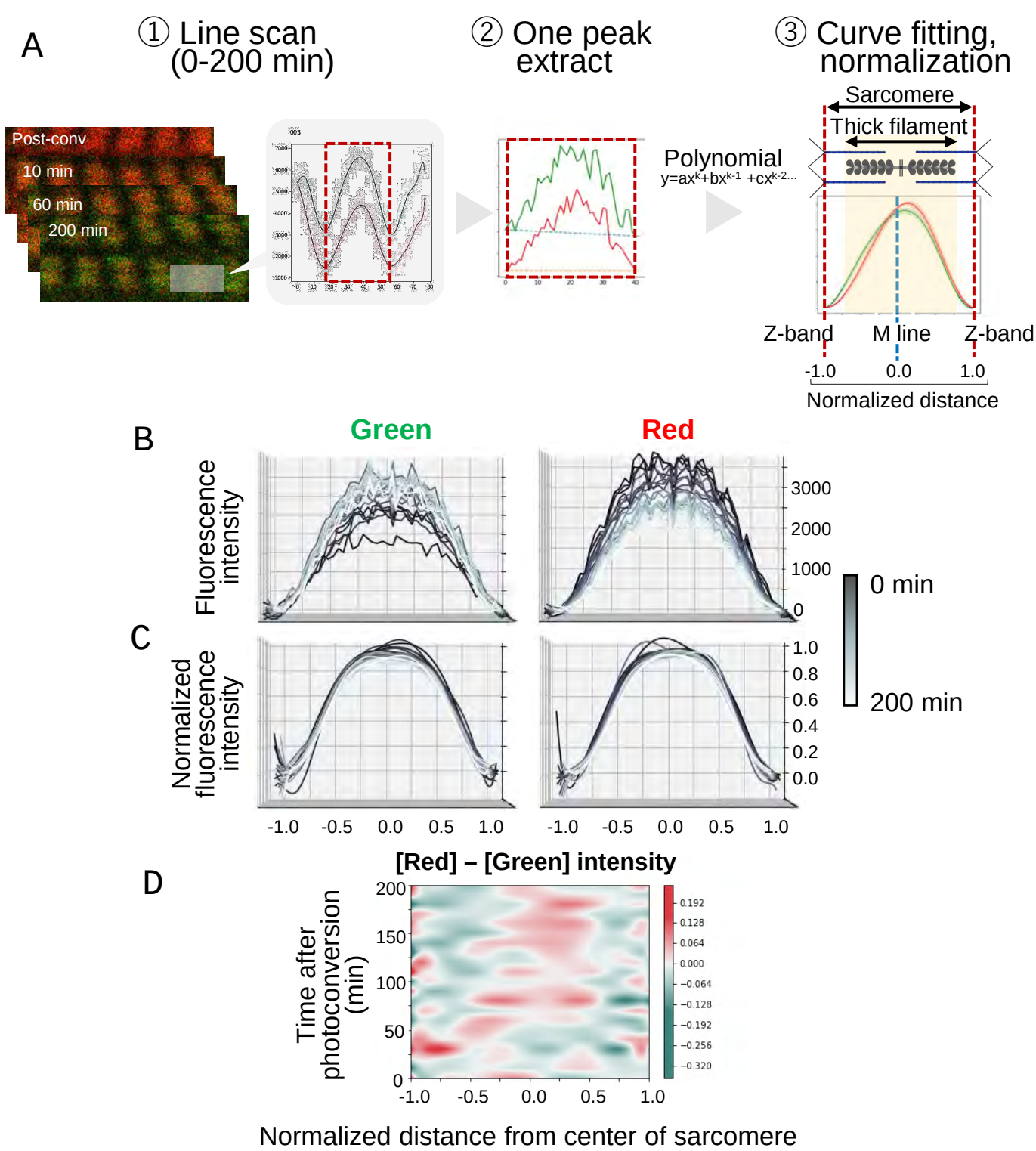

Fig. 3. Over time alteration of green and red fluorescence distribution of KikGR-Myh3 in the sarcomeres

A. A scheme of image-processing to compare fluorescence distribution between red and green of KikGR-Myh3 in each sarcomere is shown. First, the fluorescence signal was line-scanned along myofibrils to obtain mean fluorescence intensities in sarcomere with 10 minutes intervals up to 200 minutes (a dashed rectangle in A). Second, following extraction of one peak, data was curve fitted with a polynomial formula. Waveforms were normalized as a fluorescence max value and x-axis max distance from the center to be 1.0.

B–C. Twenty line-scanned images taken from 0 to 200 min with 10 min intervals following photoconversion were overlaid with each color. The unprocessed fluorescence intensity and the normalized fluorescence intensity were shown in B and C, respectively. The x-axis was the normalized distance from the center of the sarcomere. The y-axis was the unprocessed (B) and the normalized (C) fluorescence intensities. n = 7 myotubes.

D. The graph shows that the difference of two fluorescence intensities where normalized green fluorescence intensity was subtracted from normalized red fluorescence intensity. Red and green colors indicated the subtraction images of green from red. The x-axis and the y-axis indicate the normalized distance from the center of the sarcomere and the time post-photoconversion (minutes). n = 7 myotubes.

Halo-tag technique enabled us to track newly synthesized Halo-Myh3 with different fluorescence ligands. First, expressed Halo-Myh3 was labeled with the Oregon-Green (green fluorescence) ligand for 16 h, and then Halo-Myh3 was labeled with the TMR (red fluorescence) ligand for 7, 15, or 30 min (Fig. 4A). Green fluorescence-labeled Halo-Myh3 was observed in the thick filaments during the pulse-chase experiment. Following the 7 min incubation, red fluorescence-labeled Halo-Myh3 was localized to the myofibrils with diffuse cytoplasm (Fig. 4B). After incubation for 15- and 30-min, red fluorescence-labeled thick filaments were more prominently visualized.

Next, each sarcomere was line-scanned to determine the region of incorporation of the newly synthesized red fluorescence-labeled myosin into the thick filament and the fluorescence patterns were classified (Fig. 5A). The red fluorescence patterns were categorized into six groups based on the regions of the red peak signal in the thick filaments: both side, right side, left side, center, random fashion, and no incorporation (Fig. 5B). Average values in each category are shown in the upper graphs in Fig. 5B. Enumeration of the individual data in the lower panels of Fig. 5B showed that the normalized green fluorescence intensities were subtracted from the normalized red fluorescence intensities. The most frequent localization patterns involved the side groups, i.e., the both sides, left side and right side patterns during pulse-chase (~80% in each time point: Fig. 5C). The frequency of the center pattern gradually increased to ~20% at 30 min of incubation. The random pattern, in which the red and green fluorescence signal patterns were identical, slightly increased to ~20% at 15 min. The frequency of the no signal pattern, defined as no red fluorescence, was decreased in 15 min on incubation (Fig. 5C).

Finally, it was investigated where newly synthesized myosin was inserted into the thick filament. For this purpose, the distance between the red fluorescence peak and the center of the thick filament was plotted during pulse-chase labeling using the data for the side groups, since

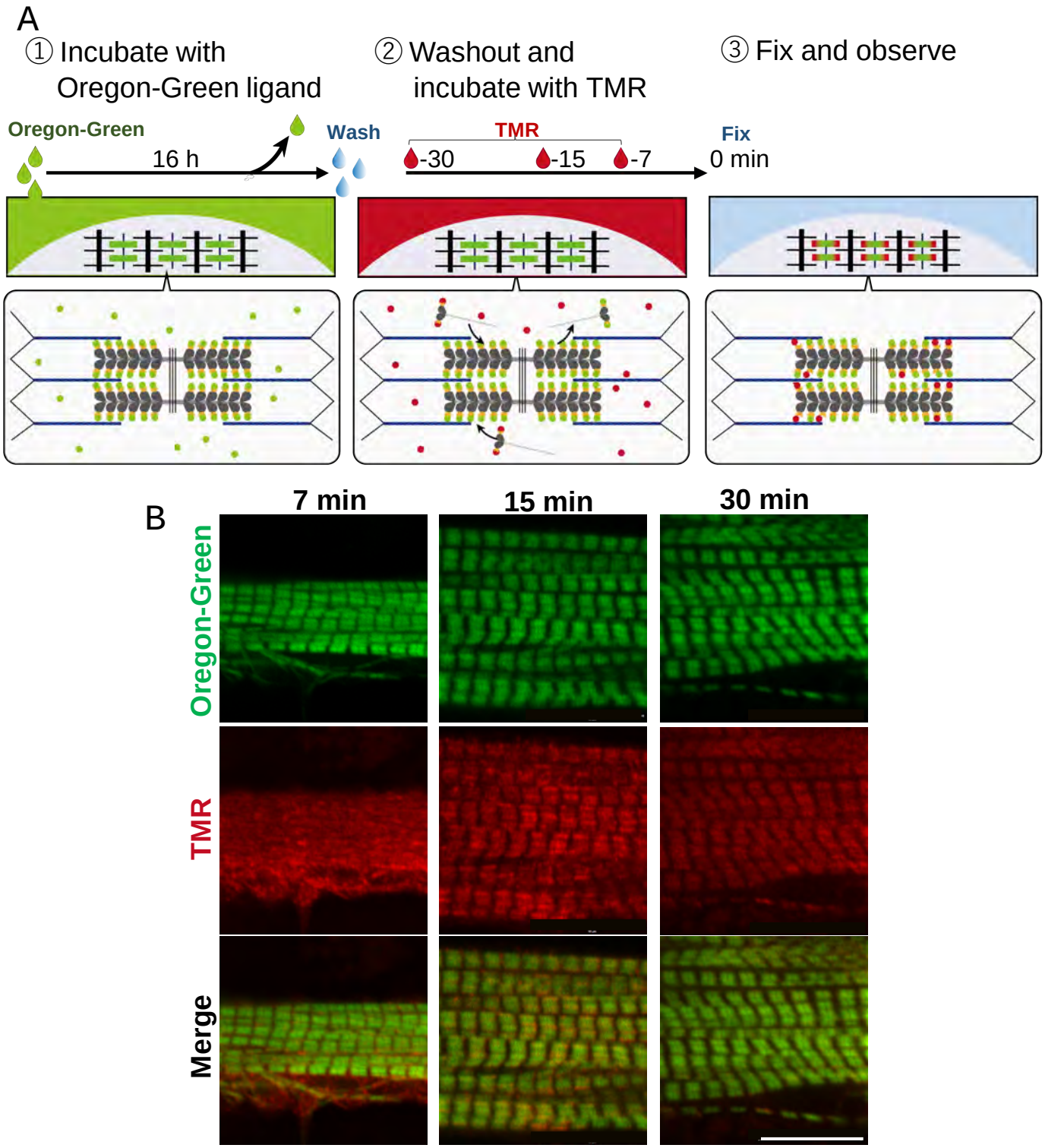

Fig. 4. Visualization of newly synthesized myosin incorporation into the thick filaments
A. Experimental procedure of different fluorescence pulse-chase labeling using Halo-Myh3 is shown. First, myotubes expressing Halo-Myh3 were incubated with Oregon-Green ligand (green fluorescence) for 16 h. Next, myotubes were reacted with TMR ligand (red fluorescence) to label newly synthesized myosin for 7, 15, or 30 min, following wash out Oregon-Green ligand. Finally, myotubes were fixed and observed with confocal microscopy.
B. Representative images of myotubes expressing Halo-Myh3 with fluorescence pulse-chase labeling. Bar, 10 μm.

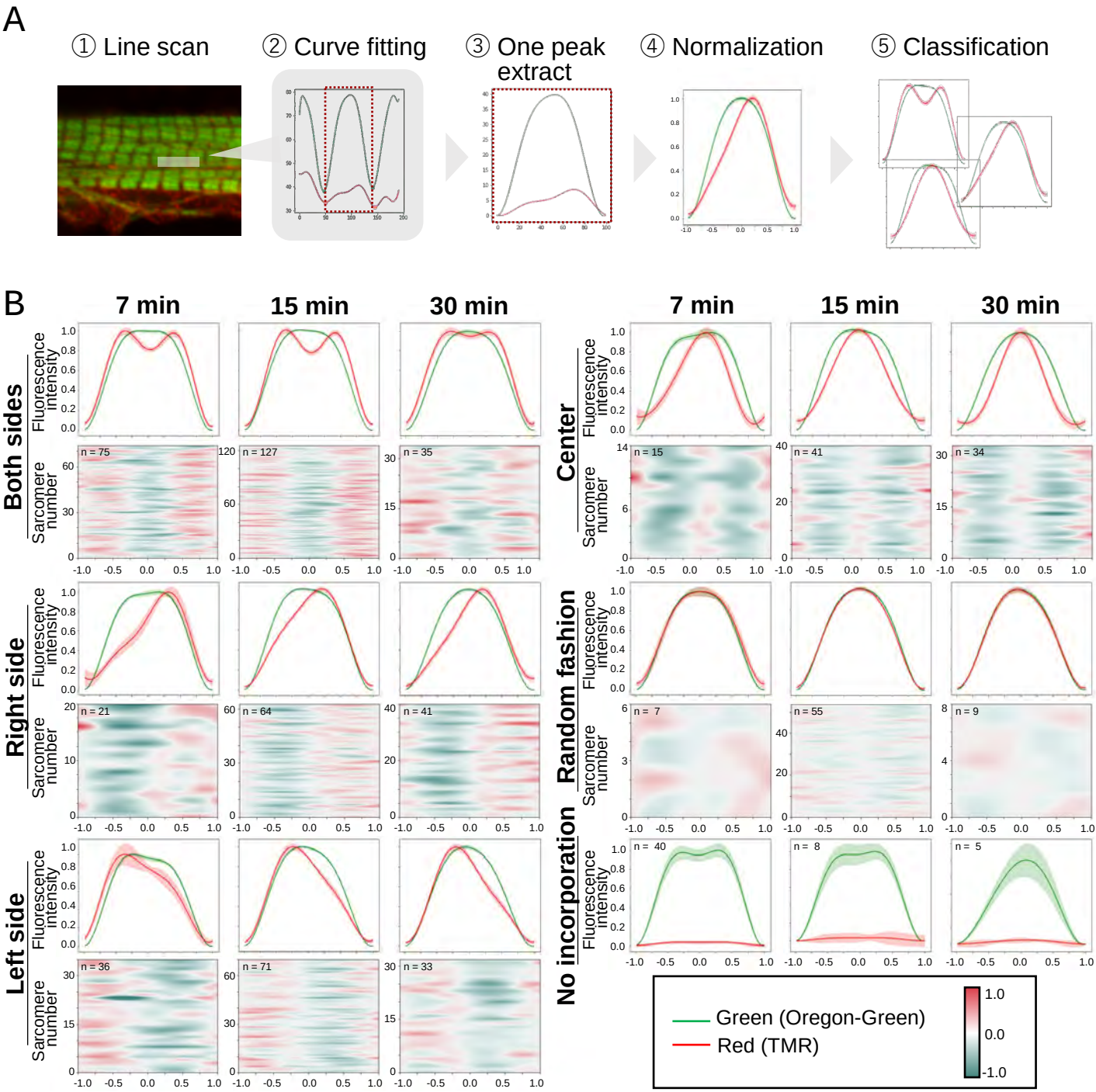
A
① Line scan
② Curve fitting
③ One peak extract
④ Normalization
⑤ Classification
B
7 min
15 min
30 min
Both sides
Right side
Left side
Center
Random fashion
No incorporation
Fluorescence intensity
Sarcomere number
n = 75
n = 127
n = 35
n = 15
n = 41
n = 34
n = 21
n = 64
n = 41
n = 7
n = 55
n = 9
n = 40
n = 8
n = 5
n = 36
n = 71
n = 33
Green (Oregon-Green)
Red (TMR)
1.0
0.0
-1.0
C
Red fluorescence localization pattern
(%)
Frequency
100
80
60
40
20
0
7 min
15 min
30 min
Both sides
One side (R+L)
Center
Random fashion
No incorporation
No incorporation
Random fashion
Center
Side

Fig.5 A variety of incorporation patterns of newly synthesized Halo-Myh3 into the thick filaments.

A . A scheme to categorize newly synthesized myosin insertion sites in the thick filaments is shown. First, each sarcomere was line-scanned. Second, line-scanned data were curve-fitted with a polynomial formula. Third, a green waveform and its corresponding red waveform were extracted. Forth, fluorescence intensities of green and red were normalized as the max value was 1. Finally, waveforms were classified into six patterns based on the red peak position.

B. Line-scanned images were categorized into six groups based on the waveforms of red fluorescence signals compared to green fluorescence signals: both sides, right side, left side, center, random fashion, and no incorporation. Solid lines show average value ± SE (pale-colored width) in the upper graphs. The lower panels are drawn by enumeration of individual subtraction of the green fluorescence signal from the red fluorescence signal. In the no incorporation group, red fluorescence intensities are shown as the relative values against green fluorescence intensities. The x-axis indicates the normalized distance from the center of the sarcomere indicated as 0.0. The normalized distance between the center of the sarcomere and the Z-bands were indicated as 1.0 and -1.0. The y-axis indicates the normalized fluorescence intensity in the upper panels and the sarcomere number in the lower panels.

C. The bar chart indicates the ratio of the myosin incorporation pattern. The stacked bar graph shows the proportion of side groups (both sides and either side), center, random fashion, and no incorporation. Values represent the mean ± SE. 7 min, n = 194 in 3 myotubes. 15 min, n = 366 in 9 myotubes. 30 min, n = 157 in 6 myotubes.

the localization patterns involving the side groups were the most frequent (Fig, 6A and B). The distance between the red fluorescence peak and the center of the thick filament was lessened during pulse-chase labeling (Fig. 6B). The myosin insertion area in the thick filaments was gradually spread from the tip of the thick filaments towards the center of the thick filaments as the red fluorescence peak shifted to the center of the thick filaments. These results indicate that newly synthesized myosin is not evenly replaced in the thick filament, i.e., newly synthesized myosin tends to be incorporated into the tips of the thick filament (Fig. 6C).

4. Myosin was re-incorporated into the thick filament once released from the thick filament.

The results showed that thick filament associate-myosin was frequently exchanged, and newly synthesized myosin was inserted at the tip of the thick filament. Next question was whether released myosin from the thick filament was re-inserted into the thick filament. I monitored the incorporation region of red converted KikGR-Myh3 in myotubes when a part of the red fluorescence-converted region was bleached following UV exposure (Fig. 7A). The red fluorescence recovery of KikGR-Myh3 was observed in the bleaching area at 10 min intervals and analyzed by a line-scan mode to detect recovery of striation pattern of KikGR-Myh3. The red fluorescence signal disappeared after bleaching (dashed rectangles in Fig. 7B), whereas the red fluorescence signals of the thick filament striation were gradually recovered. This result suggests that myosin is re-incorporated into the thick filament once released from the thick filaments.

The FRAP assay was conducted in myotubes expressing Halo-Myh3 to confirm that recycled myosin was re-inserted into the thick filament with the same result as the FRAP assay of myotubes expressing KikGR-Myh3. Myotubes were incubated with TMR ligand at a final concentration of

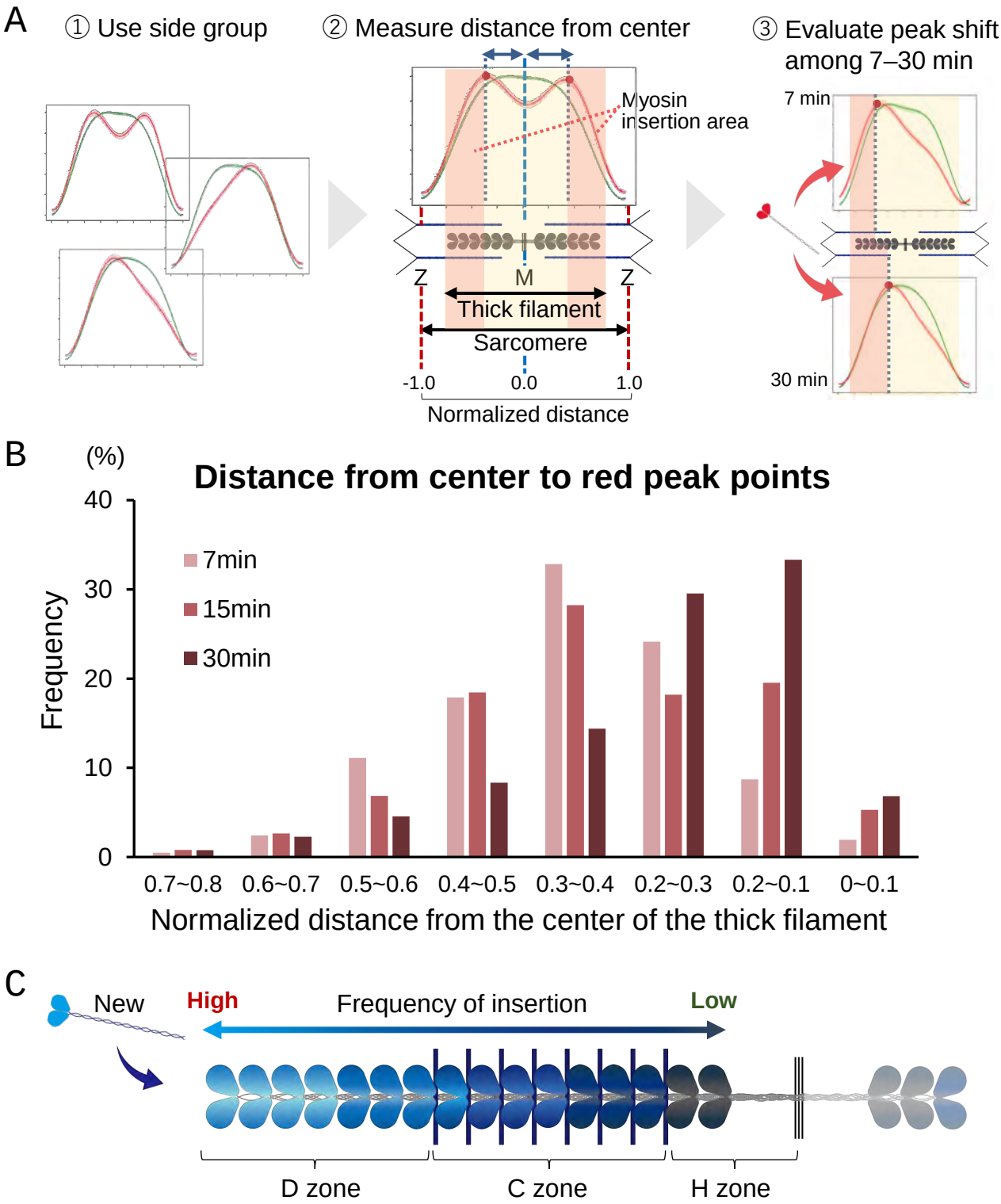

Fig. 6. Comparison of distance from the thick filament center to the peak signal of Halo-Myh3 with red fluorescence.
A. A scheme to evaluate insertion site of newly synthesized myosin with red fluorescence on the thick filaments is shown. First, the distance between red fluorescence peak and center was measured using waveforms categorized to the side group. Second, the measured distance was plotted in the histogram at indicated time points. Finally, the peak shift was evaluated during pulse-chase labeling.
B. Newly synthesized myosin incorporation sites on the thick filaments is shown as a histogram. The frequency of the myosin incorporation site, defined as the distance between the red fluorescence peak and the center of the thick filament, was shown. The x-axis indicates the normalized distance from the center of the thick filament. The center of the thick filament is located at 0, and the edge of the thick filament is located at approximately 0.7–0.8. The number of the thick filaments: 7 min, n = 194 in 3 myotubes. 15 min, n = 366 in 9 myotubes. 30 min, n = 157 in 6 myotubes.
C. Cartoon of transition of newly synthesized myosin insertion into the thick filament. The color of the thick filament reflects the frequency of myosin insertion, i.e., increasing saturation of the blue color means higher frequency

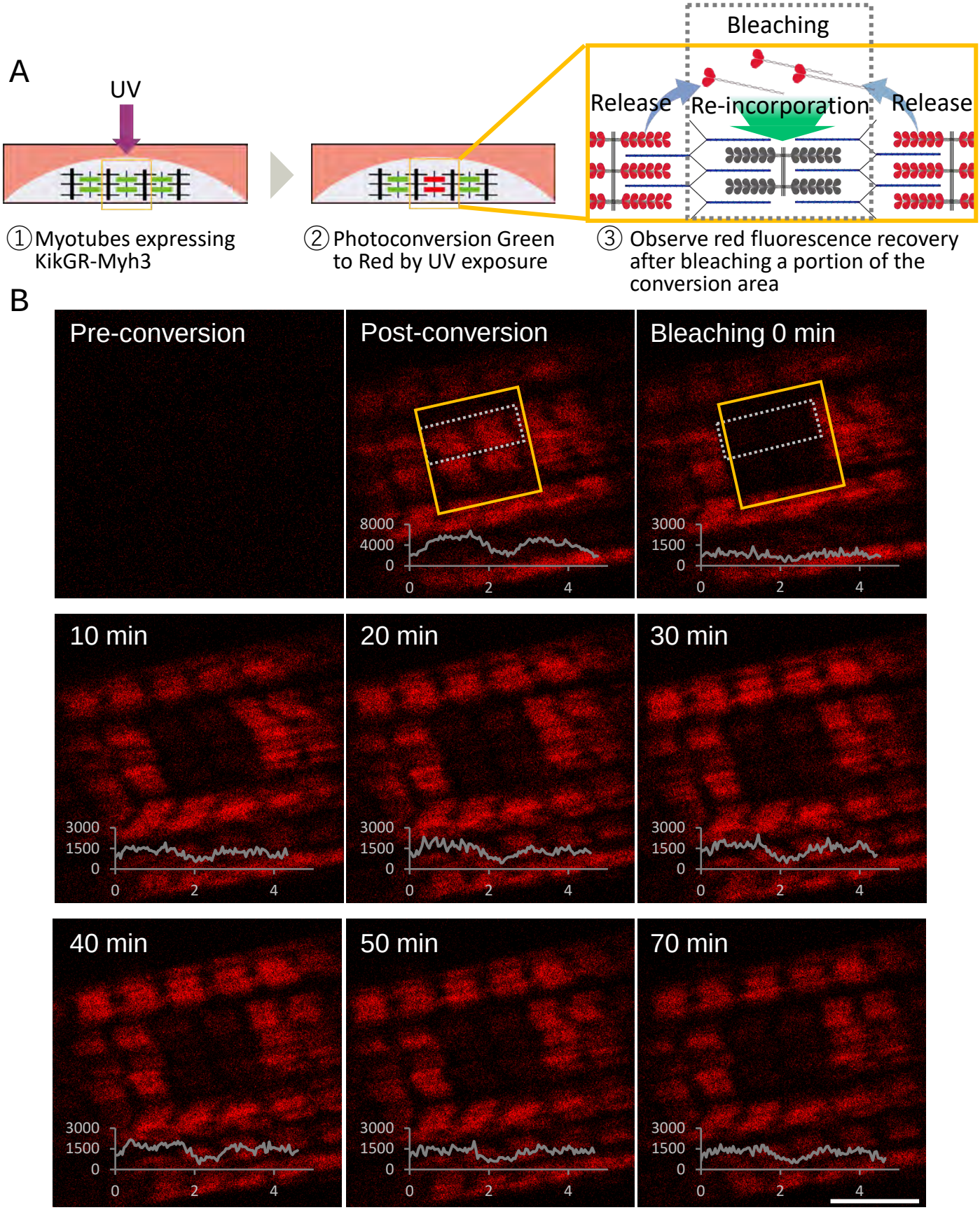

Fig.7 Localization of photoconvertible KikGR-Myh3 in the myofibrils

A. A scheme of FRAP experience is shown. First, muscle cells were transfected with KikGR-Myh3 vector and forms myotube expressing KikGR-Myh3. Second, a portion of myofibrils were photoconverted from green to red by exposure of UV light. Final, a portion of photoconverted area was bleaching and red fluorescence recovery of the area was observed at 10 min intervals.

B. Alternation of KikGR-Myh3 fluorescence signals was monitored at 10 min intervals after photoconversion. The graphs in each panel show that line scan data of the red fluorescence of KikGR-Myh3 in bleaching area. The yellow rectangles indicate bleaching area. The dashed rectangles are indicating the area using line scan. Bar is 5 μm.

0.1% in DM overnight, and then TMR ligand was washed out with PBS. Subsequently, the medium was shifted to the regular DM 1 h before the FRAP assay. If the red fluorescence signal was recovered in the bleaching area, the red labeled myosin should insert into the thick filaments. In other words, the red-labeled myosin was released from the other thick filaments to be reincorporated into the thick filament of the bleached area (Fig. 8A). As a result, the red fluorescence intensity was gradually increased in myotubes expressing Halo-Myh3 (Fig. 8B; Fig. 9).

Finally, to investigate which region of the thick filament was favored for insertion of re-incorporated myosin, the insertion pattern was analyzed using FRAP images of Halo-Myh3. Line-scan was performed using 8–14 sarcomeres per myotube and average data for each myotube was calculated. Next, total average data was normalized to max value 1. To evaluate distribution change during indicating time, the fluorescence increment and distribution change compared to pre-bleaching or 0 min were calculated using unprocessed and normalized fluorescence data (Fig. 10A). Unprocessed fluorescence intensity was depressed after bleaching, which was gradually recovered during observation (Fig. 10B). In normalized waveforms, gradual recovering of the characteristic dent pattern at M-line was observed (Fig. 10C). To confirm in which region of sarcomere fluorescence increased at first, the fluorescence intensity in sarcomere was compared between 0 min and indicating time points using unprocessed fluorescence data. The fluorescence intensity was gradually increased 60 min onward, which recovered faster in the region indicated by around -0.5 and 0.5 at the X-axis than the center of the sarcomere (Fig. 10D). Next, the distribution pattern was compared between each data of 0–300 min and pre-bleaching using normalized fluorescence data. The distribution pattern of 200 min onward became almost the same as pre-bleaching. The difference of fluorescence distribution from pre-bleaching tended to remain near the center rather than the region indicated by around -0.5 and 0.5 at the X-axis (Fig.

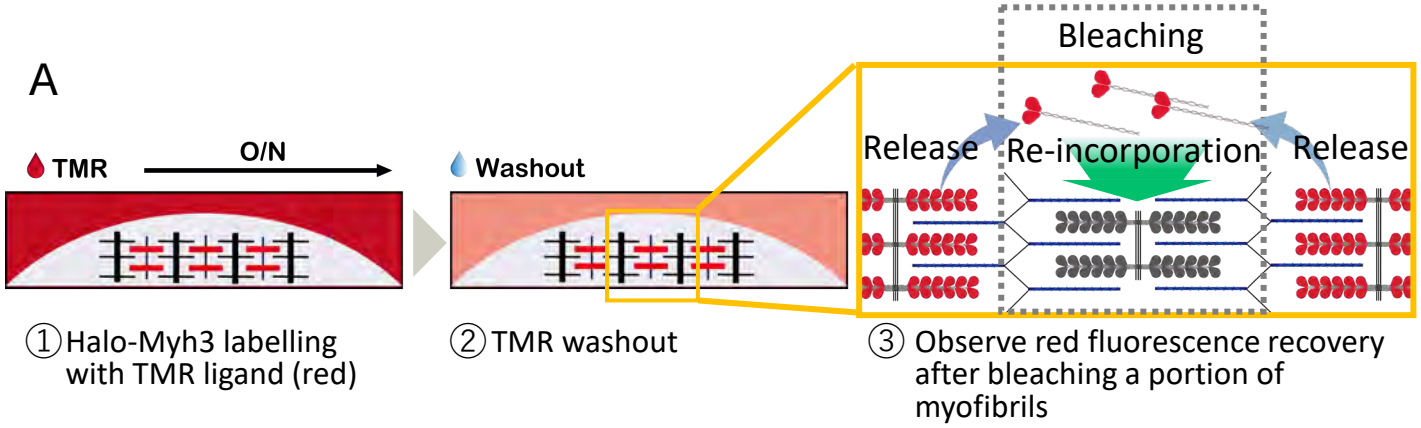
A
TMR
O/N
Washout
Bleaching
Release
Re-incorporation
Release
① Halo-Myh3 labelling with TMR ligand (red)
② TMR washout
③ Observe red fluorescence recovery after bleaching a portion of myofibrils

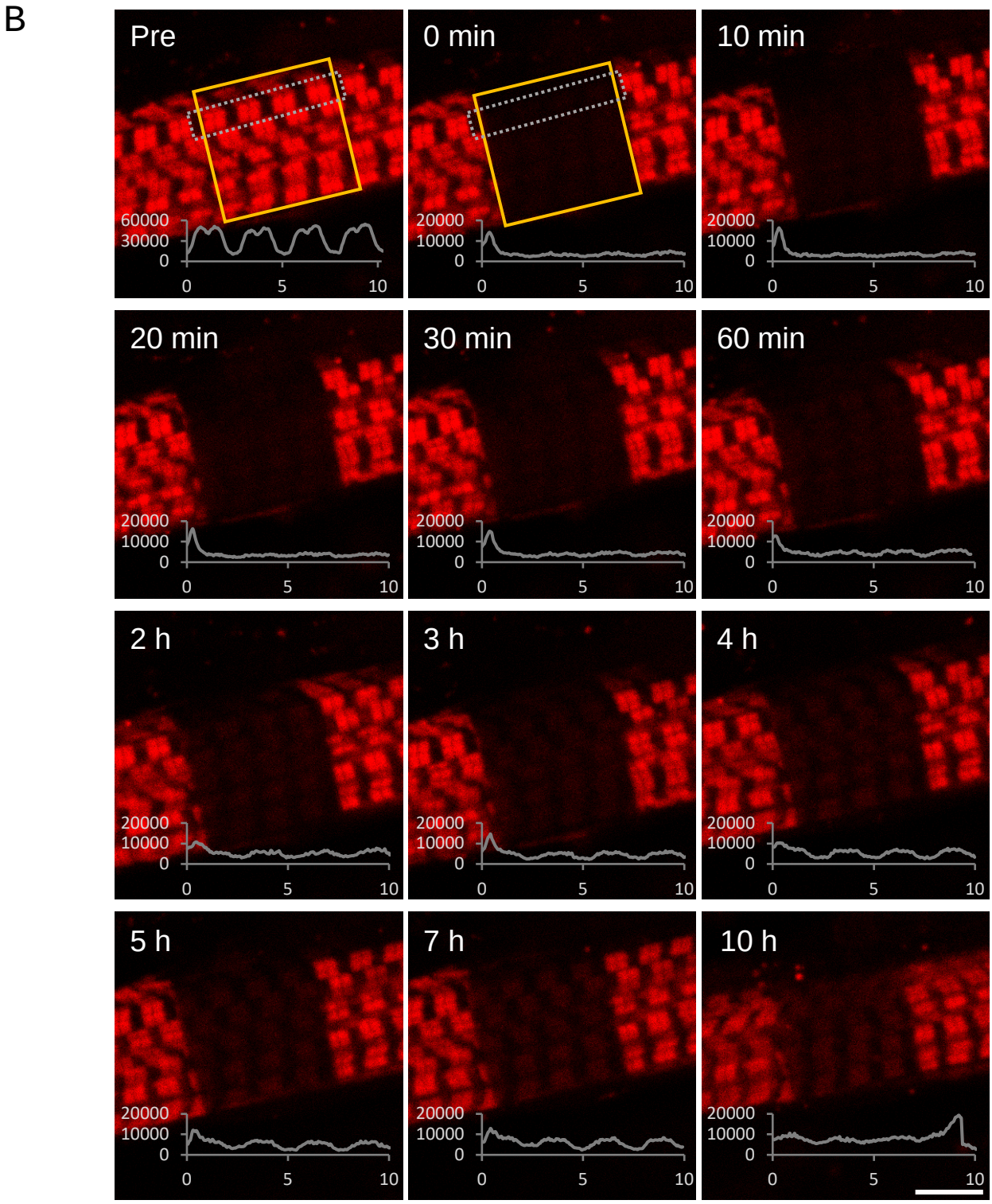
B
Pre
0 min
10 min
20 min
30 min
60 min
2 h
3 h
4 h
5 h
7 h
10 h
60000
30000
20000
10000
0
0
5
10

Fig.8. Fluorescence recovery of Halo-Myh3 after washout of TMR ligand.
A. A scheme of experience is shown. First, Halo-Myh3 was labelled with TMR ligand by overnight incubation with 0.1% TMR added medium. Second, TMR was washed out and medium was shift to normal DM. Finally, fluorescence recovery was observed under condition without newly rebelled Halo-Myh3.
B. The relative fluorescence images of the TMR labeling Halo-Myh3 are shown. The yellow rectangles indicate bleaching area. The dashed rectangles indicate that the area used for the line scan. The graphs of the line scan are shown in each image. Bar is 5 μm.

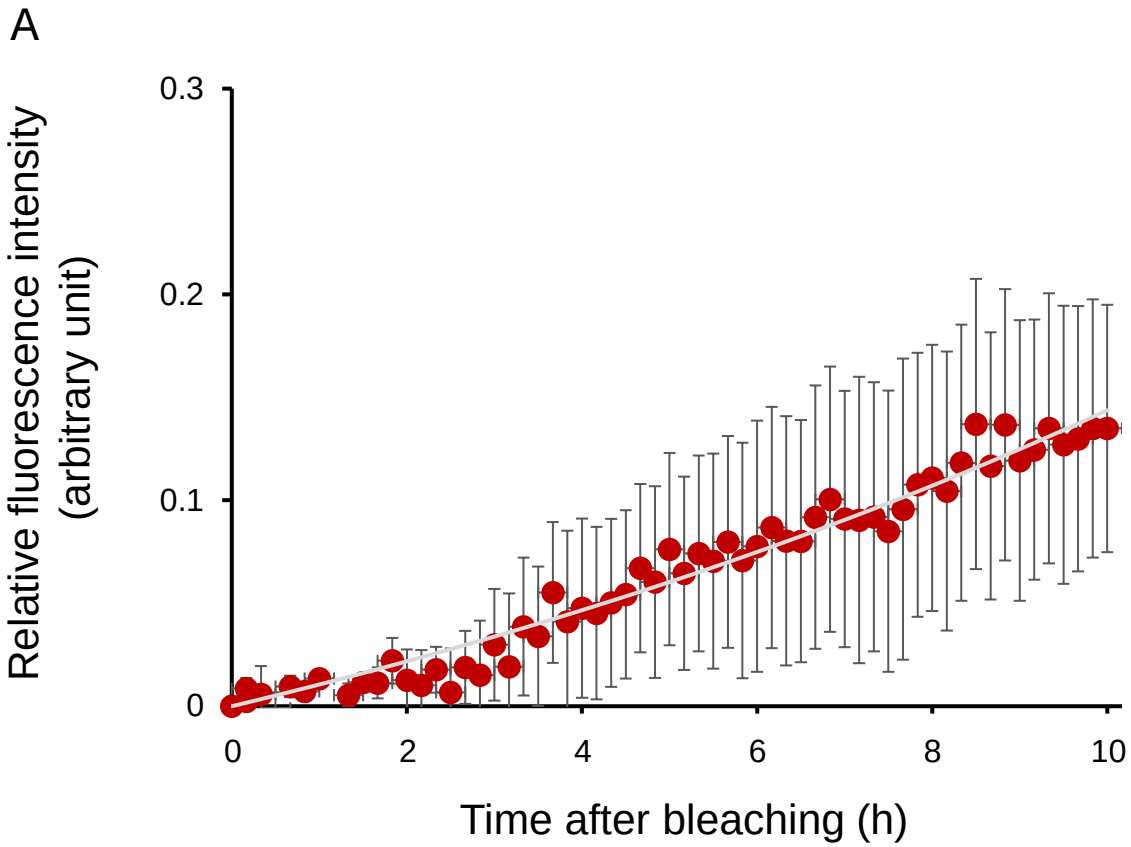

Fig.9. Fluorescence recovery of Halo-Myh3 after washout of TMR ligand.
A. Red fluorescence signals of Halo-Myh3 were measured in the bleaching area indicating yellow rectangles in Fig. 8B of myofibrils at indicated time point. Values represent the mean ± SE. n = 5.

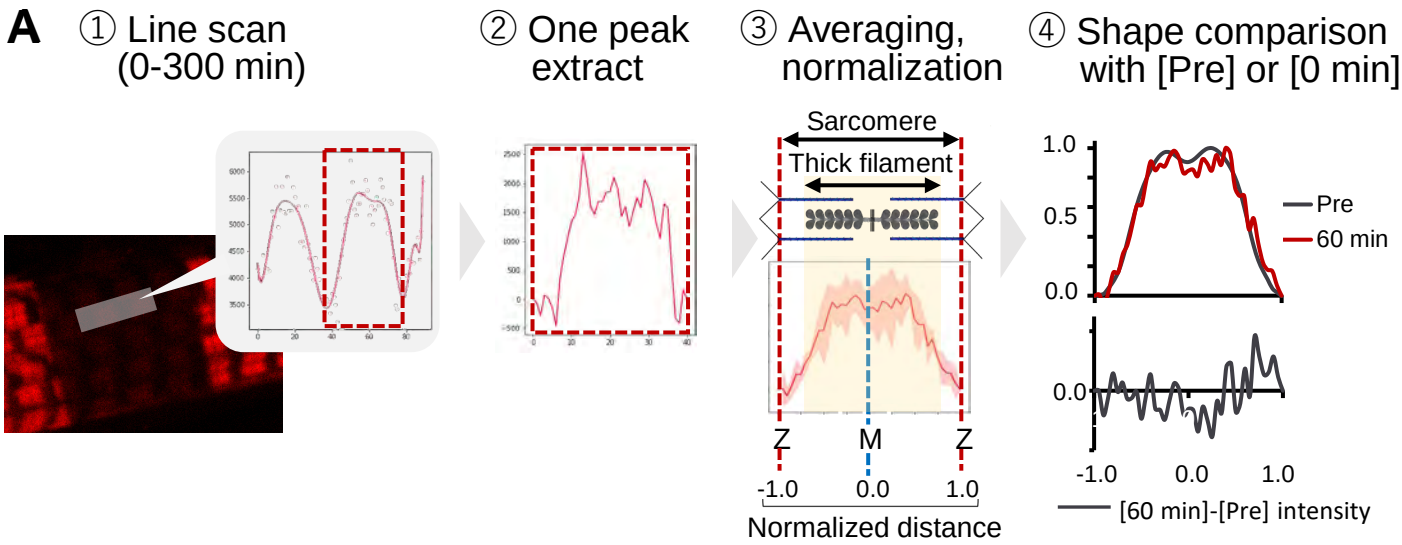

Change of fluorescence intensity during indicating time

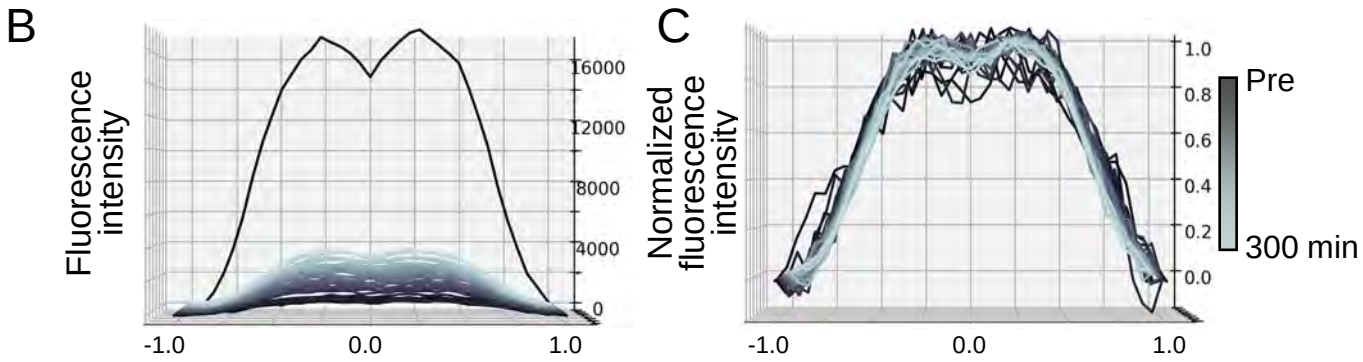

Comparison of waveforms with [Pre-bleaching] or [0 min]

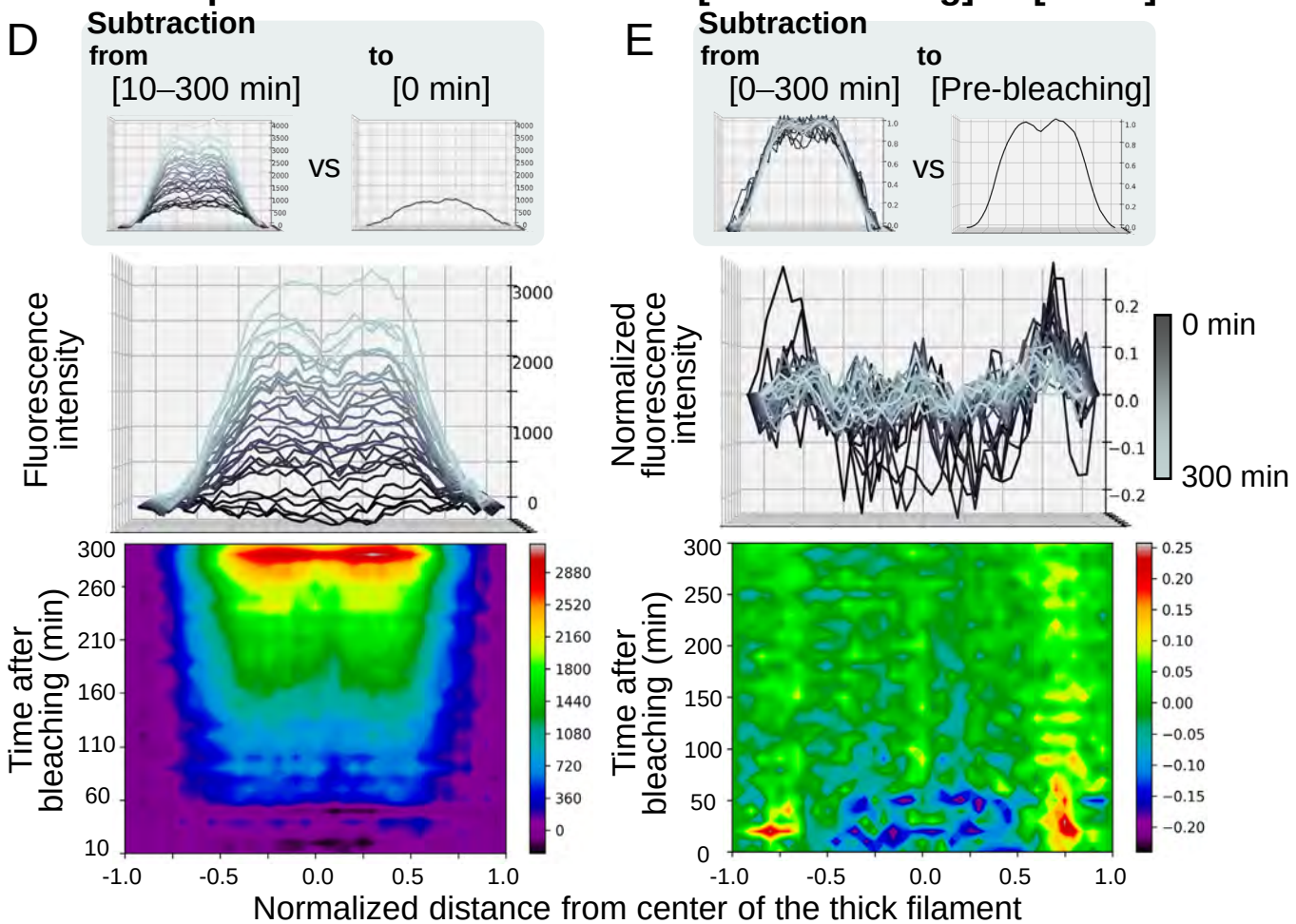

Fig. 10. Over time alteration of red fluorescence distribution of Halo-Myh3 in the sarcomeres

A. A scheme of image-processing to evaluate fluorescence distribution change during 0-300 min is shown. First, the fluorescence signal was line-scanned along myofibrils to obtain mean fluorescence intensities in sarcomere with 10 minutes intervals up to 300 minutes. Second, waveforms were extracted at the points indicating one peak. Third, waveforms were averaged and were normalized as a fluorescence max value and x-axis max distance from the center to be 1.0. Finally, fluorescence distribution change was studied by comparison between each time and 0 min or pre-bleaching. To comparison of fluorescence distribution change, the results of subtraction were obtained from data of unprocessed or normalized fluorescence intensity.

B–C. Averaged thirty line-scanned waveforms taken from 0 to 300 minutes with 10 minutes intervals following photobleaching were overlaid with each color. The unprocessed fluorescence intensity and the normalized fluorescence intensity were shown in B and C, respectively. The x-axis was the normalized distance from the center of the sarcomere. The y-axis was the unprocessed (B) and the normalized (C) fluorescence intensities. n = 5.

D. The graph shows that the difference between two fluorescence intensity distributions where unprocessed red fluorescence intensity of 0 min was subtracted from the unprocessed red fluorescence intensity of each time point. Waveforms in the upper indicate overlaid the subtraction results of each time and the color panel under indicated the subtraction image. The x-axis and the y-axis indicate the normalized distance from the center of the sarcomere and unprocessed fluorescence intensity (upper) or the time after bleaching (under, minutes). n = 5.

E. The graph shows that the difference between two fluorescence intensity distributions where normalized red fluorescence intensity of pre-bleaching was subtracted from the normalized red fluorescence intensity of each time point. Waveforms in the upper indicate overlaid the subtraction results of each time and the color panel indicated the subtraction image. The x-axis and the y-axis indicate the normalized distance from the center of the sarcomere and normalized fluorescence intensity or the time after bleaching (minutes). n = 5.

10E). These results suggested that myosin was reused for the insertion into the thick filament, and the recycled myosin also tended to be frequently incorporated into the tip of the thick filament as well as the newly synthesized myosin (Fig. 5 and 6).

Discussion

In this chapter, I demonstrated the exchange of myosin in the thick filament of cultured myotubes through a live imaging technique. These results showed that (1) myosin itself is the unit of replacement, (2) not all, but some myosins can be rapidly replaced by other myosins within 7–10 min in the thick filaments of myotubes, (3) the thick filament-dissociated myosin is reused for myosin replacement in the thick filament, and (4) the myosin replacement frequency differs depending on the region of the thick filament. Based on these results, I propose a thick filament-associated myosin replacement model in myotubes (Fig. 11).

The thick filament-associated myosin was found to have the capacity to be promptly replaced in minutes. Although our previous studies showed that about 50% of eGFP-Myh3 is replaced in the myofibrils within 3 h, we had not investigate the myosin replacement rate over a brief period (Ojima et al., 2015). The present KikGR-Myh3 experiments revealed that approximately 10% of myosin in the thick filament was replaced within 10 min (Fig. 2). Fluorescence pulse-chase assay also showed that incorporation of myosin into the thick filament was observed within 10 min (Fig. 4 and 5). This quick myosin exchange in the thick filament may in part reflect the biochemical properties of myosin, since synthetic myosin filaments are extensively exchanged for other myosin in minutes in vitro (Davis, 1993a; Saad et al., 1986, 1991). Although the thick filament-associated myosin is replaced rapidly and continuously by other myosin, it takes ~3 h to exchange half of the myosin molecules in the thick filament [Fig. 2, (Ojima et al., 2015)]; this relatively protracted amount of time is attributable to the complexity of the thick filament, which contains about 300 myosins with the thick filament-associated proteins (see below).

KikGR-Myh3 experiments showed that the thick filament-associated myosin release and the myosin incorporation into the thick filament occur concurrently. The unit of replacement is thought to be an individual myosin molecule, rather than a thick filament. One of the reasons for

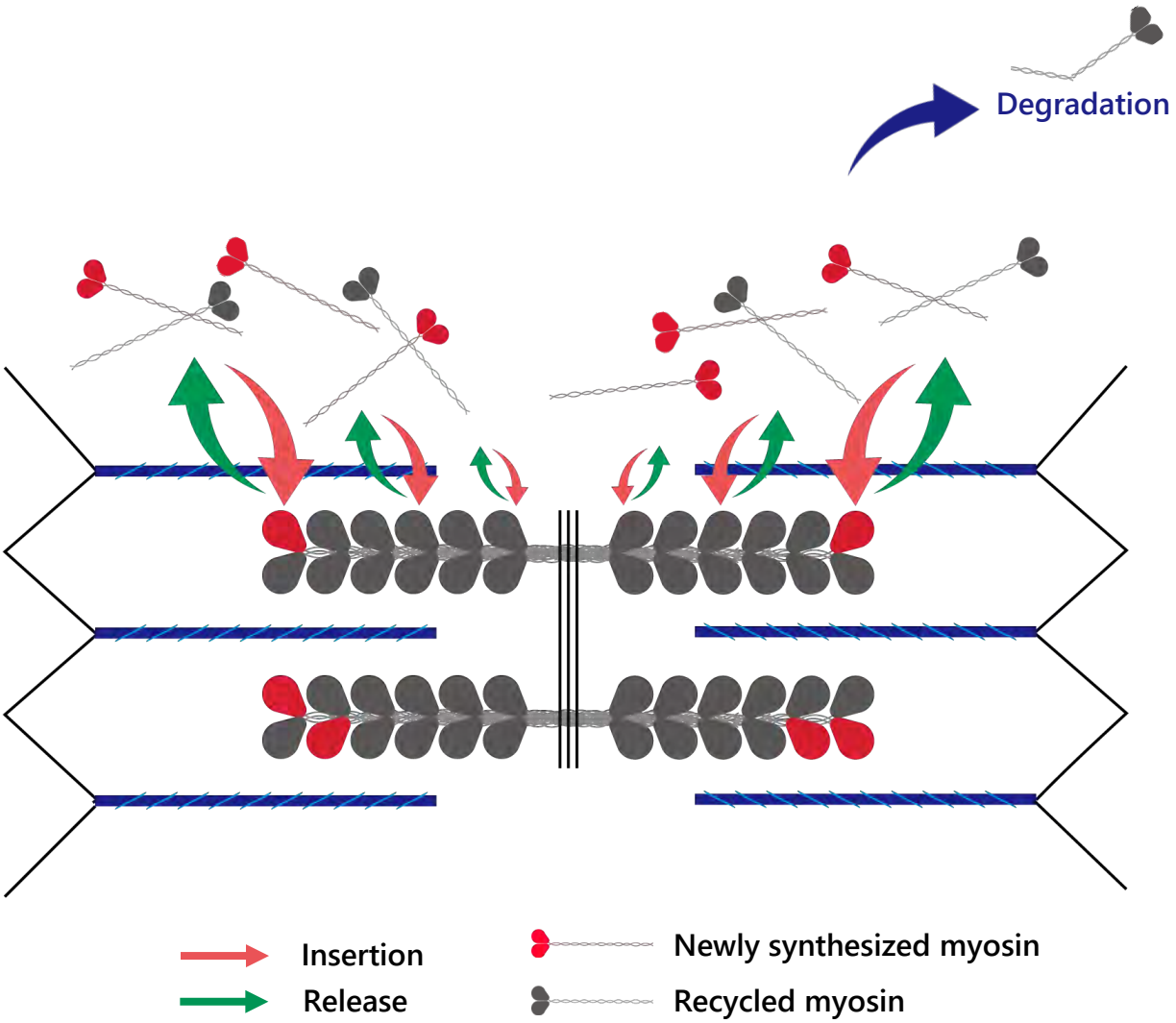

Fig. 11. A model of myosin replacement in the thick filament.
When thick filament-associated myosin is replaced, (1) the individual myosin molecule acts as an exchange unit, (2) myosin release and insertion occur concurrently, (3) myosin is more frequently replaced at the edge of the thick filament, (4) both of newly synthesized and recycled myosin were used for myosin replacement, and (5) a certain amount of myosin was selected for degradation. The size of the arrow reflects the myosin replacement rate in the thick filament conceptually. The red and gray color myosin indicate the position of inserted newly or recycled myosin, respectively.

this conclusion is that found different myosin replacement rates along the thick filament. Moreover, the thick filament-associated proteins, such as MybpC and myomesin, are also exchanged by others in the thick filaments, but their replacement rates are independent of myosin (Ojima et al., 2015). These results support the notion that the replacement unit in the myofibril is a myosin molecule rather than a thick filament.

FRAP assays using converted KikGR-Myh3 and Halo-Myh3 showed that once released myosin was recycled and incorporated into the thick filament again (Figs. 7–9). In these exams, although fluorescence recovery was detected, which recovery rate was lower and slower than that of KikGR-Myh3 experiment in Figs. 1–2 and previous study using eGFP-Myh3 [Fig. 9, (Ojima et al., 2015)]. These results indicate that the rapid replacement in minute might be mainly contributed by newly synthesized myosin. Moreover, the difference in the fluorescence recovery rate was not observed between the sarcomere located in proximity to the non-bleaching area and the sarcomere located center of the bleaching area (Fig. 7 and 8). This observation implies that the dissociated myosin might disperse immediately and uniformly within the range of ROI used in this study.

Based on the following observations, it was concluded that myosin is the most frequently replaced at the tip of the thick filament (Fig. 11). First, the red fluorescence intensity of KikGR-Myh3 was rapidly reduced at the tips of the thick filaments compared to the middle of the thick filaments. Second, newly synthesized myosin tended to be inserted into the tips of the thick filaments. Third, both the red and green intensities of KikGR-Myh3 changed biphasically. Fourth, the incorporation of recycled myosin was faster at the tip of the sarcomere than the center. The present results are consistent with the following results from several pioneering works. An in vitro biochemical study showed that myosin was incorporated into the tip of the synthetic myosin filament within 5 min, but myosin replacement was observed in the full length of the synthetic

myosin filament by 60 min (Saad et al., 1991). In glycerinated myofibrils, the thick filament dissociated from both ends under high ionic strength conditions (Higuchi et al., 1986). Finally, a study using an immune-electron microscopic technique revealed a greater exchange of new myosin at the ends of the thick filament than at other regions in rabbit cardiac cells (Wenderoth & Eisenberg, 1987). Therefore, the tip is the region with the most active exchange of myosin in the thick filament of skeletal muscle cells as well as in the filaments of cardiomyocytes and in vitro synthetic myosin.

This chapter results showed the different myosin replacement rates on the thick filament. The complexity of the thick filament may partly explain these results. The thick filament is a bipolar structure that is separated into several parts (Davis, 1988). The center of the thick filament is called the H zone, where myosin is arranged in an antiparallel fashion. A bundle of thick filaments is tied with myomesin in the H zone. Seven to eleven MybpC striped with about 43 nm intervals on the thick filament are called the C zone (Davis, 1988; Dennis et al., 1984b; Henderson et al., 2018). Both ends of the thick filament are called the D zone (Skubiszak & Kowalczyk, 2002). In addition, connectin/titin also interacts with the thick filament at multiple sites in the H and the C zones (Henderson et al., 2018; Labeit & Kolmerer, 1995). Unlike the thin filament, whose ends are capped with capping proteins such as tropomodulin at the pointed end and Cap-Z at the barbed end (Casella et al., 1987; Fowler et al., 1993), both ends of the thick filament are uncapped, leading to frequent myosin exchange at both tips of the thick filaments. These structural components of the thick filaments might be obstacles to the prompter exchange (release and insertion) of myosin on the H and the C zones of the thick filaments compared to the D zones. Furthermore, the fact that the difference in the frequency of myosin replacement is dependent on the position within the thick filament might be the reason for the biphasic replacement of myosin observed in our KikGR-Myh3 experiments.

Collectively, the present results show that myosin is actively and continuously replaced in the thick filaments in living myotubes. Given the extensive number of classic studies on in vitro synthetic myosin filaments (Davis, 1993b; Saad et al., 1986, 1991), the dynamic equilibrium of myosin is involved in the myosin replacement in myotubes. This frequent myosin exchange in the thick filament depends on both newly synthesized and recycled myosin. However, it is unclear how myosin was selected for reuse or broke down. The association of protein degradation system with myosin replacement was studied in Chapter 2.

Chapter 2

Introduction

Because of its remarkable plasticity, skeletal muscle tissue can modify its volume to adapt to exercise, disease, development, and aging (Lecker et al., 2006; Nury et al., 2007). Skeletal muscle tissue is composed of bundles of myofibers, which contain highly organized structural components named myofibrils. A single myofiber contains approximately 2,000 of myofibrils in untrained adult humans (Chen et al., 2017). Myofibrillar proteins, of which there are more than 20 types, are organized into repeated minimal contraction units referred to as sarcomeres (Clark et al., 2002; Henderson et al., 2018). Muscle tissue size is determined by the volume of each muscle fiber, which reflects the number of myofibrils. Therefore, muscle hypertrophy and atrophy depend on increase and decrease of the number of myofibrils, respectively, and muscle volume is modulated by the balance between the synthesis and degradation of myofibrillar proteins.

Myosin, an abundant myofibrillar protein in the skeletal muscle, functions as a motor protein in muscle contraction. Myosin is composed of two heavy chains and four light chains, and polymerizes into filaments under physiological ionic strength conditions (Craig & Woodhead, 2006; Davis, 1988). In myofibrils, approximately 300 myosin molecules form a single thick filament with myosin-associated proteins such as connectin/titin, myomesin, and myosin binding protein C (MybpC) (Kontrogianni-Konstantopoulos et al., 2009; Labeit & Kolmerer, 1995; Obermann et al., 1997). The interaction of myosin in the thick filaments with actin in the thin filaments induces muscle contraction, coupled with ATP hydrolysis by myosin (Walklate et al., 2016).

Skeletal muscle is classified into two categories according to the velocity of muscle contraction, *i.e.*, slow and fast types. This feature is attributed to the expression of myosin heavy

chain (Myh) isoforms with different rates of ATPase activity and muscle contraction velocity in each myofiber (Resnicow et al., 2010; Walklate et al., 2016). Slow type muscle fibers express Myh7, whereas fast type myofibers express Myh1, Myh2, and/or Myh4. Although slow and fast types of Myhs are dominantly expressed in adult skeletal muscles, other Myh isoforms such as embryonic (Myh3) and neonatal (Myh8) types are expressed during muscle development. Fast type of Myhs gradually becomes predominant a few days after birth in mice, which causes the downregulation of Myh3 and Myh8, resulting in Myh isoform shift in myofibrils (Stefano Schiaffino et al., 2015).

Proteins are regularly degraded to maintain protein quality and quantity *in vivo*. One of the main degradation systems in skeletal muscle is the ubiquitin-proteasome system (UPS), which selectively degrades target proteins (Lecker et al., 2006; Passmore & Barford, 2004). In the UPS, ubiquitin (Ub) is activated by the E1 ubiquitin-activating enzymes in an ATP-dependent manner and is transferred to an E2 ubiquitin-conjugating enzyme. The E3 ubiquitin ligase which selectively recognizes substrate proteins recruits the E2, catalyzing the transfer of Ub to a lysine (K) residue of the substrate (Passmore & Barford, 2004). Polyubiquitination on the substrate protein is classified for degradation by the proteasome (Huang & Zhang, 2020).

In striated muscle, muscle ring finger protein 1 (Murf1) and muscle atrophy F-box (MAFbx) are muscle-specific E3s that are upregulated under conditions of muscle atrophy (Bodine et al., 2001). Murf1 is a member of the Murf family, which ubiquitinates multiple myofibrillar proteins containing the slow and fast types of Myh (Cohen et al., 2009; Fielitz et al., 2007). Potential target proteins of MAFbx in sarcomeres include Myh, vimentin, and desmin (Lokireddy et al., 2011, 2012), in addition to its well-known substrates MyoD and eukaryotic translation initiation factor 3 (Lagirand-cantaloube et al., 2008; Tintignac et al., 2005). Neuralized E3 ubiquitin protein ligase 2 (Neurl2) which is referred to as Ozz, another muscle-specific E3, is upregulated during myotube

formation (Campos et al., 2010). Ozz, a member of the suppressor of cytokine signaling family, functions as an E3 in a complex containing Elongin B/C, Rbx1, and Cullin 5 (Kile et al., 2002).

Our previous studies demonstrated that the myosin in myofibrils is replaced by another myosin molecule that is newly synthesized and/or derived from a cytosolic pool of myosin (Ojima et al., 2015, 2017). In addition, I showed that myosin was replaced in the thick filament by newly synthesized myosin and recycled myosin from the myofibrils in chapter 1. However, the role of protein degradation system in myosin replacement has not been investigated. In this chapter, I examined the effect of muscle specific E3 ligase overexpression on myosin replacement.

Materials and Methods

1. Experimental animals

All experiments were performed using primary muscle cells from chick embryos. Experimental animals were reared for as outlined in Hokkaido University and NARO guidelines for the care and use of laboratory animals. This study was approved by the two committees.

2. Cell culture and transfection

Skeletal muscle cells were isolated from the pectoral muscles of 11-day-old chick embryos as described above. Obtained cell fraction containing skeletal muscle cells was seeded at a density of 7,500–10,000 cells/cm^2 on dishes coated with poly-L-Lysine (Sigma-Aldrich) and collagen Type Ⅰ-A (Nitta Gelatin). One day after seeding, the cells were transfected with expression vectors using Lipofectamine® LTX and Plus reagents. The GM was replaced by DM 1 day after transfection or after reaching 70% cell confluence. The DM was replaced every 2 days. Once myotubes were formed, 10 μM cytosine arabinoside (Tokyo Chemical Industry, Tokyo, Japan) was added to the medium to remove mitotic non-muscle cells. For MG132 treatment, MG132 (Peptide Institute, Osaka, Japan) was added to the differentiation medium at a final concentration of 1 μM for 16 h.

3. cDNA constructs

Mouse cDNAs for *Myh1* (85–5913 in NM_030679), *Myh3* (45–5868 in NM_001099635), *Myh4* (111–5930 in NM_010855), and *Myh7* (142–5949 in NM_080728) were cloned into the peGFP-C1 vector (TAKARA BIO, Kusatsu, Japan). Mouse cDNA for *Trim63* (Murf1, 105–1172 in NM_001039048) and *Neurl2* (Ozz, 157–1014 in NM_001082974) was cloned into the

pmCherry vector (TAKARA BIO). The inserted sequences of all constructs were verified with a 3730 DNA Analyzer (Applied Biosystems)

4. Reverse translation quantitative PCR assay (RT-qPCR)

Total RNA was isolated from differentiated muscle cells with ISOGEN (Nippon Gene, Tokyo, Japan) according to the manufacturer's instructions. The first-strand cDNA was synthesized using ReverTra Ace (Toyobo, Osaka, Japan). RT-qPCR was performed with a CFX96 Real-Time PCR Detection System (Bio-Rad, Tokyo, Japan) using the QuantiTect SYBR Green PCR System (Qiagen, Tokyo, Japan). The primer pairs used in this study are listed in Table 1. PCR conditions were as follows: 15 min at 95°C, 45 cycles of 15 sec at 94°C, 30 sec at 65°C and 30 sec at 72°C. GAPDH was used as an internal control.

Table 1. Primer list for RT-qPCR

Gene	Accession number		Primer sequence
cOzz (Neurl2)	XM_015296576	Forward	5’-CTCCTGGATGAGCTGTACCGCAC-3’
		Reverse	5’-GAAGTGACCCTTGAAGGCCATC-3’
cMurf1 (Trim63)	XM_015297755	Forward	5’-CTCTGTGCACGTTTTGATGCGTTCTCA-3’
		Reverse	5’-ATAGAAAAGTGTCCTGTACTGGAGCTGGAT-3’
cMurf2 (Trim55)	NM_001081281	Forward	5’-CAGCAATGACAGAGTACAAGGGATAGTCAC-3’
		Reverse	5’-GCCTCCTCCTCTCTGTCAAAATCAATTTCT-3’
cMurf3 (Trim54)	XM_015285000	Forward	5’-GAAGAAGATCACAGACATGTCCAAGGTGTC-3’
		Reverse	5’-CTTCATAGCAGTCATAGGGCTGTAGGGTTT-3’
cGAPDH	NM_204305	Forward	5’-CAACTTTGGCATTGTGGAGGGTCTTATGAC-3’
		Reverse	5’-AAACAAGCTTGACGAAATGGTCATTCAGTG-3’
mOzz (Neurl2)	NM_001082974	Forward	5’-TCTAGTGGAAATTGAGGAAAAAGAGCTGGG-3’
		Reverse	5’-CATGTCCTCCCCGTTGATGATGATGTG-3’
mMurf1 (Trim63)	NM_021447	Forward	5’-CATTTACAAACGCCAGAAGAGTGAGCTGAG-3’
		Reverse	5’-CTCACAGAGAATTGCTCCATGCTCTCATAG-3’
mMurf2 (Trim55)	NM_001081281	Forward	5’-AGGAACCTGCTCGTGGAAAACATTATTGAT-3’
		Reverse	5’-CTTCCTGATAAGAGTTCGGACATGTTCCAG-3’
mMurf3 (Trim54)	NM_001039048	Forward	5’-ACAGAAGACTGAGCTGAGTAACTGCATCTC-3’
		Reverse	5’-GCCTCTGCTATGTGTTCTAAGTCCAGAGTA-3’
GFP		Forward	5’-CTACGGCAAGCTGACCCTGAAGTTCATC-3’
		Reverse	5’-CTCGATGTTGTGGCGGATCTTGAAGTTCAC-3’

c and m indicate chicken and mouse, respectively.

5. Fluorescence recovery after photobleaching (FRAP) assay

The FRAP assay was performed using transfected myotubes cultured on glass-based dishes (IWAKI) with a Leica TCS SP5 (Leica microsystem) as described above. Cells were incubated at 37°C and 5% CO_2 on the microscope incubation system (TokaiHit) during FRAP experiments. The emission wavelengths of eGFP and mCherry were 488 and 543 nm, respectively, and band-pass filters were 500–540 nm and 600–700 nm, respectively. A 100 μm^2 region of interest (ROI)

was selected in each cell. The fluorescence of ROIs was bleached by exposure to an argon laser at a strength of 100% for 30 sec. Fluorescence recovery was monitored every hour after photobleaching. The fluorescence intensity of the ROI was quantified and normalized to that of the non-bleaching area at each time point. The normalized fluorescence intensities were used in the following exponential curve fitting formula calculated by ImageJ 1.52a (National Institutes of Health) software:

$FI=Mf*(1-e^{(-b*t)}) +c$, where FI is the normalized fluorescence intensity, Mf is the mobile fraction, b is the speed constant, c is the fluorescence intensity after bleaching, and t is the elapsed time after beaching.

Mf was used for the maximum value of fluorescence intensity change. The 5% recovery time (5% Rt) indicated the time required to reach a fluorescence recovery of 5% of prebleaching intensity, and was calculated from In [Mf/(Mf-0.05)]/b. The 5% Rt was used for the parameter of speed for fluorescence recovery at the initial rise time.

6. Immunoprecipitation and western blotting

Immunoprecipitation samples were obtained from cells co-transfected with eGFP-Myh3 and mCherry-Ozz. To increase the amount of ubiquitinated proteins, myotubes were treated with 1 μM MG132 (Peptide Institute), a proteasome inhibitor, for 16 h. Immunoprecipitation was conducted under denature condition (Koyama et al., 2008). The cytosolic fraction was obtained by treating cells with modified chemical skinned-fiber buffer [10 mM Tris-HCl pH 7.6, 150 mM CsCl, 1 mM EDTA Cs, 0.5% (v/v) Triton X-100, 0.1% (w/v) sodium dodecyl sulfate, 2% protease inhibitor cocktail (Sigma-Aldrich), 0.06 mM leupeptin (Peptide Institute), 0.7 μM calpastatin (Takara Bio), and 25 μM MG132] for 30 min at 4°C. To remove cellular debris, the soluble

fraction was centrifuged at 1,500g for 5 min. The supernatant was further centrifuged at 20,000g for 20 min to obtain the cytosolic fraction. Precipitation fraction was prepared from myotubes after chemical skinned-fiber buffer treatment. Skinned myotubes were collected in high salt lysis buffer [10 mM Tris-HCl pH 7.6, 0.6 M CsCl, 1 mM EDTA Cs, 0.5 % (v/v) Triton X-100, 0.1% (w/v) sodium dodecyl sulfate, 2% protease inhibitor cocktail, 0.06 mM Leupeptin, 0.7 μM Calpastatin, 25 μM MG132]. Samples were homogenized with 27 G syringes and rotated at 4℃ for 15 min to solubilize myosin. After centrifugation at 20,000g for 20 min, the high salt soluble fraction was used as a myofibril fraction. The cytosolic and the myofibril samples were pre-treated with agarose conjugated-protein G (Santa Cruz Biotechnology, Dallas, TX, USA) for 1 h to remove nonspecific proteins bound to the agarose beads. The supernatants were then reacted with anti-myosin antibody (1:100; clone MF20, R&D Systems, Minneapolis, MN, USA) followed by protein G conjugated agarose beads at 4℃ for 1 h. The beads were washed with modified chemical skinned-fiber buffer five times and then boiled with Laemmli sample buffer [125 mM Tris-HCl pH 6.8, 20% (v/v) glycerol, 4% (w/v) SDS, 0.02% (w/v) bromophenol blue, and 0.2 M dithiothreitol] at 95℃ for 5 min.

7. Western blotting (WB)

Samples were analyzed by sodium dodecyl sulfate polyacrylamide gel electrophoresis (SDS-PAGE) followed by transfer to PVDF membranes (Merck, Tokyo, Japan). Membranes were blocked with 0.5% (w/v) bovine serum albumin (FUJIFILM Wako Pure Chemical Corporation, Osaka, Japan) at room temperature for 30 min and then incubated at 4℃ for 16 h with one of the following antibodies: mouse anti-myosin heavy chain (1:1,000; clone MF20, R&D Systems),

mouse anti-ubiquitin (1:1,000; clone VB2880, VIVA Bioscience, Shanghai, China), and mouse anti-mRFP (1:1,000; clone mix of 1G9 and 3B5, MBL, Tokyo, Japan). Following incubation with peroxidase-conjugated mouse secondary antibodies (NICHIREI BIOSCIENCES, Tokyo, Japan), bands were visualized with the POD immunostain kit (FUJIFILM Wako Pure Chemical Corporation) or ECL Western Blotting Detection Reagents (GE HealthCare, Tokyo, Japan). For band quantification, signal intensities of bands were analyzed by ImageJ 1.52a. As T. Nastasi, et al (Nastasi et al., 2004) described previously, the ratios of Ub-Myh band intensity to Myh band intensity were calculated as follows: (the signal intensity of Ub-Myh band/ the lower Ig band) / (the signal intensity of Myh band / the lower Ig band). The ratios were then normalized with values of controls.

8. Immunofluorescence staining

Myotubes cultured in 8-well chambers (Thermo Fisher Scientific) were treated with MG132 for 16 h before fixing and washing with 0.5% (v/v) Triton X-100 in PBS. Then, myotubes were blocked with 0.5% (w/v) bovine serum albumin (FUJIFILM Wako Pure Chemical Corporation) at room temperature for 30 min. After blocking, myotubes were reacted with mouse anti-ubiquitin antibody (1:100; clone VU-1, LifeSensors, Malvern, PA, USA) and rabbit anti-pan sarcomeric myosin heavy chain antibody (1:4,000; kindly gifted by Prof. Howard Holtzer, Univ. Penn), followed by incubation with FITC and TRITC secondary antibodies (anti-Rabbit, 611-102-122, Rockland, PA, USA) (anti-mouse, #55527, Cappel, NC, USA). Specimens were mounted with mounting media (Thermo Fisher Scientific) and observed using the Leica TCS SP5 (Leica microsystem).

9. Statistics

All data are expressed as the mean ± standard error (SE) with individual datapoints. Control and each trial data were compared using the t-test. Statistical significance was set at $p < 0.05$. All statistical tests were performed using EZR on R commander ver. 1.40.

Results

1. Overexpressing Murf1 facilitated the myosin replacement of eGFP-Myh3 and eGFP - Myh4

The protein turnover process occurs in all living organisms. Myofibrils of skeletal muscle cells are thought to require protein turnover to replace old proteins with new ones and to change the isoforms of myofibril proteins. Therefore, to examine the UPS involvement in myosin replacement, I focused on tripartite motif-containing 63 (Trim63; Murf1) because Murf1 is one of the specific E3 ligases to recognize myosin for ubiquitination (Bodine et al., 2001). First, to study myosin replacement in myotubes overexpressing Murf1, cultured muscle cells were transfected with expression vectors eGFP-Myh3 and mCherry-Murf1. In myotubes, exogenously expressed mCherry-Murf1 was observed in M-lines, the middle of the eGFP-Myh3 positive thick filaments (Fig. 12D and F), whereas solely expressed mCherry was diffusely distributed in the cytoplasm (Fig. 12A). Overexpression of mCherry-Murf1 and mCherry did not inhibit the formation of myofibrils, *i.e.*, the striation pattern of eGFP-Myh3 was observed in myotubes (Fig. 12B and E). Exogenously expressed mCherry-Murf1 was also detected at mRNA (Fig. 12G) and protein (Fig. 12H) levels. The effect of exogenously overexpressed Murf1 on the mRNA expression levels of endogenous Murf1 and other Murf families was examined by RT-qPCR. The mRNA expression levels of endogenous *Murf1* and other Murf family, *Murf2* and *Murf3* were not significantly different with or without mCherry-Murf1 expression (Fig.12I–K).

To evaluate myosin replacement in myotubes overexpressing Murf1, one of the Myhs (Myh1, Myh3, Myh4, and Myh7) was co-expressed with Murf1 because Murf1is associated with multiple myosin isoforms (Cohen et al., 2009; Fielitz et al., 2007) (Fig. 13). FRAP experiments revealed that fluorescence recoveries of eGFP-Myh3 and eGFP-Myh4 were facilitated in the presence of

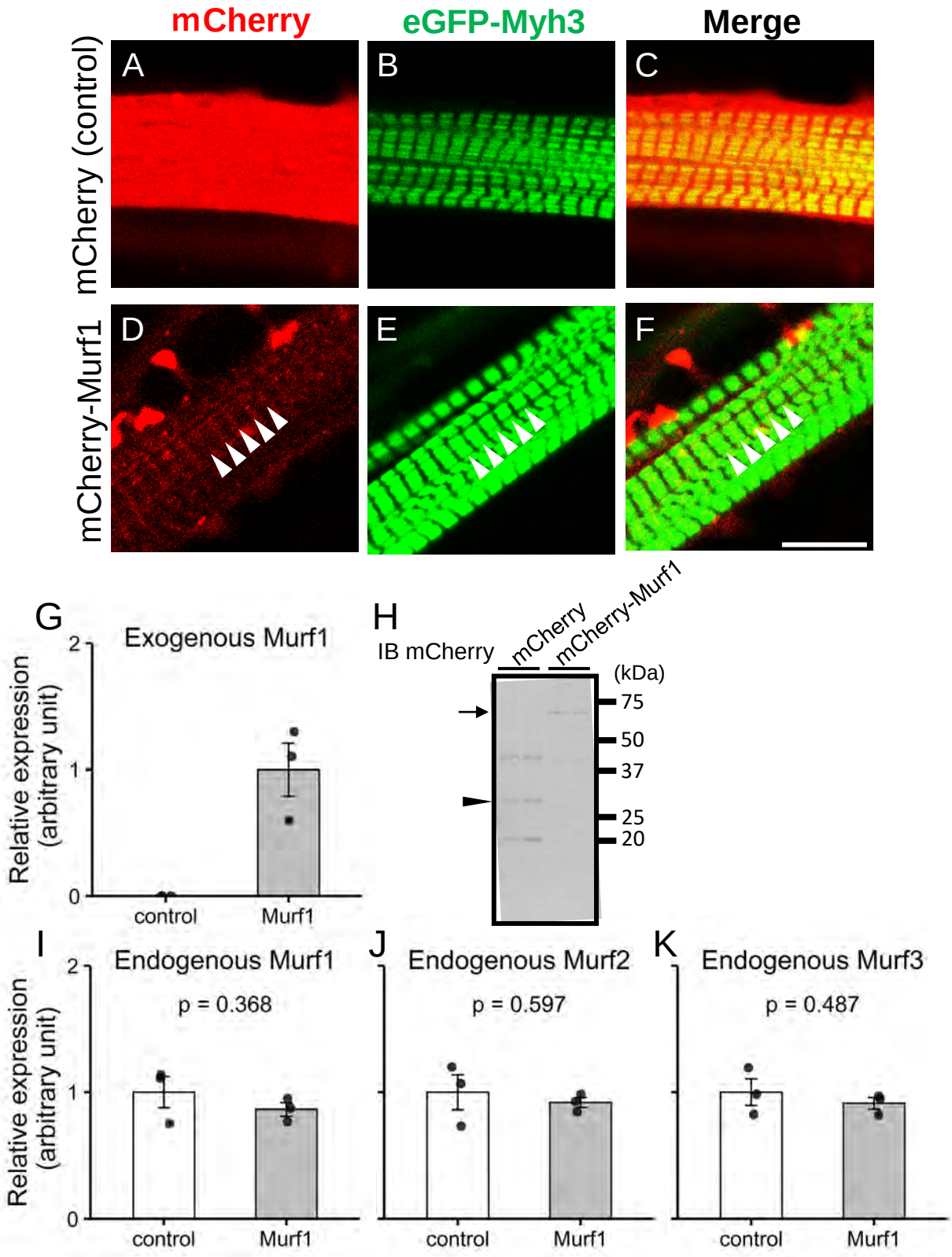

Fig.12. Localization and expression level of exogenously expressed mCherry-Murf1 in muscle cells.

A–F. Localization of exogenously expressed eGFP-Myh3 and mCherry-Murf1 observed by confocal microscopy. eGFP-Myh3 localized to the A-bands of myotubes (green). mCherry-Murf1 was localized to M-line in myotubes (red in D and F). mCherry expressed alone as a control showed a diffuse distribution in myotubes (red in A and C). C and F are merged images of A and B, and D and E, respectively. Bars, 10 μm.

G, H. The expression of mCherry-Murf1 and mCherry proteins in myotubes was detected by western blotting. An arrow and an arrowhead indicate the bands corresponding to mCherry-Murf1 and mCherry, respectively.

I–M. The expression levels of mCherry-Murf1, endogenous Murf1, and endogenous Murf1~3 were quantified by RT-qPCR in myotubes co-expressing eGFP-Myh3 and either mCherry (control) or mCherry-Murf1. GAPDH was used as the internal control, and the relative expression levels were calculated as a ratio of the signal intensity of the target gene to the signal intensity of GAPDH. Fold change was normalized to the mCherry-Murf1 group (H) or mCherry group (I-K). Values represent the mean ± SE. n = 3 for each group.

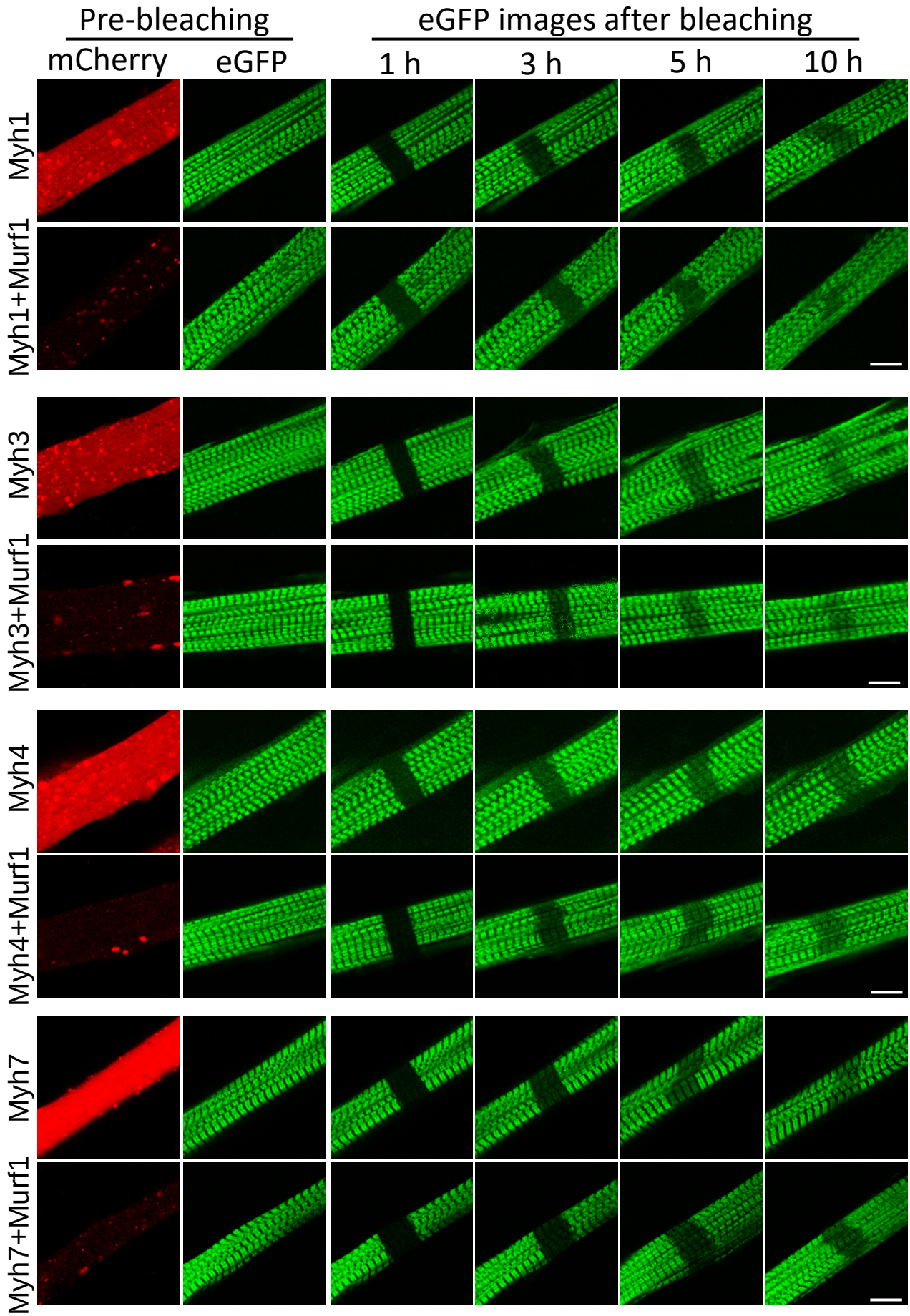

Fig. 13. Fluorescence images of eGFP in myotubes overexpressing mCherry-Murf1.
Representative FRAP images of myotubes co-expressing indicating eGFP tagged Myhs and either mCherry (control) or mCherry-Murf1. Images were obtained at 1 h intervals after photobleaching. Bar is 10 μm.

overexpressed mCherry-Murf1 while those of eGFP-Myh1 and eGFP-Myh7 were not significantly changed in myotubes overexpressing mCherry-Murf1 (Fig. 14 and 15). Mfs of Myh3 and Myh4 were significantly higher in myotubes overexpressing mCherry-Murf1 than control myotubes expressing mCherry (Fig. 15A). No significant change of $t_{1/2}$ was observed in all groups (Fig. 15B). These results suggest that the effects of Murf1 overexpressing on myosin replacement depend on the combination of Murf1 and Myh isoform. Although this result alone made it difficult to determine whether overexpression Murf1 was attributed to the direct or indirect effect on myosin replacement, this result showed that Murf1 was involved in myosin replacement.

2. Overexpressed Ozz localizes to the cytosol and does not alter the expression levels of eGFP-Myh3 and endogenous Ozz

Overexpression of Murf1 was partially enhanced Myh1 and Myh4 replacement rates, probably because of the broad targets of Murf1. We further investigated the effect of Myh3 associate ubiquitin E3 ligase (Campos et al., 2010), neuralized E3 ubiquitin-protein ligase 2 (Neurl2, or OZZ), on the Myh3 replacement. First, we tested whether exogenously expressed Ozz was localized to specific regions in the myofibrils. Cultured skeletal muscle cells were transfected with expression vectors encoding eGFP-Myh3 and mCherry-Ozz. Although exogenously expressed mCherry-Ozz was mainly distributed as puncta between myofibrils, the mCherry-Ozz puncta did not affect the structure of eGFP-positive thick filaments (Fig. 16A–F). The molecular weight of exogenously expressed mCherry-Ozz in myotubes was examined by immunoblot (Fig. 16G). The effect of exogenously overexpressed Ozz on the expression levels of endogenous Ozz and exogenous eGFP-Myh3 was examined by RT-qPCR. The results showed that the mRNA expression levels of endogenous Ozz did not differ significantly between the Ozz overexpressing

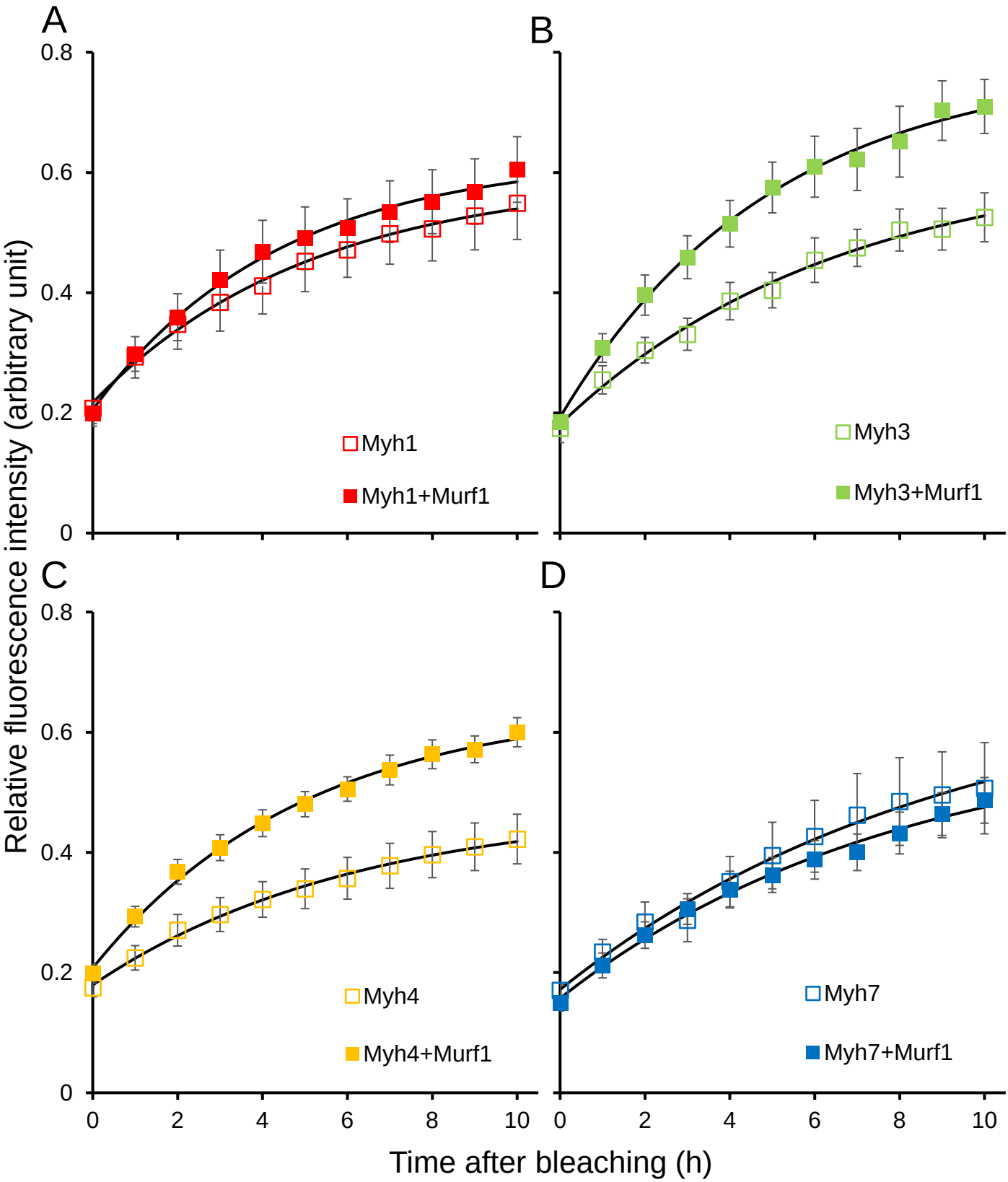

Fig. 14. Fluorescence recovery of eGFP-Myh1, -Myh3, -Myh4, or -Myh7 in myotubes expressing mCherry-Murf1. A-D. Normalized fluorescence intensities of eGFP were obtained from myotubes co-expressing indicating eGFP tagged Myh and mCherry (control) or mCherry-Ozz.Values represent the mean ± SE., Myh1, n = 9. Myh1+Murf1 n = 11. Myh3, n = 8. Myh3+Murf1, n = 7. Myh4, n = 12. Myh4+Murf1, n = 10. Myh7, n = 5. Myh7+Murf1, n = 12.

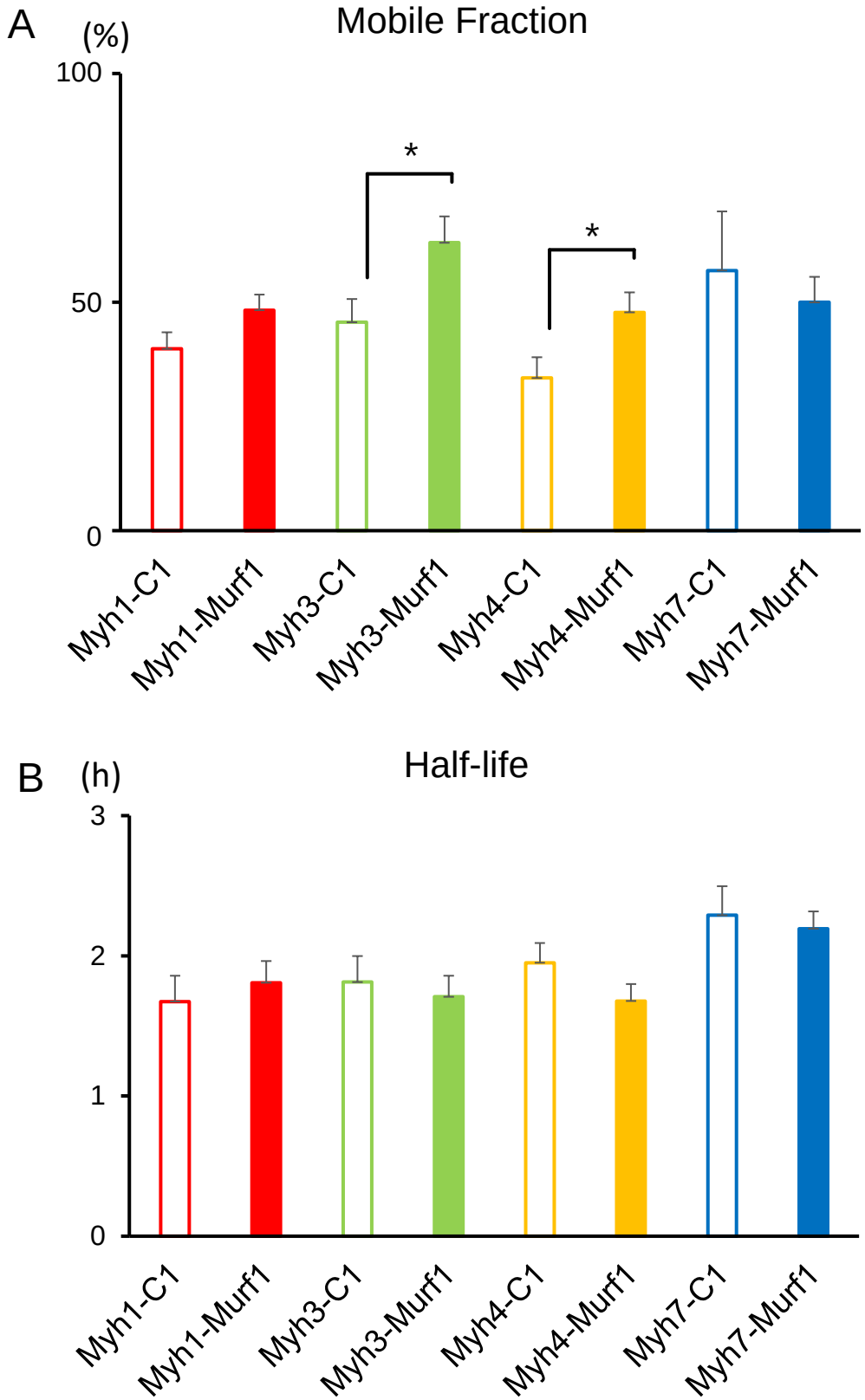

Fig. 15. Fluorescence recovery rate of eGFP-Myh1, -Myh3, -Myh4, or –Myh7 in myotubes expressing mCherry-Murf1.

A. Mobile fractions (%): 48.2% ± 3.5% in Myh1+Murf1 vs. 39.8% ± 3.6% in Myh1; 63.0% ± 5.8% in Myh3+Murf1 vs. 45.6% ± 5.1% in Myh3; 47.8% ± 4.3% in Myh4+Murf1 vs. 33.4% ± 4.5% in Myh4; 50.0% ± 5.6% in Myh7+Murf1 vs. 56.9% ± 13.0% in Myh7

B. Half-lives (h): 1.81 ± 0.16h in Myh1+Murf1 vs. 1.67 ± 0.18 h in Myh1; 1.71 ± 0.15 h in Myh3+Murf1 vs. 1.81 ± 0.19 h in Myh3; 1.67 ± 0.12 h in Myh4+Murf1 vs. 1.95 ± 0.14 h in Myh4; 2.19 ± 0.12 h% in Myh7+Murf1 vs. 2.29 ± 0.21 h in Myh7

Values represent the mean ± SE. Myh1, n = 9. Myh1+Murf1 n = 11. Myh3, n = 8. Myh3+Murf1, n = 7. Myh4, n = 12. Myh4+Murf1, n = 10. Myh7, n = 5. Myh7+Murf1, n = 12. $p > 0.05$

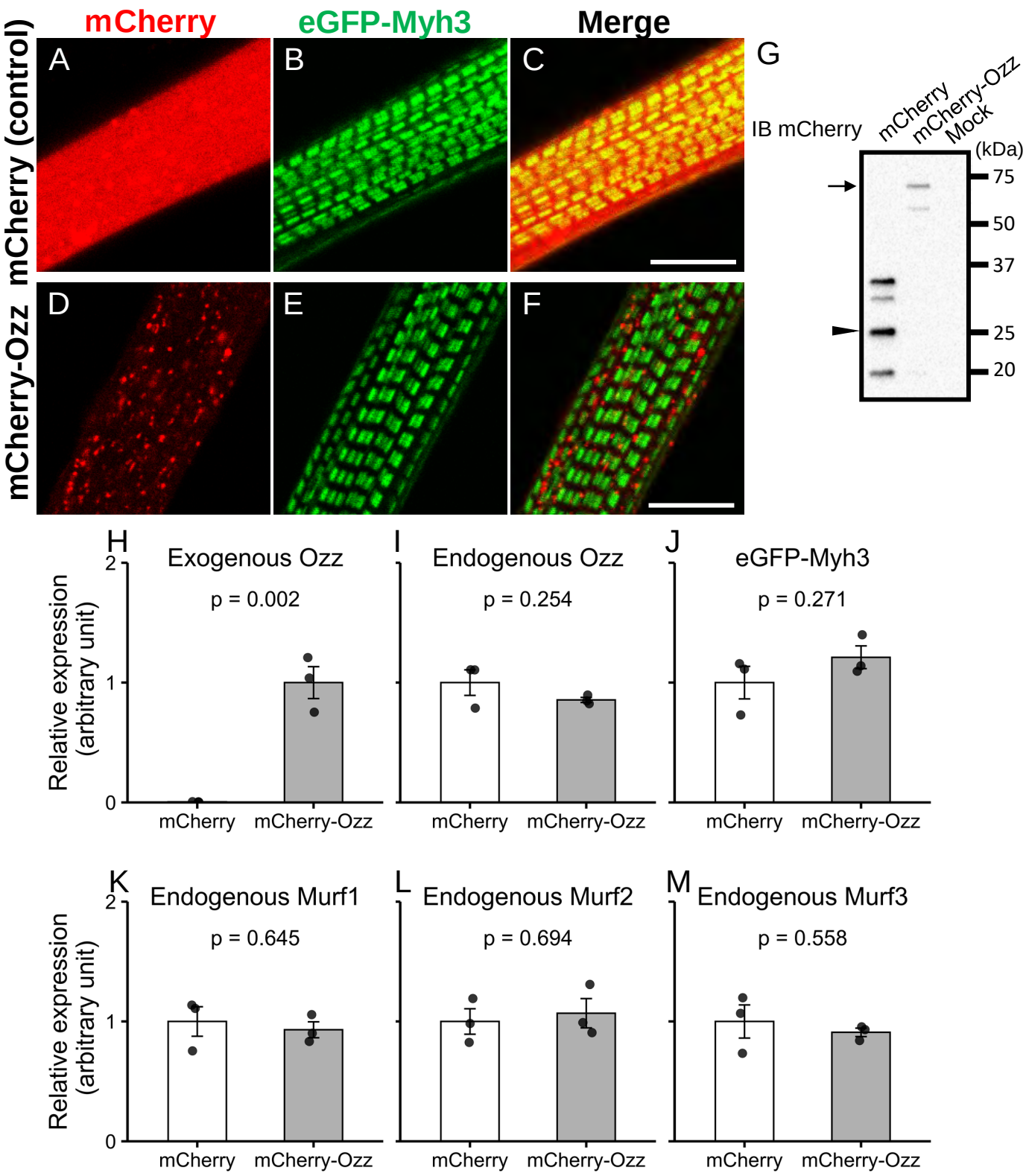

Fig.16. Localization and expression level of exogenously expressed mCherry-Ozz in muscle cells.

A–F. Localization of exogenously expressed eGFP-Myh3 and mCherry-Ozz observed by confocal microscopy. eGFP-Myh3 localized to the A-bands of myotubes (green). mCherry-Ozz was distributed as small puncta in myotubes (red in D and F). mCherry expressed alone as a control showed a diffuse distribution in myotubes (red in A and C). C and F are merged images of A and B, and D and E, respectively. Bars, 10 μm.

G. The expression of mCherry-Ozz and mCherry proteins in myotubes was detected by western blotting. An arrow and an arrowhead indicate the bands corresponding to mCherry-Ozz and mCherry, respectively.

H–M. The expression levels of mCherry-Ozz, endogenous Ozz, eGFP-Myh3 and endogenous Murf1~3 were quantified by RT-qPCR in myotubes co-expressing eGFP-Myh3 and either mCherry (control) or mCherry-Ozz. GAPDH was used as the internal control, and the relative expression levels were calculated as a ratio of the signal intensity of the target gene to the signal intensity of GAPDH. Fold change was normalized to the mCherry-Ozz group (H) or mCherry group (I-M). Values represent the mean ± SE. n = 3 for each group.

and the control groups (Fig. 16H–I), and eGFP-Myh3 was expressed at comparable levels in the two groups (Fig. 16J). Furthermore, Ozz overexpression did not change the expression levels of endogenous Murf family members (Fig. 16K–M). These results indicate that exogenously expressed mCherry-Ozz did not alter the expression levels of endogenous Ozz and Murf family, and exogenous eGFP-Myh.

3. mCherry-Ozz overexpression decreases the replacement rate of eGFP-Myh3

To examine effect of Ozz overexpression on eGFP-Myh3 replacement, myotubes co-expressing eGFP-Myh3 and mCherry-Ozz were analyzed using the FRAP assay. Changes in fluorescence intensity at the bleaching area were measured at 1 h intervals after fluorescence bleaching to determine the fluorescence recovery of eGFP-Myh3 in myotubes overexpressing mCherry or mCherry-Ozz (Fig. 17). The eGFP-Myh3 fluorescent recovery rate was lower in myotubes expressing mCherry-Ozz than in control myotubes, although the recovery time of eGFP-Myh3 did not differ significantly from that of the control (Fig. 18A–C). These results indicate that overexpression of Ozz decreased the eGFP-Myh3 replacement rate in myofibrils.

4. Ozz does not alter the replacement rate of eGFP-Myh1 and eGFP-Myh7

Because overexpression of Ozz decreased the replacement rate of eGFP-Myh3 (the embryonic myosin isoform), I tested the effects of Ozz on the replacement rates of other myosin isoforms such as Myh1 and Myh7. eGFP-Myh1 and eGFP-Myh7 were localized to the A-bands in myotubes overexpressing mCherry and mCherry-Ozz (Fig. 19 and 21). The results of the FRAP assays showed that the replacement rate of eGFP-Myh1 in myotubes co-expressing mCherry-Ozz did not differ significantly from that in control myotubes overexpressing mCherry (Fig. 20A–C).

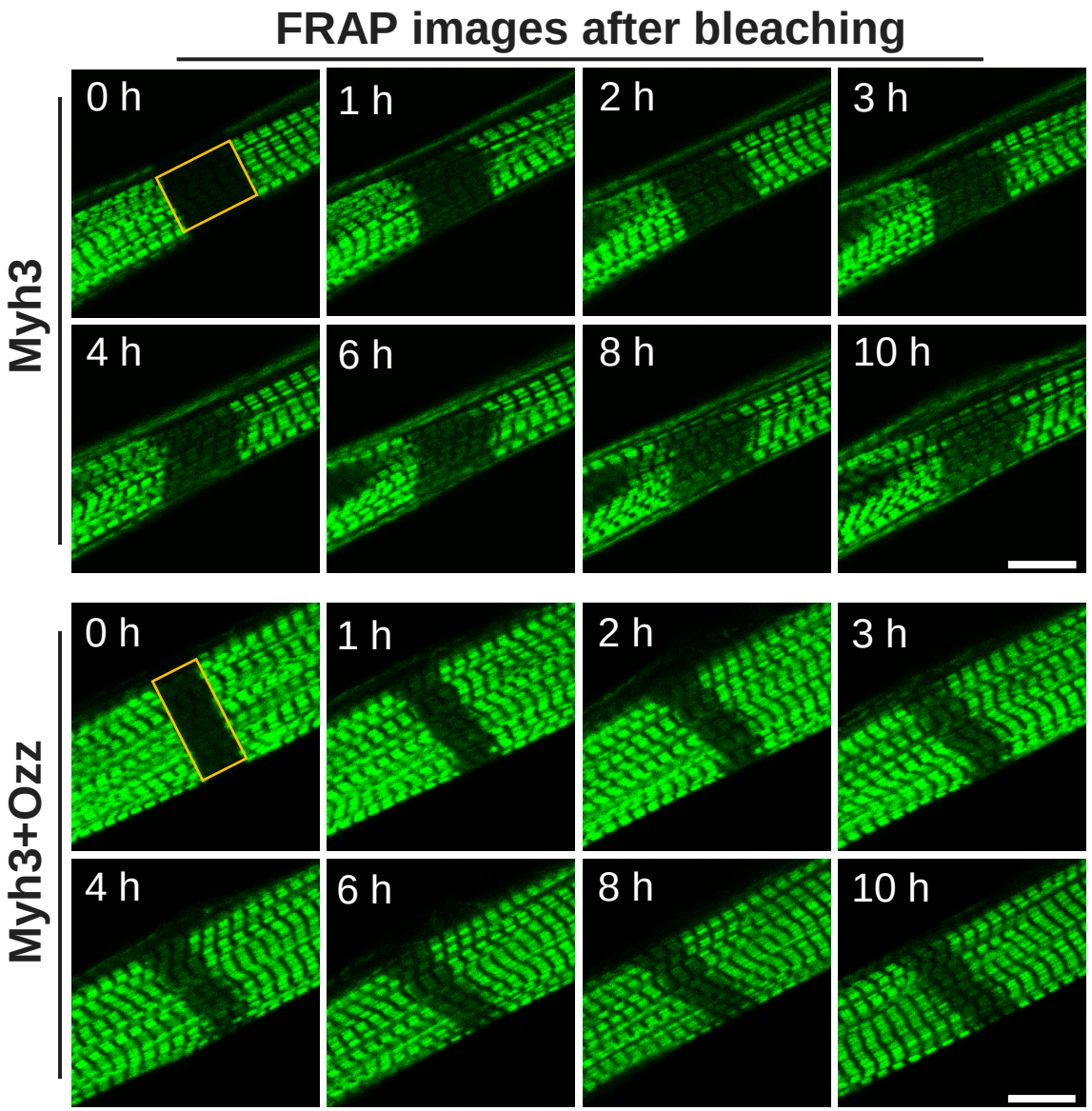

Fig. 17. Fluorescence images of eGFP-Myh3 in myotubes overexpressing mCherry-Ozz.
Representative FRAP images of myotubes co-expressing eGFP-Myh3 and either mCherry or mCherry-Ozz. Images were obtained at 1 h intervals after photobleaching. Bleached areas are indicated by yellow rectangles. Bar is 10 μm.

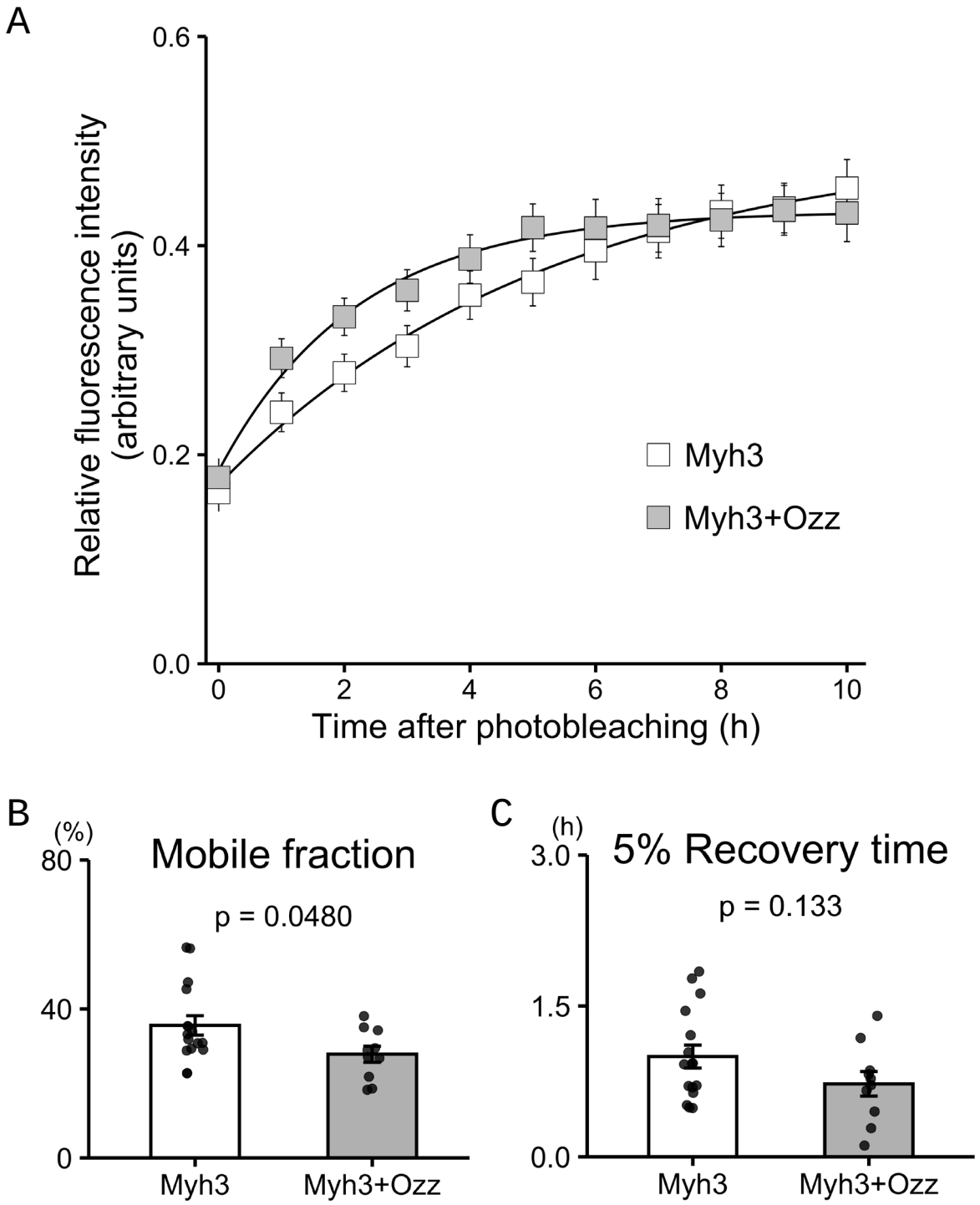

Fig. 18. Fluorescence recovery of eGFP-Myh3 in myotubes overexpressing mCherry-Ozz.
A. Normalized fluorescence intensities of eGFP-Myh3 were obtained from myotubes co-expressing eGFP-Myh3 and mCherry (control) or mCherry-Ozz.
B–C. Mobile fractions and 5% fluorescence recovery times were calculated from the graph as described in the Materials and Methods section. Mobile fraction (%): 27.8 ± 2.1% in Myh3+Ozz vs. 35.6% ± 2.6% in Myh3, 5% Rt (h): 0.73 ± 0.12 h in Myh3+Ozz vs. 0.99 ± 0.11 h in Myh3, Values represent the mean ± SE. Myh3, n = 16. Myh3+Ozz, n = 10.

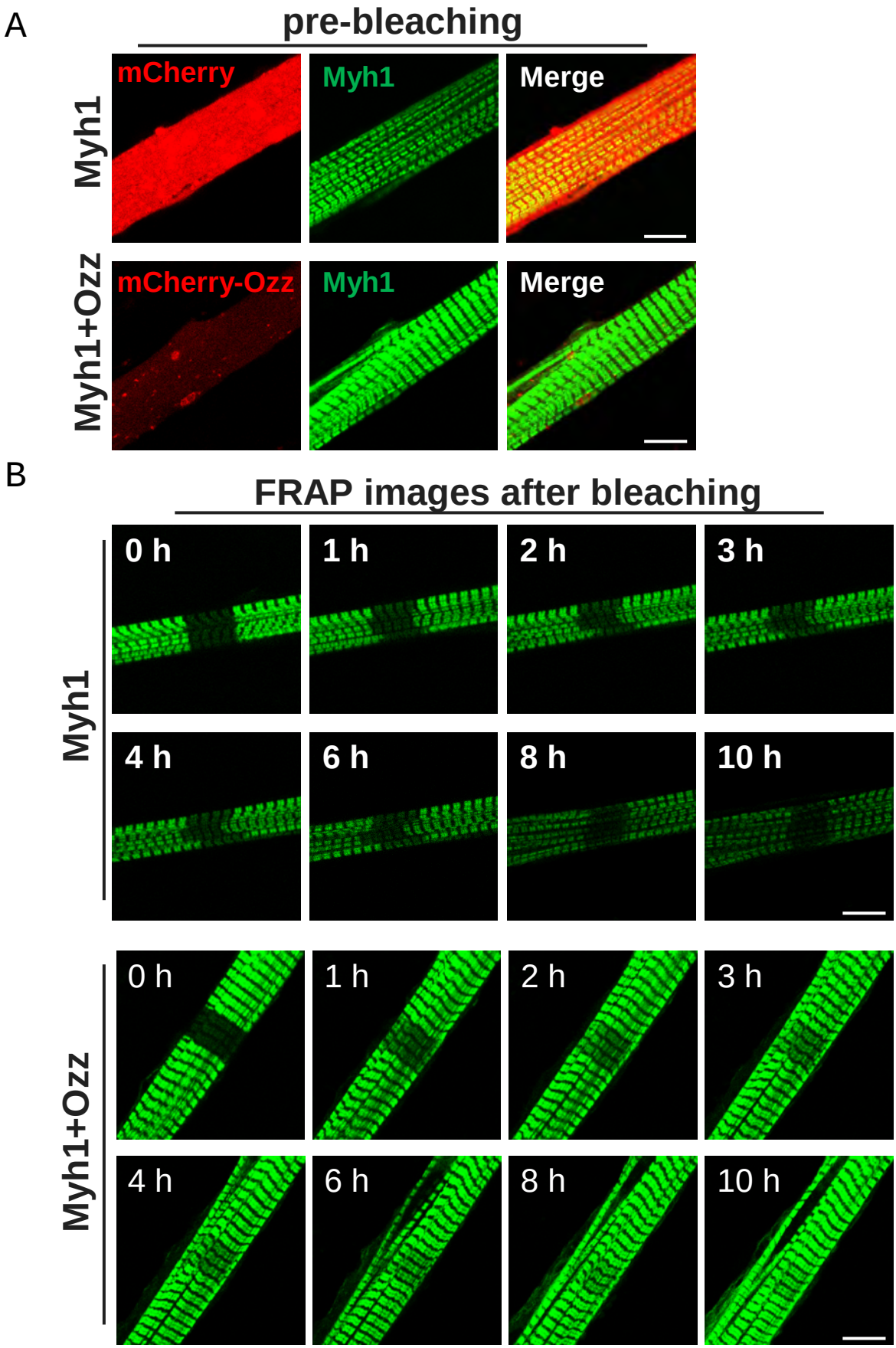

Fig. 19. Fluorescence images of eGFP-Myh1 in myotubes overexpressing mCherry-Ozz.
A. Localization of exogenously co-expressed eGFP-Myh1 and either mCherry or mCherry-Ozz. eGFP-Myh1 were localized to the A-bands of myotubes (green). mCherry and mCherry-Ozz was distributed diffusely or as small puncta in myotubes (red). Bars, 10 μm.
B. Representative FRAP images of myotubes co expressing eGFP-Myh1 and either mCherry or mCherry-Ozz. Images were obtained at 1 h intervals after photobleaching.

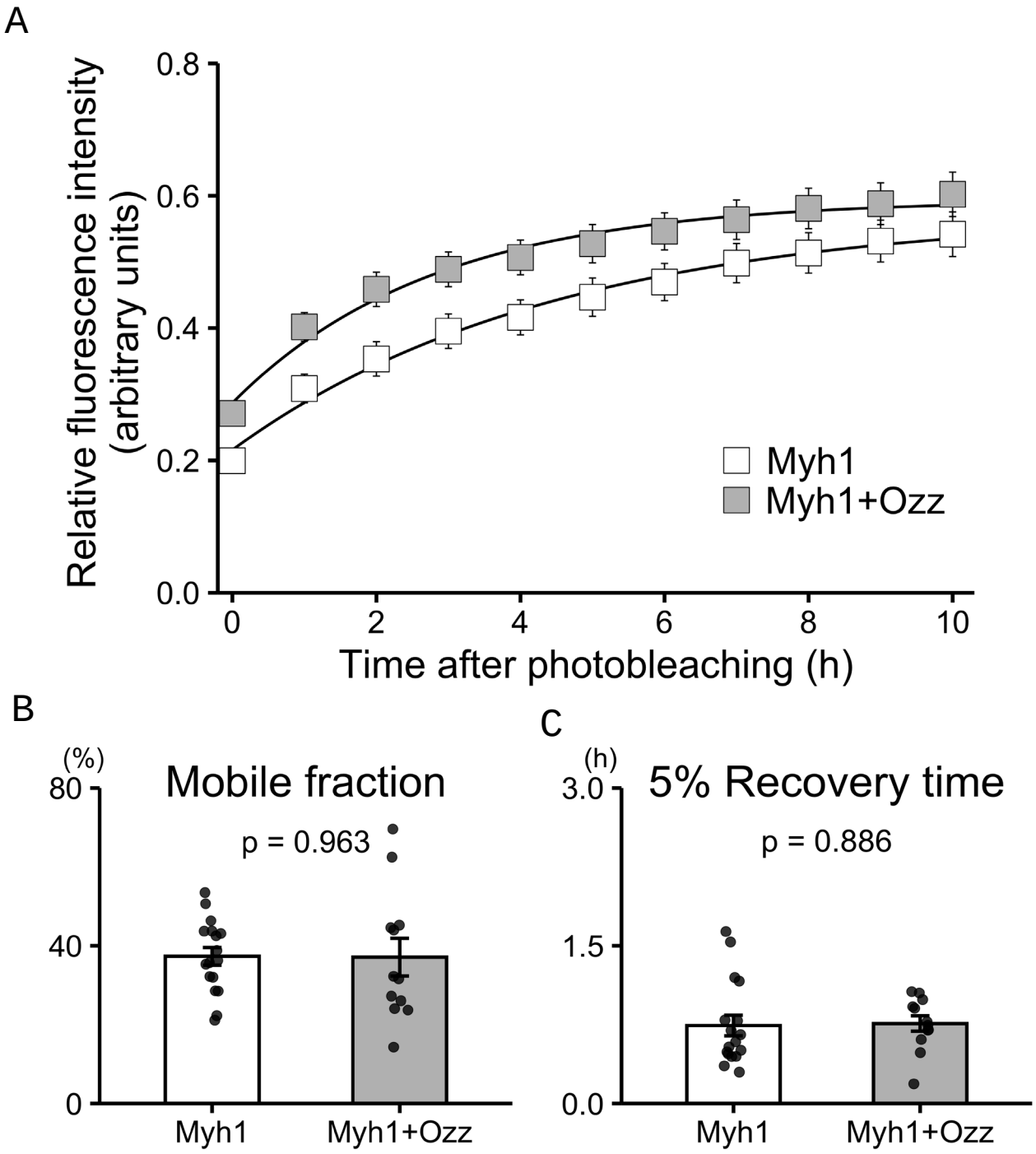

Fig. 20. Fluorescence recovery of eGFP-Myh1 in myotubes overexpressing mCherry-Ozz.
A. Fluorescence recovery of eGFP-Myh1 was measured in myotubes co-expressing mCherry-Ozz (grey squares) or mCherry (white squares).
B–C. Mobile fraction (%): 37.1 ± 4.8% in Myh1+Ozz vs. 37.3% ± 2.2% in Myh1, 5% Rt (h): 0.76 ± 0.07 h in Myh1+Ozz vs. 0.74 ± 0.10 h in Myh1, Data are expressed as the mean ± SE. Myh1, n = 17. Myh1+Ozz, n = 12

Similarly, Ozz overexpression did not decrease the replacement rate of eGFP-Myh7 in myotubes overexpressing mCherry-Ozz (Fig. 22A–C). These results indicate that overexpression of Ozz specifically reduced the replacement rate of eGFP-Myh3, whereas it did not affect that of eGFP-Myh1 and eGFP-Myh7.

5. Ozz induces myosin ubiquitination in myotubes.

Since Ozz functions as a Myh3-specific Ub ligase (Campos et al., 2010), I hypothesized that the Ozz-induced decrease in the myosin replacement rate was caused by the effect of Ozz overexpression on targeting eGFP-Myh3 for degradation. To address this, cultured muscle cells were separated into a cytosolic fraction and a myofibril fraction, and ubiquitinated myosin was detected by immunoprecipitation and immunoblotting in each fraction. Cells were treated with MG132 to detect ubiquitinated myosin, because ubiquitin bands were scarcely detected without MG132 treatment (Fig. 23A and C). In the cytosolic fraction, the relative signal intensity of ubiquitinated-Myh detected by immunoblotting was significantly higher in muscle cells overexpressing Ozz than in control muscle cells (Fig. 23A–B). In the myofibril fraction, the signal intensity of ubiquitinated-Myh was not different between Ozz overexpression and control groups (Fig. 23C–D). Intriguingly, the band intensities captured by anti-ubiquitin antibody were scarcely detectable in the myofibril fraction with MG132. These results indicate that overexpression of Ozz increased Myh ubiquitination and probably enhanced UPS-mediated degradation in the cytosol.

6. Ubiquitinated-Myh is abundant in the cytosolic fraction but not replaced in the thick filament

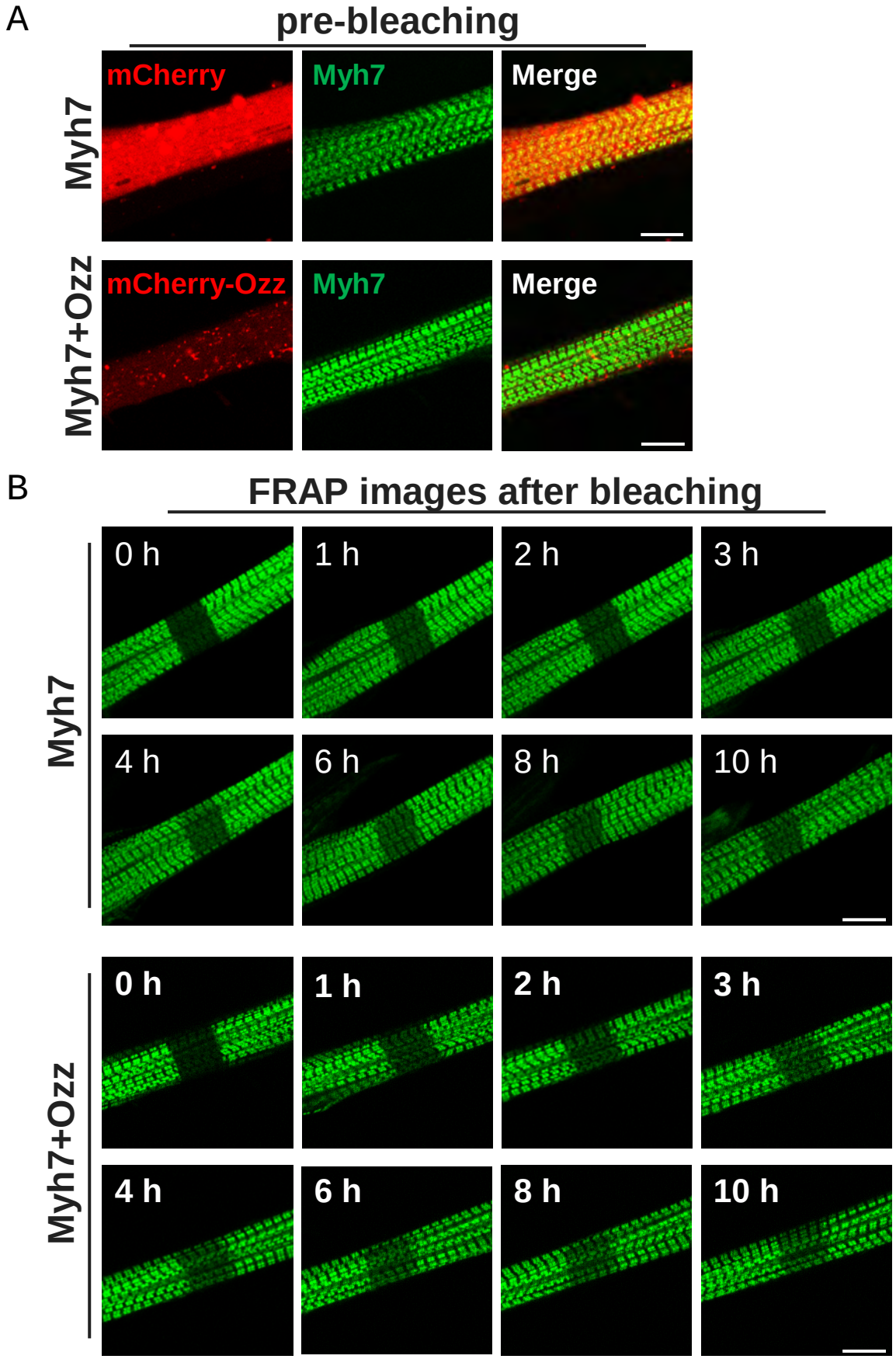

Fig. 21. Fluorescence images of eGFP-Myh7 in myotubes overexpressing mCherry-Ozz.
A. Localization of exogenously co-expressed eGFP-Myh7 and either mCherry or mCherry-Ozz. eGFP-Myh7 were localized to the A-bands of myotubes (green). mCherry and mCherry-Ozz was distributed diffusely or as small puncta in myotubes (red). Bars, 10 μm.
B. Representative FRAP images of myotubes co expressing eGFP-Myh7 and either mCherry or mCherry-Ozz. Images were obtained at 1 h intervals after photobleaching.

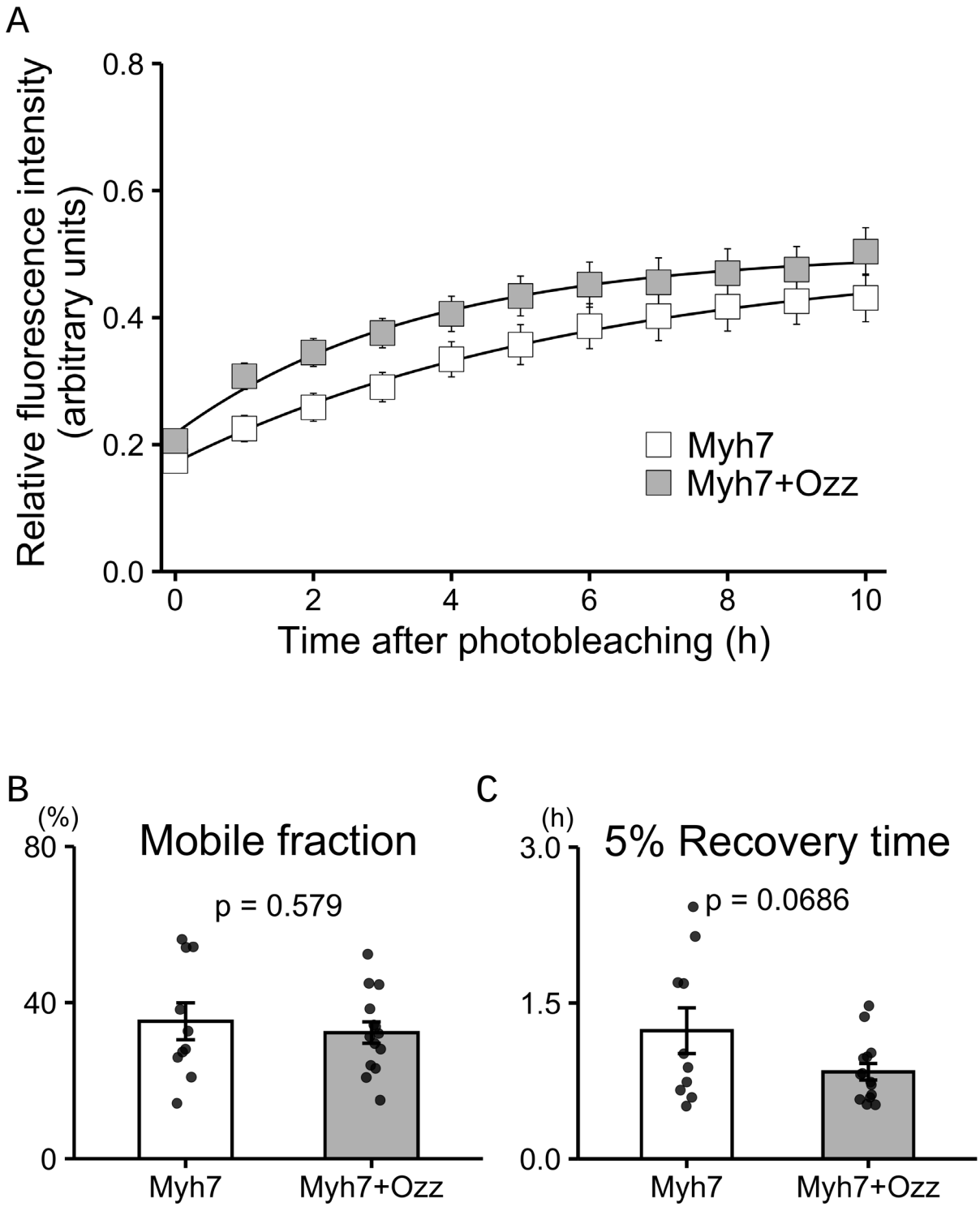

Fig. 22. Fluorescence recovery of eGFP-Myh7 in myotubes overexpressing mCherry-Ozz.
A. Fluorescence recovery of eGFP-Myh7 was measured in myotubes co-expressing mCherry-Ozz (grey squares) or mCherry (white squares).
B–C. Mobile fraction (%): 32.3 ± 2.7% in Myh7+Ozz vs. 35.2% ± 4.7% in Myh7, 5% Rt (h): 0.83 ± 0.08 h in Myh7+Ozz vs. 1.23 ± 0.22 h in Myh7, Data are expressed as the mean ± SE. Myh7, n = 10. Myh7+Ozz, n = 14

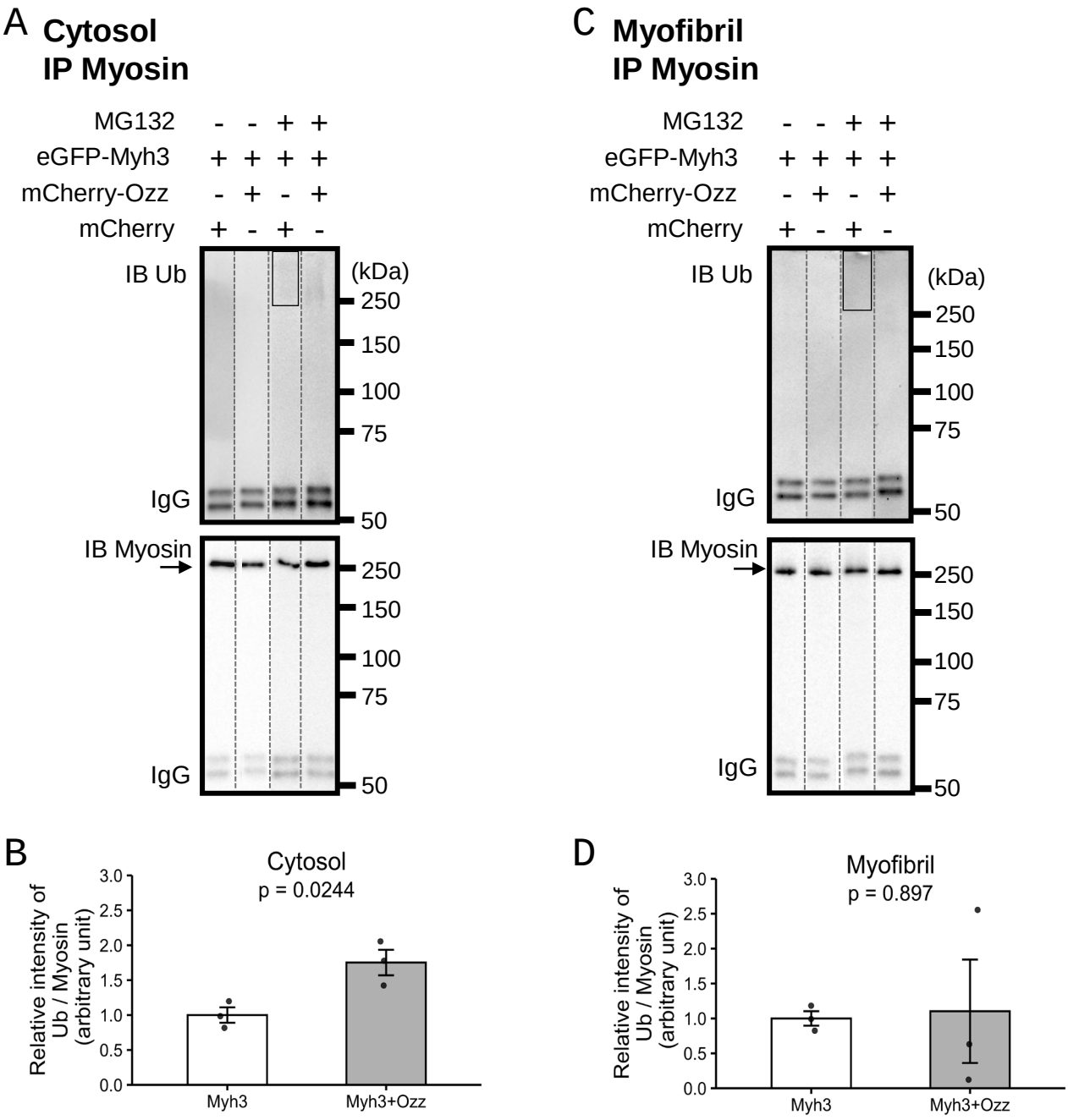

Fig. 23. Enhanced ubiquitination of Myh in muscle cells overexpressing mCherry-Ozz.
A, C. eGFP-Myh3 and mCherry or mCherry-Ozz were co-expressed in muscle cells treated with or without MG132. Cytosolic in A and myofibril in C fractions were obtained as 0.15 or 0.6 M TNE buffer soluble fractions. Samples were immunoprecipitated with anti-Myh antibody (MF20) and subjected to western blotting against anti-Myh or anti-ubiquitin antibody. Arrows indicate bands corresponding to Myh.
B, D. The band intensity of ubiquitinated Myh in MG132-treated samples was quantified in the area indicated by rectangles in A and C. Relative intensity of Ub-Myh to Myh was calculated as described in the Materials and methods section. Data are expressed as the mean ± SE. n = 3 for each group.

The results indicate that Ozz decreased the Myh3 replacement rate by promoting myosin degradation. Therefore, I explored the effect of inhibition of protein degradation on myosin replacement. Cultured muscle cells were treated with the proteasome inhibitor MG132, which does not inhibit ubiquitination but does inhibit protein degradation by UPS. MG132 treatment increased the level of ubiquitinated proteins in the cytosolic and myofibril fractions (Fig. 24A). To test the effect of inhibition of protein degradation on myosin replacement, myotubes expressing eGFP-Myh3 in the presence or absence of MG132 were analyzed using the FRAP assay. eGFP-Myh3 was detected in the thick filaments of myofibrils in myotubes treated with MG132, indicating that MG132 did not disrupt the myofibrils structure (Fig. 24B). FRAP assays revealed that the replacement rate of eGFP-Myh3 was significantly lower in MG132-treated myotubes than in the control group (Fig. 24C–E). These results suggest that ubiquitinated myosin is not frequently replaced in myofibrils in the presence of MG132. Next, the localization of ubiquitin in myotubes treated with or without MG132 was investigated. Ubiquitin was not detected in the thick filaments, but rather in the cytoplasm diffusely or as small puncta. Microscopic observation also supported the findings that ubiquitinated myosin was predominantly localized in the cytoplasm, which was proved by immunoblotting. These results suggest that ubiquitinated myosin is not the primary source for myosin substitution in the myofibrils (Fig. 24F).

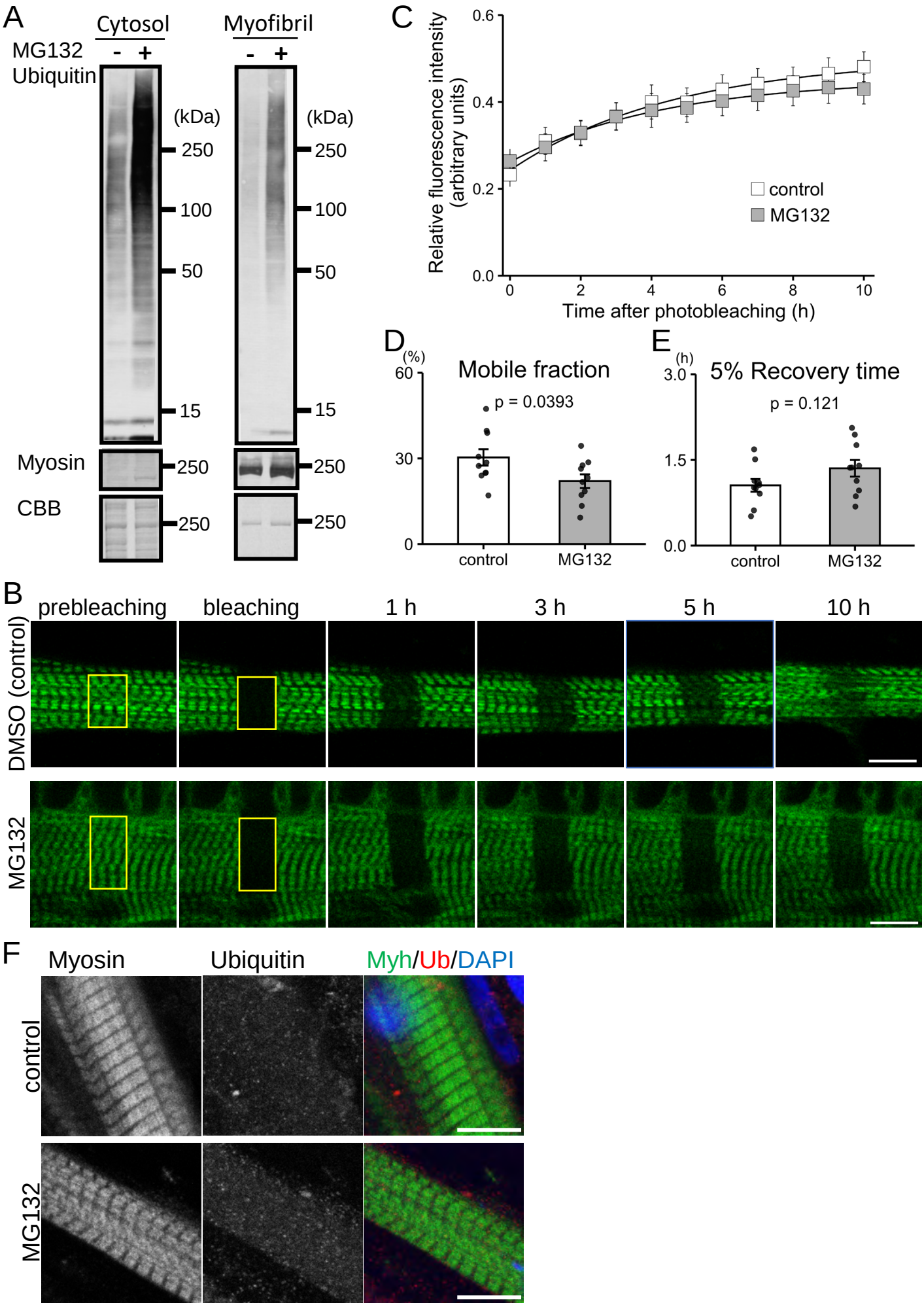
A
Cytosol
Myofibril
MG132
- + - +
Ubiquitin
(kDa)
250
100
50
15
Myosin
CBB
C
Relative fluorescence intensity (arbitrary units)
0.6
0.4
0.2
0.0
0 2 4 6 8 10
Time after photobleaching (h)
control
MG132
D
(%)
Mobile fraction
p = 0.0393
60
30
0
control
MG132
E
(h)
5% Recovery time
p = 0.121
3.0
1.5
0.0
control
MG132
B
prebleaching
bleaching
1 h
3 h
5 h
10 h
DMSO (control)
MG132
F
Myosin
Ubiquitin
Myh/Ub/DAPI
control
MG132

Fig. 24. Fluorescence recovery of GFP-Myh3 in myotubes treated with MG132.

A. Ubiquitinated proteins were detected by western blotting. Samples were obtained from muscle cells treated with or without MG132.

B. Representative FRAP images of in myotubes expressing eGFP-Myh3 in the presence of DMSO (control) or MG132. Images were obtained at 1 h intervals after photobleaching. Bleached areas are indicated by yellow rectangles.

C. Normalized fluorescence intensities of eGFP-Myh3 were obtained from DMSO (control) or MG132-treated myotubes.

D, E. Mobile fraction (%): 30.3 ± 2.9% in DMSO vs. 22.0% ± 2.4% in MG132, 5% Rt (h): 0.21 ± 0.04 h in DMSO vs. 1.35 ± 0.15 h in MG132, Data are expressed as the mean ± SE. n = 10 for each group.

F. Myotubes treated with or without MG132 were stained with anti-myosin antibody (green) and anti-ubiquitin antibody (red). Nuclei were visualized with DAPI. Bars, 10 μm.

Discussion

In this chapter, overexpression of Ozz decreased the Myh3 replacement rate in myotubes probably through promoting the ubiquitination and degradation of Myh3. MG132 treatment led to the accumulation of ubiquitinated-Myh in the cytosol rather than in the myofibrils of myotubes, suggesting that the myosin in myofibrils was not replaced by ubiquitinated myosin. Myosin in the cytosol is one of the main source for myosin replacement (Ojima et al., 2017). The decrease of replaceable myosin in the cytoplasm of myotubes caused by increased ubiquitination by Ozz and UPS-mediated degradation led to a low myosin replacement rate in myofibrils.

In the present study, Ozz overexpression specifically decreased eGFP-Myh3 replacement rate. Because Myh3 is a substrate of the E3 ligase Ozz (Campos et al., 2010), I hypothesized that Ozz overexpression promoted the ubiquitination and proteasomal degradation of eGFP-Myh3. The increased degradation rate of Myh3 may have limited the supply of Myh3 for myosin substitution, thereby decreasing the eGFP-Myh3 replacement rate. This hypothesis was supported by the results showing that Ozz overexpression increased myosin ubiquitination in the cytosol, and not in the myofibrils (Fig. 23). The finding that overexpressed mCherry-Ozz did not localize to the myofibrils suggests that Ozz promotes the degradation of myosin in the soluble cytosolic fraction rather than in the myofibril. This is similar to other E3s such as Murfs (Cohen et al., 2009; Solomon & Goldberg, 1996), which capture myosin in the soluble cytosolic fraction of skeletal muscle cells. In addition, Ozz may target impaired or expendable myosin for degradation in the cytosolic fraction rather than in the myofibrils. It is unlikely that Ozz captures impaired or expendable myosins in the thick filaments because Ozz interacts with myosin through the assembly competence domain of Myh3 (1873–1901 aar) (Campos et al., 2010), which is essential for the formation of thick filaments and is concealed in the thick filament (Sohn et al., 1997). Therefore, interaction with Ozz may interfere with the incorporation of the Myh-Ozz complex

into thick filaments, leading a decrease in the myosin replacement rate in myotubes overexpressing Ozz.

Another possible explanation for the reduction in Myh3 replacement rate in myotubes overexpressing Ozz and myotubes treated with MG132 is that ubiquitination of Myh3 changes its biochemical properties. Ubiquitination is a post-translational modification (Passmore & Barford, 2004) that functions not only as a tag for degradation, but also as a modification factor for protein solubility (Dao et al., 2018; Sharkey et al., 2018). Biochemical studies demonstrated that in the presence of MG132, ubiquitinated myosin accumulated in the cytosol rather than in myofibrils. Furthermore, immunofluorescence studies showed that ubiquitin did not colocalize with myosin in thick filaments but was distributed diffusely in the cytosol (Fig. 24F). The modification of myosin with ubiquitin may increase its solubility to prevent the formation of aggregates, which form under physiological ionic conditions (Davis, 1988). Although MG132-treated myotubes contained ubiquitinated myosin in the cytosol, the myosin replacement rate was slow. Thus, it is likely that ubiquitinated myosin in the cytosol is not replaceable in the thick filaments. Moreover, ubiquitinated myosin scarcely accumulated in the absence of MG132 in both the cytosolic and myofibril fraction, suggesting that ubiquitinated myosin is immediately disassembled (Fig. 23A and C). The increase in myosin solubility caused by ubiquitination may improve the degradation efficiency by suppressing myosin insertion into myofibrils. Taken together, these observations indicate that ubiquitinated myosin tends to stay in the cytosol rather than being incorporated into thick filaments.

The myosin replacement rates differed between slow and fast myosins, *i.e.*, eGFP-Myh7 showed the slowest myosin replacement speed (5% Rt 1.23 ± 0.22 h) among 3 myosin isoforms (0.74 ± 0.10 h in eGFP-Myh1, and 1.00 h ± 0.11 h in eGFP-Myh3) and replacement speed is statistically different between Myh1 and Myh7 (Fig. 19–22). Because the intracellular

environment was identical in myotubes expressing eGFP-Myh7, eGFP-Myh1, or eGFP-Myh3, these results suggest that differences in the replacement rate were caused by the intrinsic properties of the different myosin isoforms. The amino acid sequence homology of the myosin isoforms is relatively high: Myh7 and Myh1, 81.9%. However, amino acid sequence variations are found in the tail region of Myhs, which play pivotal role in myosin filament assembly. Because amino acid composition determines the myosin axial arrangement (Atkinson & Stewart, 1992; Sohn et al., 1997), differences in the composition of the tail among myosin isoforms may change the assembly properties of myosin.

The effect of overexpression of Murf1 on the myosin replacement was different depending on the co-expressed Myh isoform (Fig. 14–16). It is possible that the different isoforms of myosin are differentially regulated by the UPS. The Murf family (Murf1, Murf2, and Murf3) of muscle-specific ubiquitin ligases is myosin-associated protein (Cohen et al., 2009; Fielitz et al., 2007; Pizon et al., 2002). Murfs work cooperatively, and double knockout of Murf1 and Murf3 or Murf2 and Murf3 in mice causes myosin aggregation and myopathy (Fielitz et al., 2007; Lodka et al., 2016). However, Murf expression is muscle type-specific in vivo: Murf1 is predominantly expressed in slow type myofibers, Murf2 is expressed in fast type myofibers, and Murf3 is expressed ubiquitously (Moriscot et al., 2010; Perera et al., 2012). Murfs may preferentially recognize specific myosin isoforms, which may affect the myosin replacement rate.

A model of myosin replacement in the presence of Ozz overexpression was proposed (Fig. 25). Overexpression of Ozz increases Myh3 ubiquitination and probably degradation, which decreases the eGFP-Myh3 replacement rate. In the differentiation stage and during muscle remodeling, Myh in thick filaments shifts from the embryonic to the adult isoform (Stefano Schiaffino et al., 2015). The upregulation of Ozz during muscle differentiation (Nastasi et al., 2004) results in the selective degradation of ubiquitinated Myh3, which promotes an isoform shift

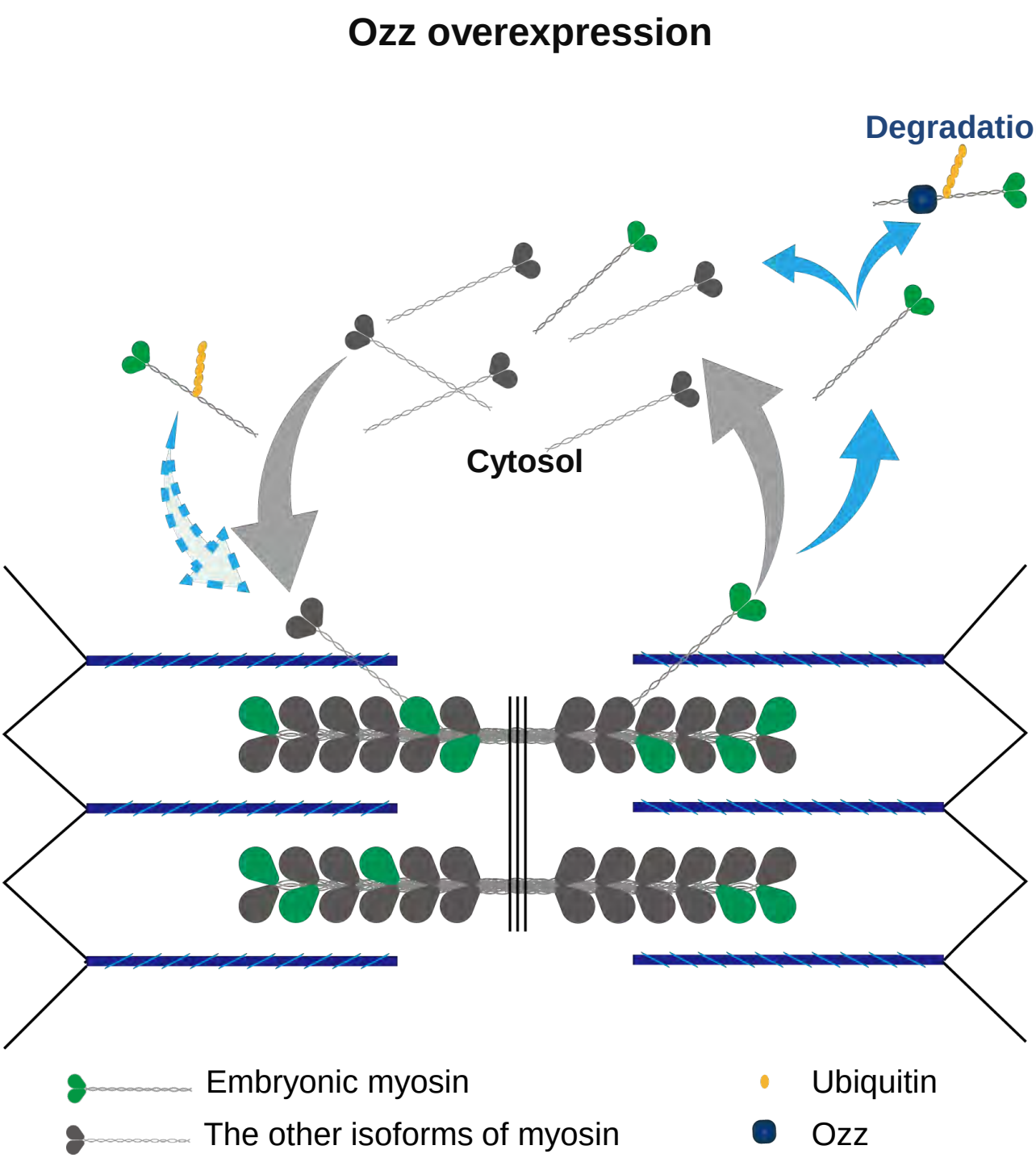

Fig. 25. A model of myosin replacement in the presence of overexpressed Ozz.
Ozz overexpression in myotubes promotes ubiquitination and degradation of embryonic myosin (Myh3) in the cytosol, and/or addition of ubiquitin chain to Myh3 decrease the insertion of Myh3 into thick filaments. Replacement rates of the other myosin isoforms are not affected by Ozz overexpression. Blue and grey arrows indicate flows of embryonic and the other myosin isoforms, respectively.

from embryonic myosin to neonatal/adult myosins (Campos et al., 2010). Therefore, Ozz may regulate the myosin replacement rate by catalyzing the modification of Myh3 to ensure an efficient myosin isoform shift in thick filaments.

Chapter 3

Introduction

Skeletal muscle is classified into two categories according to muscle contraction velocity, *i.e.*, slow and fast types. This feature is attributed to the expression of myosin heavy chain (Myh) isoforms with different rates of ATPase activity and muscle contraction velocity in each myofiber (Resnicow et al., 2010; Walklate et al., 2016). Myh4 has the highest ATPase activity, followed by Myh1, Myh2, and Myh7 (He et al., 2000; Resnicow et al., 2010). Fast muscle contraction velocity is also arranged in the following order, Myh4, Myh1, Myh2, and Myh7 (Galler et al., 1997), whereas contraction velocity is influenced by the combination of Myh isoforms and light chain isoforms (Reggiani et al., 2000). The muscle fiber type was determined based on the property as a motor protein, *i.e.*, fast myofibers express one or a combination of Myh1, Myh2, and Myh4, whereas slow myofibers express Myh7. Interestingly, Myh4 is expressed explicitly in rodents but not in large animals such as human, bovine (Chikuni et al., 2004; Stefano Schiaffino & Reggiani, 2011). Although slow and fast types of Myhs are dominantly expressed in adult skeletal muscles, other Myh isoforms such as embryonic (Myh3) and neonatal (Myh8) types are expressed during muscle development. Fast type of Myhs gradually becomes predominant a few days after birth in mice, which causes the downregulation of Myh3 and Myh8, induced by the downregulation of Myh3 and Myh8 (Stefano Schiaffino et al., 2015).

Myofibers have not different velocity properties but also different metabolic properties among myofiber types. Slow type fibers have many mitochondria, high oxidative energy production and high fatigue resistance (Hoppeler & Billeter, 1991). On the other hand, fast-type fibers with low oxidizing capacity anaerobically produce energy (S Schiaffino & Reggiani, 2011). In protein metabolism, the capacity of protein synthesis and degradation activity is relatively high

in slow-type fibers. Nuclear density and total RNA are higher in slow fibers than in fast fibers (Habets et al., 1999). In addition, slow fibers have higher levels of E3 ligase expression per tissue weight than fast fibers (Van Wessel et al., 2010). These imply that slow fibers are more capable of protein turnover than fast fibers, and the intercellular environment depends on the type of fiber.

In chapter 2, it was shown that the myosin replacement pattern was different between Myh1 and Myh7 (Fig. 19–22) though expressing these isoforms same environment. These results suggest that the myosin replacement rate was controlled not myofiber environment described above but also by the potential of myosin own. Then, I focused on post-translation modification (PTM), which is controls protein stability, protein interaction, translocation, and activity (Biggar & Li, 2015; Huang & Zhang, 2020; Narita et al., 2019; X. Zhang et al., 2015). Ub described in chapter 2 is one of the ubiquitous PTM (Avram & Aaron, 1998). In addition, phosphorylation, methylation, acetylation, glycosylation, and lipidation are known to be frequently observed as protein modification (Blom et al., 2004; Humphrey et al., 2015; Mejuch & Waldmann, 2016; Narita et al., 2019; X. Zhang et al., 2015). Previous studies have shown that myosin acetylation and arginylation affect the contractile ability of myosin (Cornachione et al., 2014; Samant et al., 2015). In this study, I hypothesized that myosin replacement is adjusted by modification with different amino acids or different modification types. To test this possibility, it was investigated (1) whether myosin replacement differs between Myh1 and Myh7 expressing the same myotubes, (2) myosin modified PMT in vivo and modification is different among isoforms, ages, or fractions, and (3) whether the position of modification differs between Myh1 and Myh7.

Material and Methods

1. Experimental animals

All experiments were performed using mouse muscle or primary muscle cells from chick embryos. Experimental animals were reared for as outlined in the guidelines of Hokkaido University.

2. Cell culture and transfection

Skeletal muscle cells were isolated from the pectoral muscles of 11-day-old chick embryos as described above. One day after seeding, the cells were transfected with expression vectors using Lipofectamine® LTX and Plus reagents (Thermo Fisher Scientific). The DM was replaced every 2 days. Once myotubes were formed, 10 μM cytosine arabinoside (Tokyo Chemical Industry) was added to the medium to remove mitotic non-muscle cells.

Satellite cells were isolated from the hindlimb of mice expressing eGFP-Myh7 or KusabiraOrange tagged Myh1 (KuO-Myh1) instead of expressing wild-type Myh7 or Myh1 (KuO-Myh1 mouse and GFP-Myh7 mouse). Isolated satellite cells were passaged several times and seeded on 60 mm dishes coated with collagen Type I-A. These mouse muscle cells were cultured in the growth medium [20% (v/v) fetal bovine serum (Thermo Fisher Scientific), 1% (v/v) penicillin-streptomycin-glutamine ×100 (Thermo Fisher Scientific), and 2.5 ng/ml human FGF-2 (R&D Systems) in Hams F-10 Nutrient Mixture (Thermo Fisher Scientific)] until 80% confluent. After shifting from the growth medium to the differentiation medium [5% (v/v) horse serum (Thermo Fisher Scientific), and 1% (v/v) penicillin-streptomycin-glutamine ×100 in Dulbeccos Modified Eagle Medium (Thermo Fisher Scientific)], the medium was changed every two days.

3. cDNA constructs

Mouse cDNAs for *Myh1* (85–5913 in NM_030679), *Myh3* (45–5868 in NM_001099635), *Myh4* (111–5930 in NM_010855), and *Myh7* (142–5949 in NM_080728) were cloned into the peGFP-C1 vector (TAKARA BIO) or the monomeric pKuO-C1 vector (Medical & Biological Laboratories Co., Ltd., Nagoya, Japan). The inserted sequences of all constructs were verified with a 3730 DNA Analyzer (Applied Biosystems)

4. Fluorescence recovery after photobleaching (FRAP) assay

The FRAP assay was performed using transfected myotubes cultured on glass-based dishes (IWAKI) with a Leica TCS SP5 (Leica microsystem) as described above. Cells were incubated at 37°C and 5% CO_2 on the microscope incubation system (TokaiHit) during FRAP experiments. The emission wavelengths of eGFP and KuO were 488 and 543 nm, respectively, and band-pass filters were 500–540 nm and 550–650 nm. The fluorescence of the region of interest (ROI), 100 μm^2 in each cell, was bleached by exposure to laser emission length 488 and 543 nm at a strength of 100% for 90 sec. Fluorescence recovery was monitored every hour after photobleaching. The fluorescence intensity of the ROI was quantified and normalized to that of the non-bleaching area at each time point. The normalized fluorescence intensities were used in the following exponential curve fitting formula calculated by ImageJ 1.52a software:

$FI=Mf*(1-e^{(-b*t)}) +c$, where FI is the normalized fluorescence intensity, Mf is the mobile fraction, b is the speed constant, c is the fluorescence intensity after bleaching, and t is the elapsed time after beaching. Mf and 5%Rt were calculated from recovery curve to use for the parameter of fluorescence recovery rate.

5. Fractionation of muscle tissues

Muscle tissue was obtained from eGFP-Myh7 and KuO-Myh1 instead of expressing wild-type Myh7 and Myh1 (hybrid mouse)(Oe et al., 2021). Tibialis anterior (TA) and soleus (SOL) muscles were isolated from 1-, 2–3-, 12-, or 24-months old mouse. These dissected muscles were frozen in liquid nitrogen immediately after excision and stored at -80℃ until the next process. Following slicing frozen muscles using microtome at 30 μn thickness, muscles were homogenized by 27G syringe in 0.15M TNE buffer [10 mM Tris-HCl pH 7.6, 150 mM CsCl, 1 mM EDTA Cs, 0.5% (v/v) Triton X-100, 0.1% (w/v) sodium dodecyl sulfate, 2% protease inhibitor cocktail (Sigma-Aldrich), 0.06 mM leupeptin (Peptide Institute), 0.7 μM calpastatin (Takara Bio), 25 μM MG132 (Peptide Institute), 2% phosphatase inhibitor cocktail (ab201112, Sigma-Aldrich)] and rotated at 4℃ for 15 min. After centrifugation at 20,000g for 20 min, the supernatant was obtained as a 0.15M soluble fraction. Remained precipitations were re-suspended in 9M Urea Buffer [9M Urea, 2% (v/v) Triton X-100, and 1% (w/v) Dithiothreitol] as a myofibril fraction. Obtained each fraction sample was boiled for 5 min with Laemmli sample buffer.

6. Fractionation of mouse muscle cells

eGFP-Myh1 mouse cells and KuO-Myh7 mouse cells were sampled after 1–5 days muscle differentiation. Cells were immersed with modified chemical skinned buffer [10 mM Tris-HCl pH 7.6, 150 mM CsCl, 1 mM EDTA Cs, 0.5% (v/v) Triton X-100, 0.1% (w/v) sodium dodecyl sulfate, 2% protease inhibitor cocktail, 0.06 mM leupeptin, 0.7 μM calpastatin, and 25 μM MG132, 2% phosphatase inhibitor cocktail] for 30 min at 4℃. Solubilized fractions were centrifuged at 1,500g for 5 min. The supernatant was further centrifuged at 20,000g for 20 min to obtain the cytosolic fraction. Precipitation fraction was prepared from myotubes with modified

chemical skinned buffer. Samples were homogenized with 27 G syringes and boiled for 5 min with Laemmli sample buffer.

7. Western blotting (WB)

Samples were subjected to sodium dodecyl sulfate-polyacrylamide gel electrophoresis (SDS-PAGE) followed by transfer to PVDF membranes (Merck). The membranes were blocked with 5% (w/v) skim milk (FUJIFILM Wako Pure Chemical Corporation) at room temperature for 30 min and then incubated at 4℃ for 16 h with one of the following antibodies: mouse anti-myosin heavy chain (1:1,000; clone MF20, R&D Systems), rabbit anti-Ubiquitin (1:1,000, ab19247, abcam, Tokyo, Japan), rabbit anti-di-Methyl lysine motif (1:1,000; #14117, Cell Signaling Technology, Tokyo, Japan), rabbit anti-tri-Methyl lysine Motif (1:1,000; #14680, Cell Signaling Technology), rabbit anti-lysine Acetylated (1:1,000, #600-401-939, Rockland), rabbit anti-L-Lactyl lysine antibody (1:1,000; # PTM-1401, PTM Biolabs, IL Chicago, USA), rat anti-GFP (1:1,000; clone GF090R, Nacalai Tesque), rabbit anti-Kusabira Orange (1:1,000; clone 3B3, Medical & biological laboratories). Membranes were incubated with one of the following peroxidase-conjugated secondary antibodies: anti-mouse (1:1,000; #315-036-003, Jackson Immuno Research, PA West Grove, USA), anti-rabbit (1:1,000; #111-036-003, Jackson Immuno Research). Bands were visualized with ECL Western Blotting Detection Reagents (GE HealthCare). The membranes were stained with Coomassie Brilliant Blue R250 (CBB-R) after ECL visualization. Antibodies used in this study were listed in Table 2. For band quantification, signal intensities of bands were analyzed by ImageJ 1.52a (National Institutes of Health). The ratios of modified myosin band intensity to Myh band intensity were calculated as follows: (the signal intensity of modified band) / (the signal intensity of Myh band in membrane stained by CBB-R). The ratios were normalized with values of 2–3-month-old mice.

8. In gel digestion

The muscle and the cultured cell samples were subjected to SDS-PAGE and gels were stained with CBB-R. Bands corresponding to eGFP-Myh7 or KuO-Myh1 were cut into 2–3 blocks. The gel samples were stored at -80℃ until in-gel digestion. The gels were washed with water 1 time and with washing solution [25 mM NH_3HCO_3 in 50% (v/v) acetonitrile] for 2 times to distain CBB-R. Then, gels were incubated with 100% acetonitrile for 5 min. After removing acetonitrile, 0.1 M NH_3HCO_3 was added to the tubes. Additionally, an equal volume of 100% acetonitrile was added to the tube. After incubation for 15 min at RT, the acetonitrile solution was removed, and gels were dried with a vacuum centrifugal concentrator. Each specimen was reduced with 10 mM DTT and 0.1 M NH_3HCO_3 for 45 min at 56℃, sulfenilated with 55 mM iodoacetamide in 0.1M NH_3HCO_3 for 30 min room temperature and treated with trypsin 10 μg/ml trypsin (Promega, Madison, WI, USA) in 0.1 M NH_3HCO_3 for 20 h at 37℃. Trypsinized samples were extracted with 25 mM NH_3HCO_3 in 50% (v/v) acetonitrile. Samples were concentrated with a vacuum centrifugal concentrator.

9. LC-MS/MS analysis

The samples were analyzed using liquid chromatography-tandem mass spectrometry. The peptide samples applied to the capillary column (EASY-Spray column, Thermo Fisher Scientific) in EASY-nLC1000 system (Thermo Fisher Scientific). For peptide separation, samples were flowed at 300 nl/min and eluted with buffer B [0.1% (v/v) formic acid in acetonitrile] gradually diluted at rage 0% to 100% in buffer A [0.1% (v/v) formic acid in water]. Separated and eluted peptides were ionized and analyzed with LTQ Orbitrap Velos (Thermo Fisher Scientific). Mass analyzer scanned peaks over the range 350–1500 m/z with a resolution of 15,000.

10. MS analysis

The obtained mass data was analyzed by Masscot Server version:2.7 (MATRIX SCIENCE, London, UK). For mass spectra search, monomethyl, dimethyl, and trimethyl were selected as variable modifications. The modification rate was calculated using the identified peptide list. First, peptides identified as associated with modification were listed and their positions in mouse Myh1 and Myh7 were examined to identify modification sites. Subsequently, modification sites satisfying the following conditions were selected for statistical analysis; ones that the same location was identified in more than half of the samples with or without modification, and ones that multiple samples had the same modification at the site. The modification rate at a particular position per peptide sample was calculated as follows: (Abundance of precursors of peptides with the desired modification) / (Abundance of precursors of all peptides including the site of interest)

11. Statistics

All data are expressed as the mean ± standard error (SE). Student's *t-test* was used to compare differences between two groups. The Tukey test was used for multiple comparisons. Statistical significance was set at $p < 0.05$. Student's *t-test* and Tukey test were performed using EZR on R commander ver. 1.54. Uniform manifold approximation and projection (UMAP) analysis was conducted with Collaboratory (Google LLC).

Results

1. The different replacement rate of Myh1 and Myh7 is observed in identical myotubes

Myosin replacement rates of each isoform were examined in different myotubes in Chapters 1 and 2. The next question was how the intracellular environment was involved in the myosin replacement. To address this, different myosin isoforms were forced to be simultaneously expressed in identical myotubes, *i.e.*, eGFP-Myh7 and KuO-Myh1 were expressed in identical myotubes. Exogenously expressed Myh1 and Myh7 were incorporated into the myofibrils (Fig. 26 and 28A). The fluorescence recovery rates of GFP tagged Myh1 and Myh7 were not different from KuO tagged those despite different fluorescence protein tags, indicating that replacement rates of myosin isoform were not affected by the types of fluorescence protein tags (Fig. 27B, C, E, and F). Subsequently, fluorescence recovery of two types of myosin isoform was simultaneously monitored using myotubes expressing eGFP-Myh7 and KuO-Myh1. In these myotubes, Mf of KuO-Myh1 was higher and 5%Rt of KuO-Myh1 was lower than those of eGFP-Myh7 (Fig. 28C and D). These results showed that the myosin replacement rates depended on expressing myosin isoform.

2. Methylated myosin is detected in muscle tissues

What factor(s) does regulate myosin replacement rates in myotubes? Our previous studies demonstrate that the myosin replacement rate depends on the intracellular amount of myosin, intracellular Ca^{2+} concentration, and myosin chaperone activity (HSP90) (Ojima et al., 2018), indicating that the intracellular environment affects the myosin replacement rate. However, our present results show that the myosin replacement rates differed between myosin isoforms under

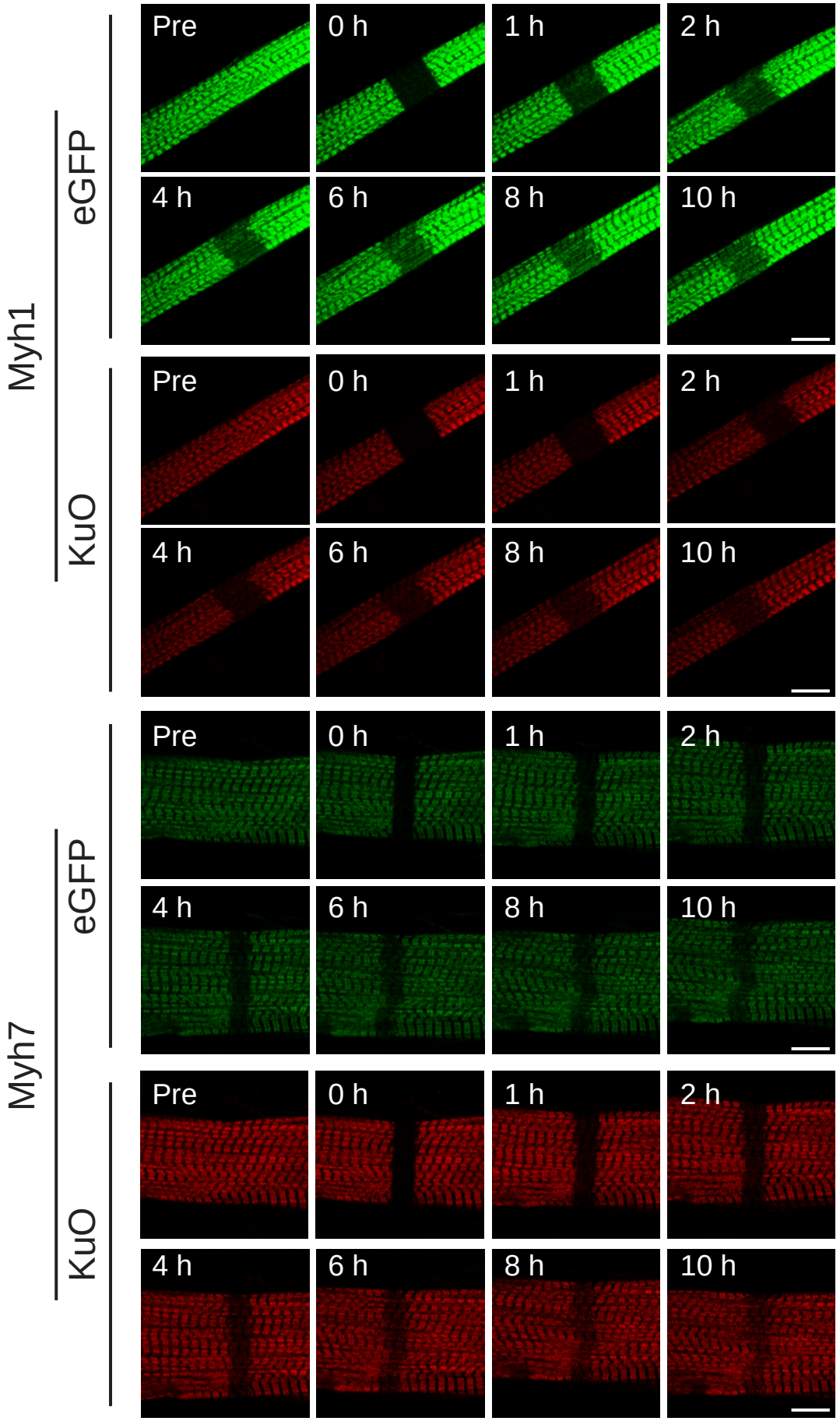

Fig. 26. Fluorescence images of eGFP or KuO tagged Myhs in cultured myotube.
A. Representative FRAP images of myotubes co-expressing eGFP-Myh1 and KuO-Myh1 or eGFP-Myh7 and KuO-Myh7. Images were obtained at 1 h intervals after photobleaching. Bleached areas are indicated by yellow rectangles. Bar is 10 μm.

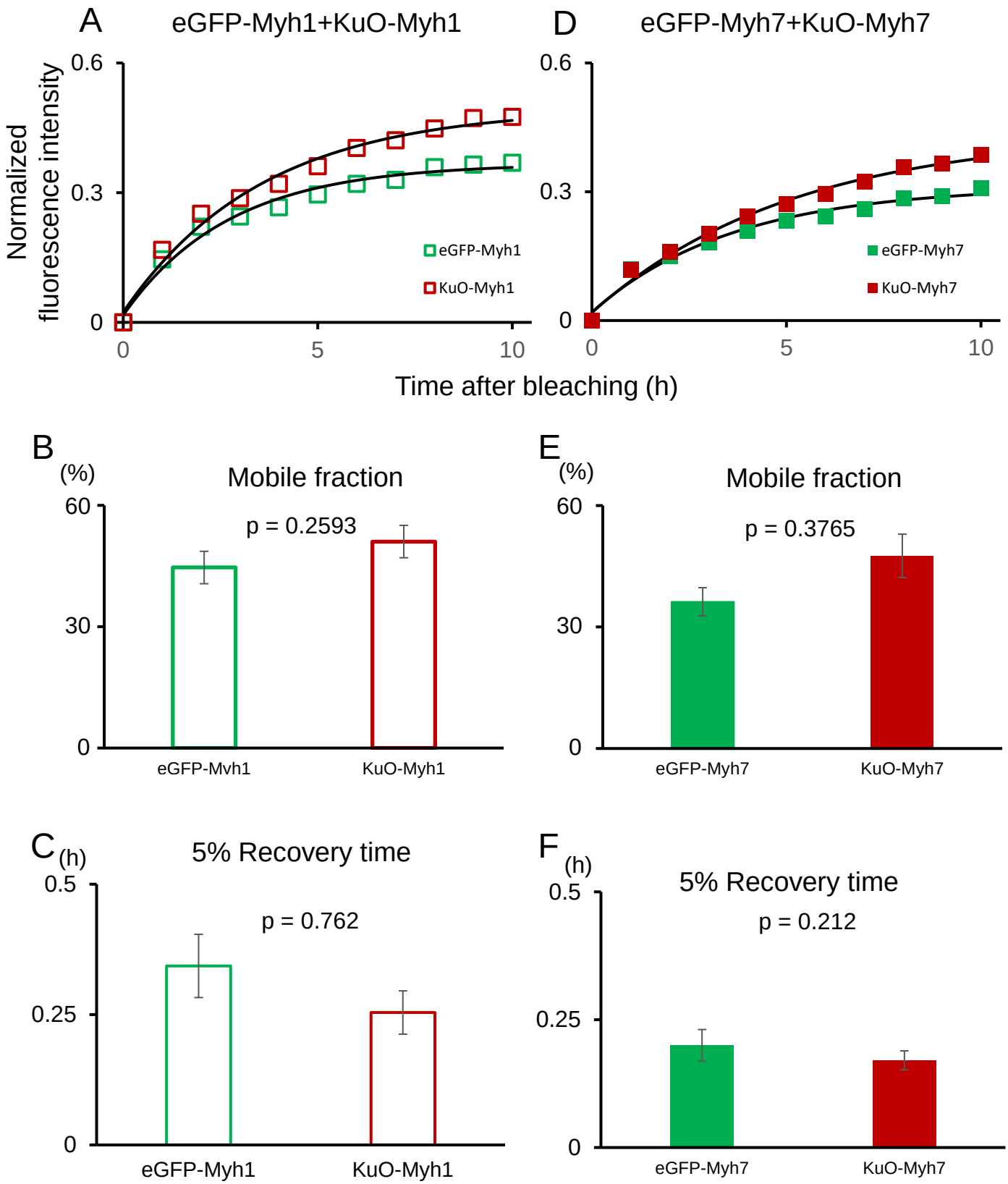

Fig. 27. Fluorescence recovery of eGFP or KuO tagged Myhs in cultured myotubes.
A, C. Normalized fluorescence intensities of eGFP or KuO were obtained from myotubes co-expressing eGFP-Myh1 and KuO-Myh1 or eGFP-Myh7 and KuO-Myh7.
B, C, E, F. Mobile factions (%): KuO-Myh1, 52.9 ± 5.3%; eGFP-Myh1, 39.3% ± 3.5%; KuO-Myh7, 47.7 ± 6.1%; eGFP-Myh7, 36.8% ± 4.0%, 5% Rt (h): KuO-Myh1, 0.50 ± 0.07 h; eGFP-Myh1, 0.53 ± 0.08 h; KuO-Myh7, 0.81 ± 0.08 h; eGFP-Myh7, 1.00 ± 0.12 h, Values represent the mean ± SE. eGFP-Myh1+ KuO-Myh1, n = 10. eGFP-Myh7 + KuO-Myh7, n = 12.

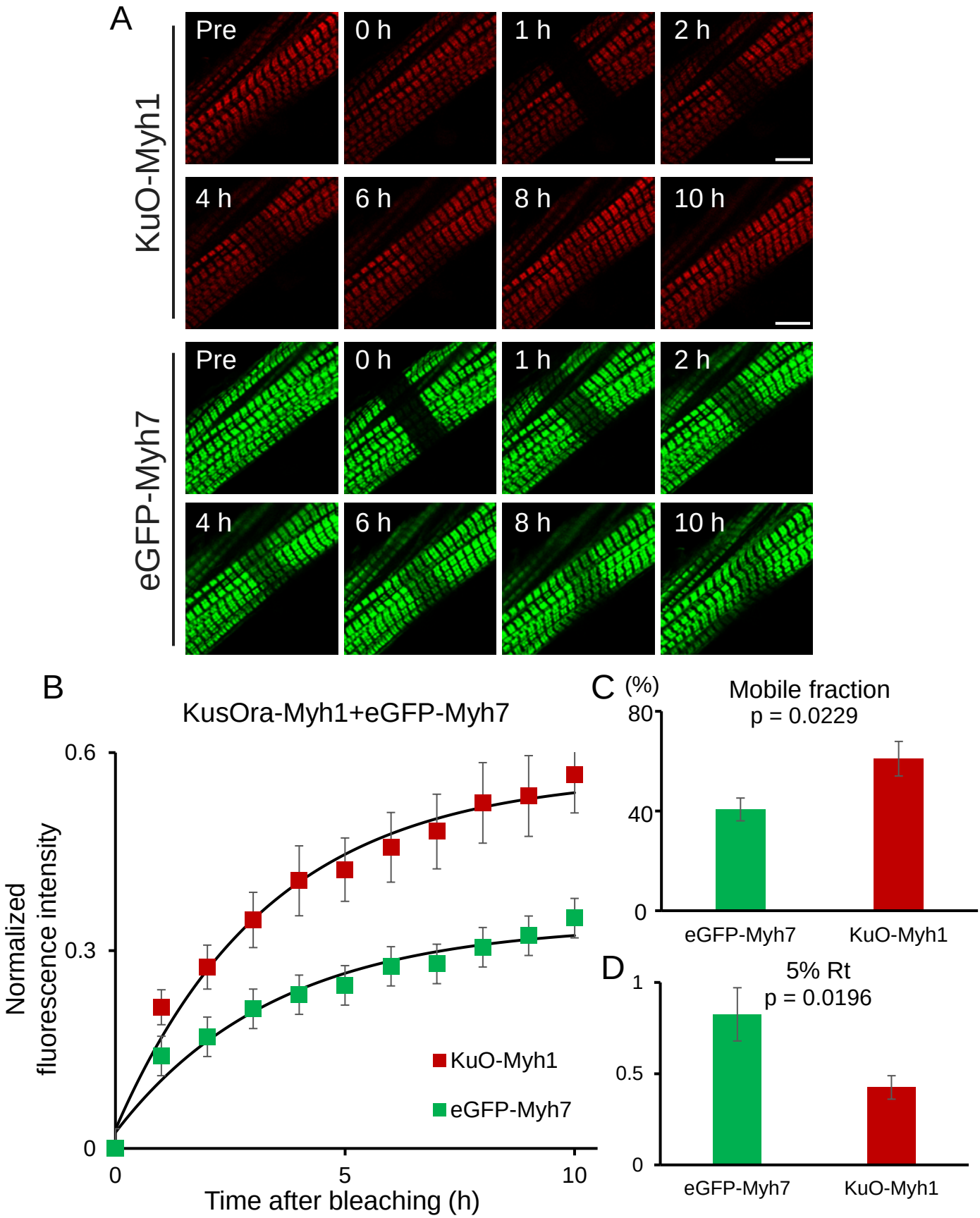

Fig. 28. Fluorescence recovery of eGFP-Myh7and KuO-Myh1 in cultured myotubes.

A. Representative FRAP images of myotubes co-expressing eGFP-Myh7 and. Images were obtained at 1 h intervals after photobleaching. Bleached areas are indicated by yellow rectangles. Bar is 10 µm.

B. Normalized fluorescence intensities of eGFP or KuO were obtained from myotubes co-expressing eGFP-Myh7 and KuO-Myh1.

C, D. Mobile factions (%): KuO-Myh1, 60.9 ± 6.9%; eGFP-Myh7, 40.6 ± 4.6%. 5% Rt (h): KuO-Myh1, 0.42 ± 0.06 h; KuO-Myh7, 0.83 ± 0.15 h. Values represent the mean ± SE. eGFP-Myh7+KuO-Myh1, n = 12

identical intracellular conditions, suggesting that myosin isoform itself is one of the keys to understanding different myosin replacement rates.

As post-translational modification (PTM) tunes biochemical properties of target proteins. To test this hypothesis, the following modification was detected by WB: methyl and acetyl groups that are known to affect protein-protein interaction, and lactyl group that is found as a newly histone and non-histone modification (Liberti & Locasale, 2020; D. Zhang et al., 2019). Protein samples were prepared from TA and SOL of 2–3-month-old mice in which eGFP-Myh7 and KuO-Myh1 were replaced by wild type Myh7 and Myh1 (Kigaki, 2020; Oe et al., 2021). Each muscle specimen was fractionated into the soluble (at the physiological ion strength) and insoluble fractions, designated as cytosolic and myofibril fractions, respectively. CBB-stained gels showed that KuO-Myh1 and eGFP-Myh7 were detected as bands just above bands of endogenous Myhs' bands (Fig. 29). Immunoblot studies revealed that bands corresponding to Myhs were positive for antibodies against anti-dimethyl lysine motif (dme-K), anti-trimethyl lysine motif (tme-K), anti-acetyl lysine (Ac-K), and anti-lactyl lysine (Lac-K). All antibodies captured positive bands corresponding to Myhs particularly in the myofibril fraction. Interestingly, the signal intensity of the dme-K bands corresponding to Myhs was stronger in SOL than in TA despite the muscle fractions (Fig. 29). These results indicated that post-translationally modified myosin was present in vivo skeletal muscles, and the modification rate was different between the origin of muscle tissues. Methylated Myhs including di- and tri- were the most predominantly found in SOL muscle.

To investigate the myosin modifications during ageing (1-, 2–3-, 12-, and 24-month-old), TA and SOL muscles were examined by immunoblotting. In addition to methyl and acetyl groups, Ub was analyzed for the evaluation of age-related accumulation of ubiquitinated myosin. The myosin modification rates of di- or tri-methylation were changed depending on ages, isoforms or

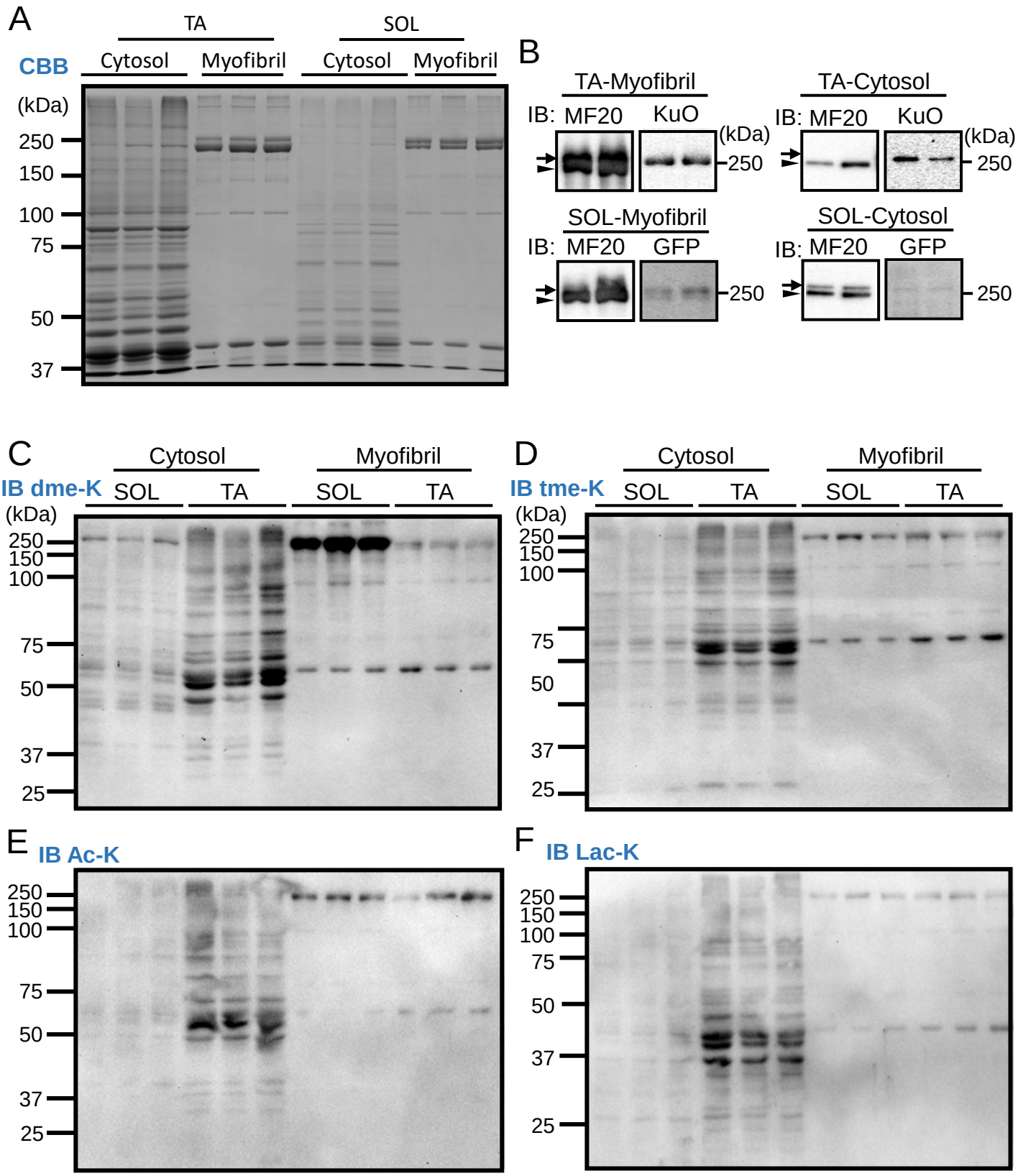

Fig. 29. Detection of post translational modification in hybrid mouse skeletal muscle.

A. Cytosolic fraction and myofibril fraction of TA and SOL were obtained from hybrid mice. The cytosolic fraction was obtained as 0.15 M TNE buffer soluble fraction, and myofibril fraction was obtained 0.15 M TNE buffer insoluble (precipitate) fraction. Each sample were subjected in SDS-PAGE and stained with CBB-R.

B. Each fraction sample from TA and SOL were western blotted using antibodies to myosin (MF20), GFP and KuO. Arrow indicates GFP or KuO tagged myosin and arrow heads indicates endogenously expressing other myosin isoforms.

C–F. Each fraction sample from TA and SOL were western blotted using antibodies to dme-K, tme-K, Ac-K, and Lac-K.

fractions, while Ace-K and Ub showed relatively constant modification rates among ages, isoforms, or fractions (Fig. 30–33). In other words, the demethylation rate of eGFP-Myh7 was consistently high in both cytosolic and myofibril fractions of SOL, and trimethylation rate of eGFP-Myh7 was also high in myofibril fraction of SOL (Fig. 32). In the TA myofibril fraction, the dimethylation ratio of KuO-Myh1was the highest in 4-week-old mice among ages we examined (Fig. 30). These results indicated that the myosin methylation rate was changed with age and isoforms.

3. Methylation sites of Myh1 and Myh7 are identified by LC-MS/MS

The WB results showed the quantitative changes of myosin modification, in which methylated ratio was the most distinct feature between Myh1 and Myh7. Next, samples from mouse skeletal muscle tissues were analyzed with a liquid chromatography-mass spectrometry (LC-MS/MS) to search for methylation sites in Myh1 and Myh7 isoforms. A total of 72 methylation sites were identified with LC-MS/MS analyses (Fig. 34A). Approximately half of methylation sites were located in the LMM domain Myh1 and Myh7. In addition, about 80% methylation sites were identified in the rod domain (S2 and LMM). The rod domain is formed by α helical coiled-coil structure, which consists of the heptad repeat pattern of amino acid residues indicated as "a–g" in Fig. 34 D. The amino acid resides that located at “a” and “d” positions and to the inner surface of the coiled-coil structure are generally hydrophobic (Parry et al., 2008). As protein surface polarity and hydrophobicity are critical for myosin polymerization (Colegrave & Peckham, 2014), identified methylation amino acid residues were applied to the “a–g” heptad repeat. Methylation sites were relatively uniformly distributed except for the “d” position, but methylation of the “f” position was specifically identified in the LMM (Fig. 34D).

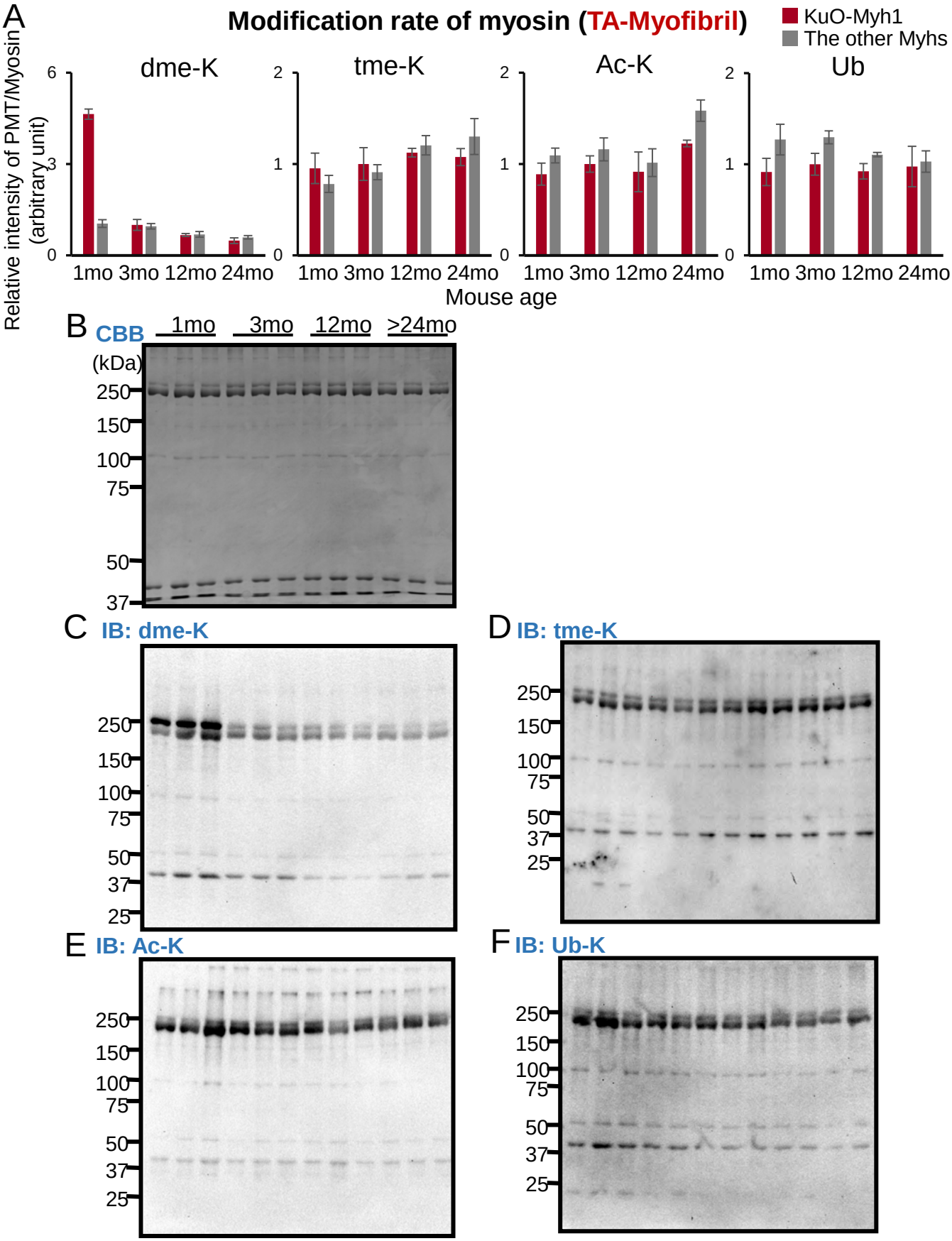

Fig. 30. Comparison of myosin modification rate among ages in TA myofibril fraction.

A. Tissue samples were obtained from 1-, 2–3-, 12-, and 24-month-old hybrid mice. The relative intensity of PMT/Myosin was calculated using band intensities of C–F. The bands just above and under 250 kDa were used as modified KuO-Myh1 and the other modified Myhs, respectively. The method of calculation is described in the Materials and methods section. Data are expressed as the mean ± SE. n = 3 for each group.

B–F. Myofibril fraction samples from TA were stained with CBB-R or western blotted using antibodies to dme-K, tme-K, Ac-K, and Ub.

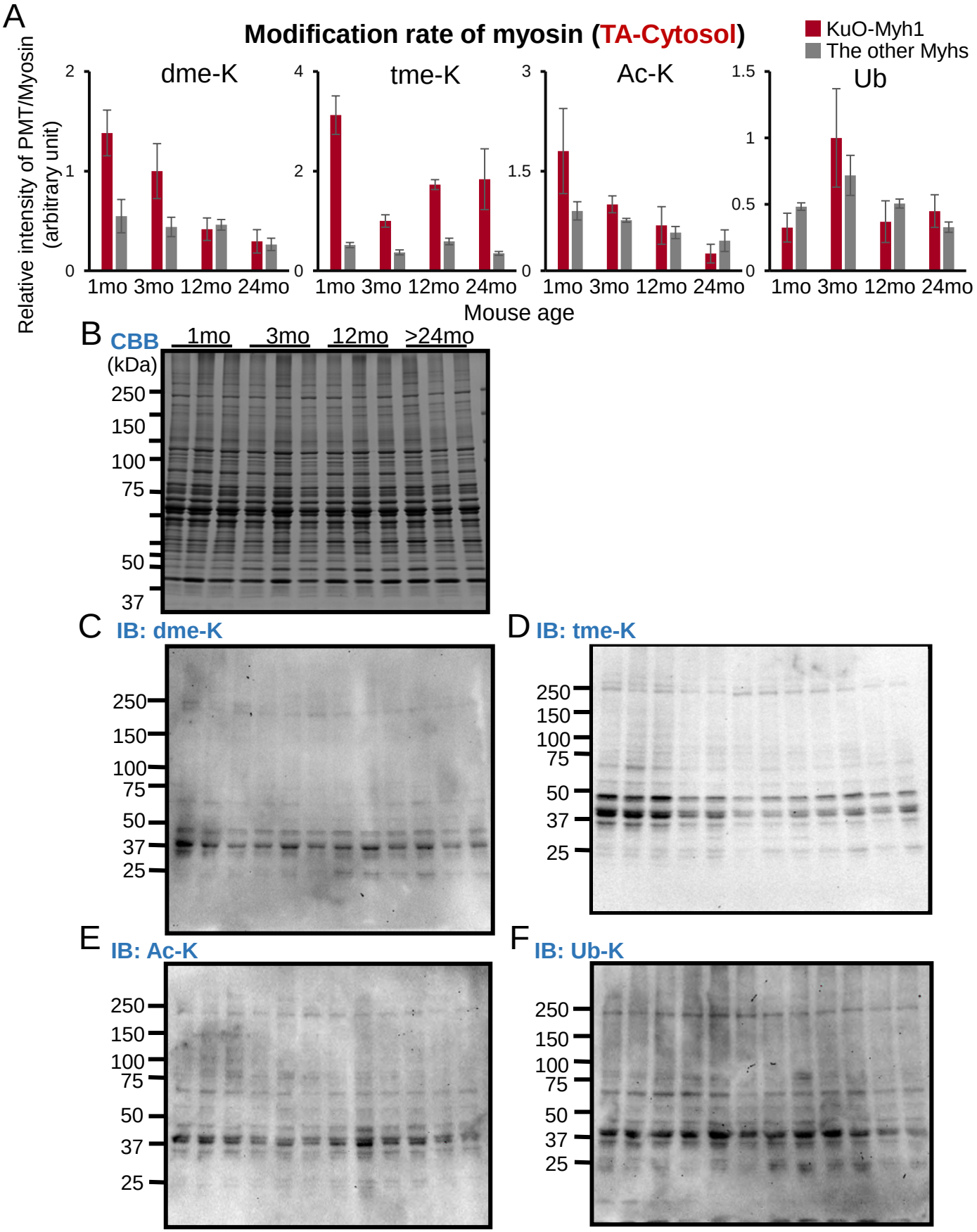

Fig. 31. Comparison of myosin modification rate among ages in TA cytosolic fraction.

A. Tissue samples were obtained from 1-, 2–3-, 12-, and 24-month-old hybrid mice. The relative intensity of PMT/Myosin was calculated using band intensities of C–F. The bands just above and under 250 kDa were used as modified KuO-Myh1 and the other modified Myhs, respectively. The method of calculation is described in the Materials and methods section. Data are expressed as the mean ± SE. n = 3 for each group.

B–F. Cytosolic fraction samples from TA were stained with CBB-R or western blotted using antibodies to dme-K, tme-K, Ac-K, and Ub.

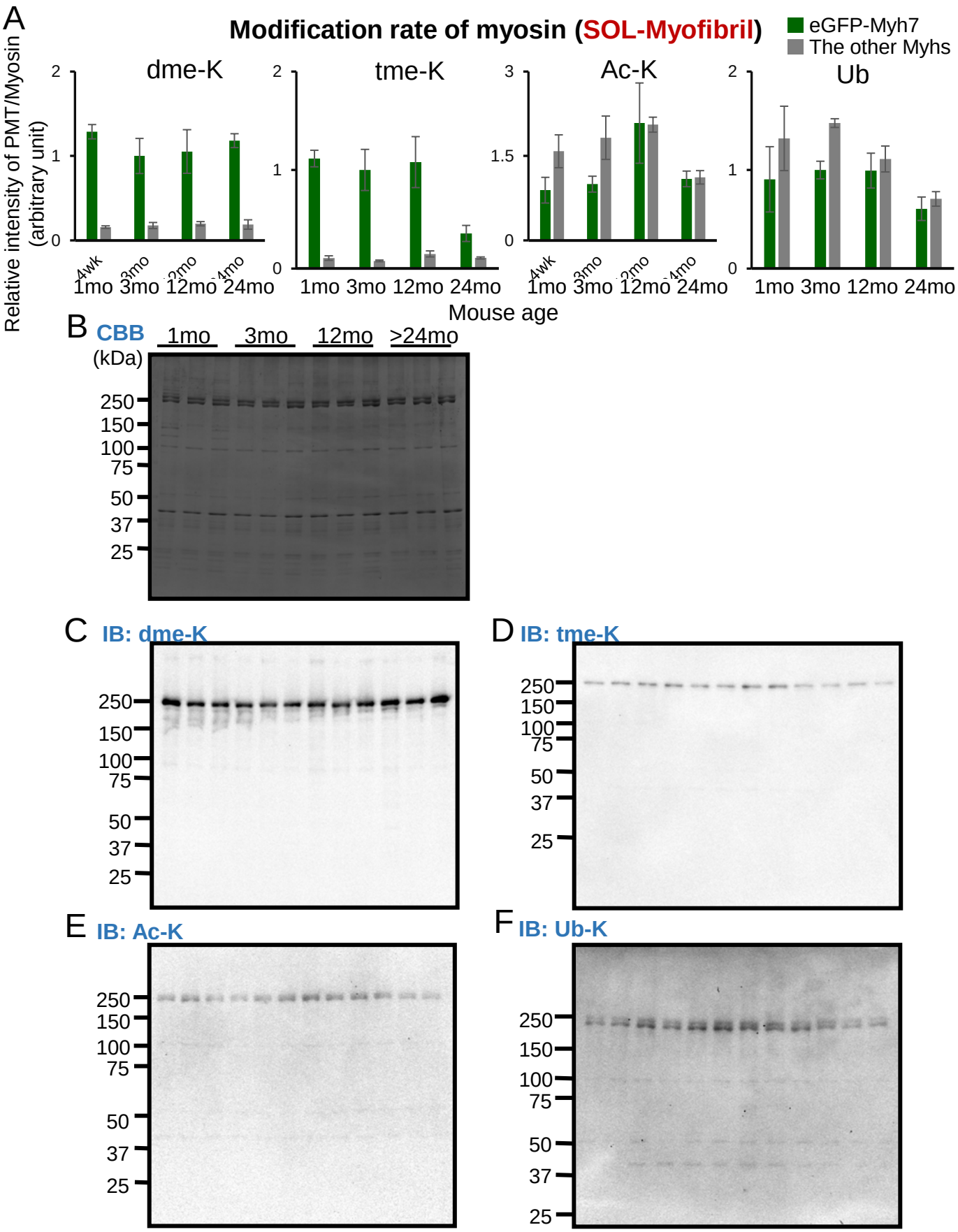

Fig. 32. Comparison of myosin modification rate among ages in SOL myofibril fraction.

A. Tissue samples were obtained from 1-, 2–3-, 12-, and 24-month-old hybrid mice. The relative intensity of PMT/Myosin was calculated using band intensities of C–F. The bands just above and under 250 kDa were used as modified KuO-Myh1 and the other modified Myhs, respectively. The method of calculation is described in the Materials and methods section. Data are expressed as the mean ± SE. n = 3 for each group.

B–F. Myofibril fraction samples from SOL were stained with CBB-R or western blotted using antibodies to dme-K, tme-K, Ac-K, and Ub.

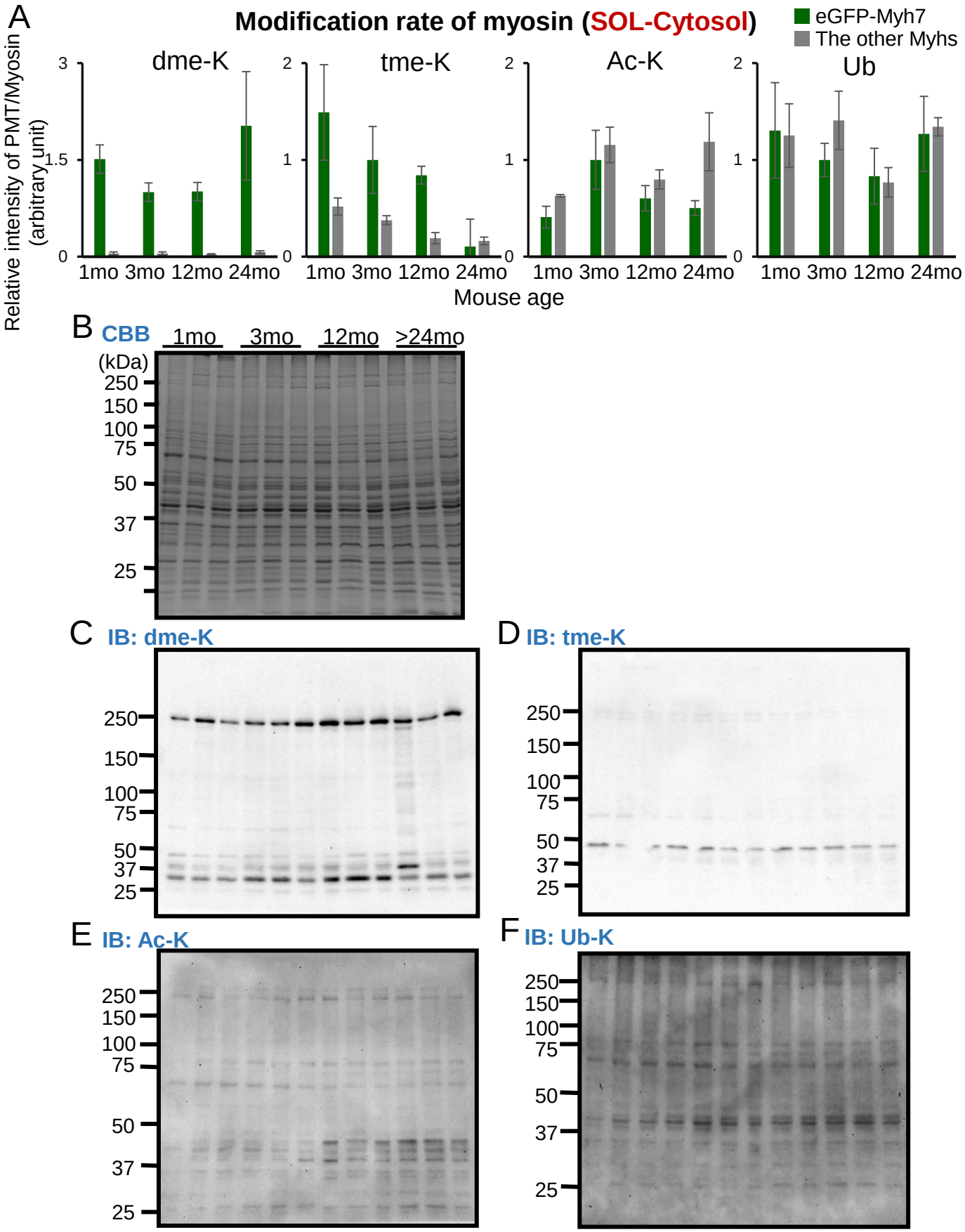

Fig. 33. Comparison of myosin modification rate among ages in SOL cytosolic fraction.

A. Tissue samples were obtained from 1-, 2–3-, 12-, and 24-month-old hybrid mice. The relative intensity of PMT/Myosin was calculated using band intensities of C–F. The bands just above and under 250 kDa were used as modified KuO-Myh1 and the other modified Myhs, respectively. The method of calculation is described in the Materials and methods section. Data are expressed as the mean ± SE. n = 3 for each group.

B–F. Cytosolic fraction samples from SOL were stained with CBB-R or western blotted using antibodies to dme-K, tme-K, Ac-K, and Ub.

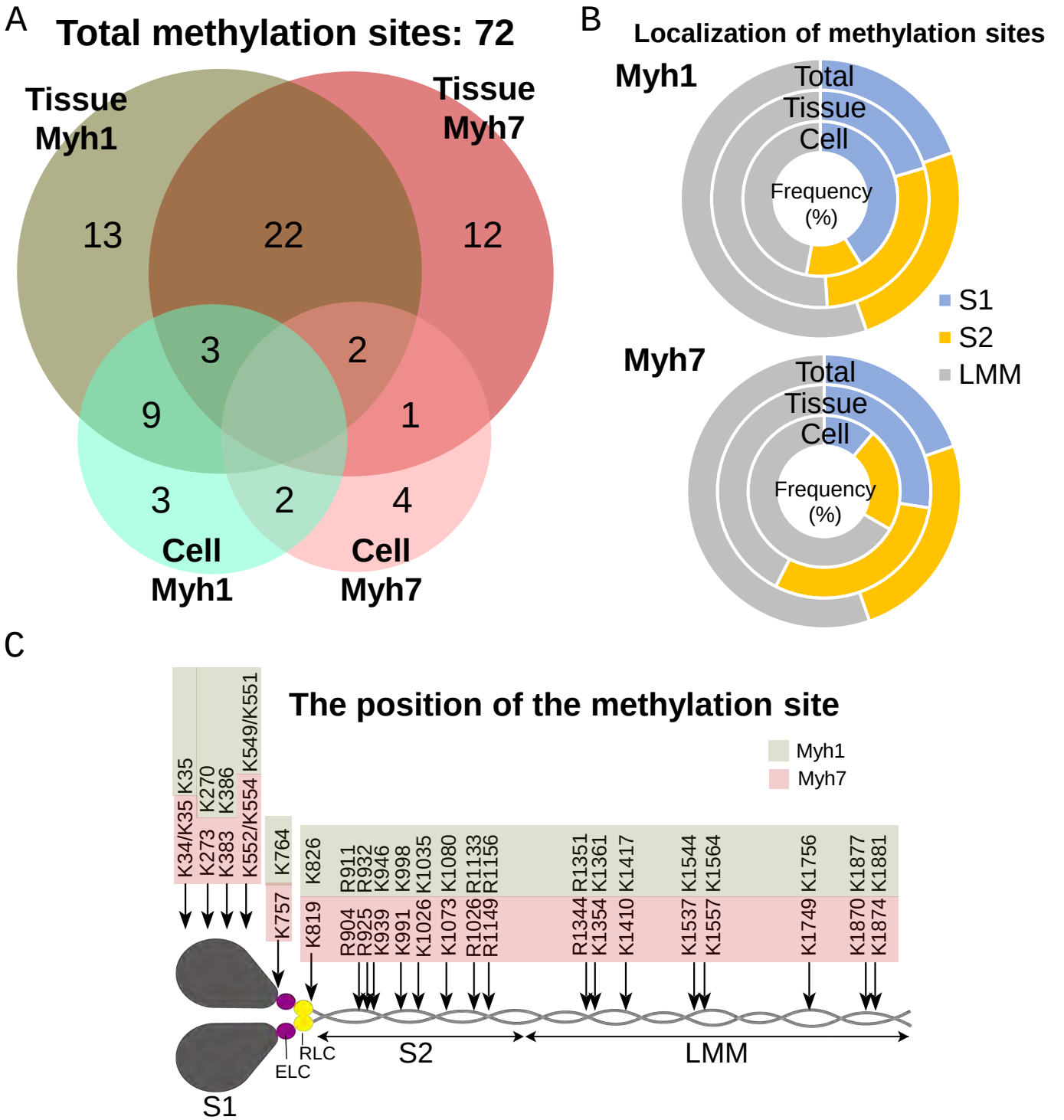
A
Total methylation sites: 72
Tissue Myh1
Tissue Myh7
Cell Myh1
Cell Myh7
13
22
12
3
2
9
1
3
2
4
B
Localization of methylation sites
Myh1
Myh7
Total
Tissue
Cell
Frequency (%)
S1
S2
LMM
C
The position of the methylation site
Myh1
Myh7
K34/K35 K35
K273
K270
K383
K386
K552/K554 K549/K551
K764
K757
K826
K819
R911 R925 R932 K939 K946 K991 K998 K1026 K1035 K1073 K1080 R1026 R1133 R1149 R1156
R904
R1344 R1351 K1354 K1361 K1410 K1417
K1537 K1544 K1557 K1564
K1749 K1756
K1870 K1877 K1874 K1881
RLC
ELC
S1
S2
LMM
D
Localization of methylation sites in heptad repeat
(%)
Frequency
100
80
60
40
20
0
Myh1
Myh7
Myh1
Myh7
S2
LMM
a
b
c
d
e
f
g
a
b
c
d
e
f
g
a'
b'
c'
d'
e'
f'
g'

Fig. 34. Methylation sites of Myh1 and Myh7 from tissue or muscle cell and its frequency of localization
A. The number of unique or common methylation sites identified by mass spectrometry is shown in the Venn diagram. The total number indicates the total number of methylation sites from hybrid mouse tissue and muscle cells. The intersection number is the number of sites commonly identified among the overlapping groups.
B. The frequency of the methylated sites in each domain of Myh1 or Myh7. The frequency was calculated by samples from mouse tissue or muscle cell. Total means the total frequency of tissue and cell.
C. The locations of identified methylated amino acid are shown in diagram. The residues are shown in diagram is used statistical analysis after Fig.35.
D. The frequency of the methylation sites in the “a–g” heptad repeat was calculated using Myh1 and Myh7 data from hybrid mice.

4. Methylation sites are found in Myh isoforms and fractions

To evaluation of methylation at the rod domain in more detail, I selected 22 methylation amino residues that had relatively high detection rates. The methylation rates of these 22 sites were calculated and compared between the following two groups: “Isoform (Myh1 vs Myh7)” or “Fraction (cytosol vs myofibril)”. The Venn diagram shows the number of unique or common methylation sites, and the numbers in parentheses in the intersection show the number of sites with significant differences in modification rates between the two groups (Fig. 35). In a comparison between isoforms, there were 7 amino acid residues where methylation was detected only in Myh1 and 2 amino acid residues where methylation was detected only in Myh7 (Fig. 35A and C). In comparison between fractions, half of the myofibril-specific methylation sites were detected at the LMM, and the sites with significant differences in the methylation rate located in S2 (Fig. 35B and D). Subsequently, each fraction was divided into isoform for comparison. In Myh1, sites with cytoplasmic or higher modification rates tended to be detected in S2, and sites with myofibril-specific or higher modification rates tended to be detected in LMM (Fig. 36A and E). In Myh7, many myofibril-specific or higher modification rate methylation sites were identified in S2 and LMM (Fig. 36B and F). However, the modification sites of S2 and LMM were generally less in Myh7 than in Myh1 (Fig. 36).

5. Age different samples were classified into 1-monthe old and the other ages.

Finally, to study whether age-dependent methylation of myosin was present or not, the methylation rate of myosin was quantified during ageing. Methylated amino acid residues were found in Myh1 and Myh7 at specific age (Fig. 37A, B, E, F). In comparison between divided fractions, methylation rates of 1-month-old mice were significantly higher than that of the other

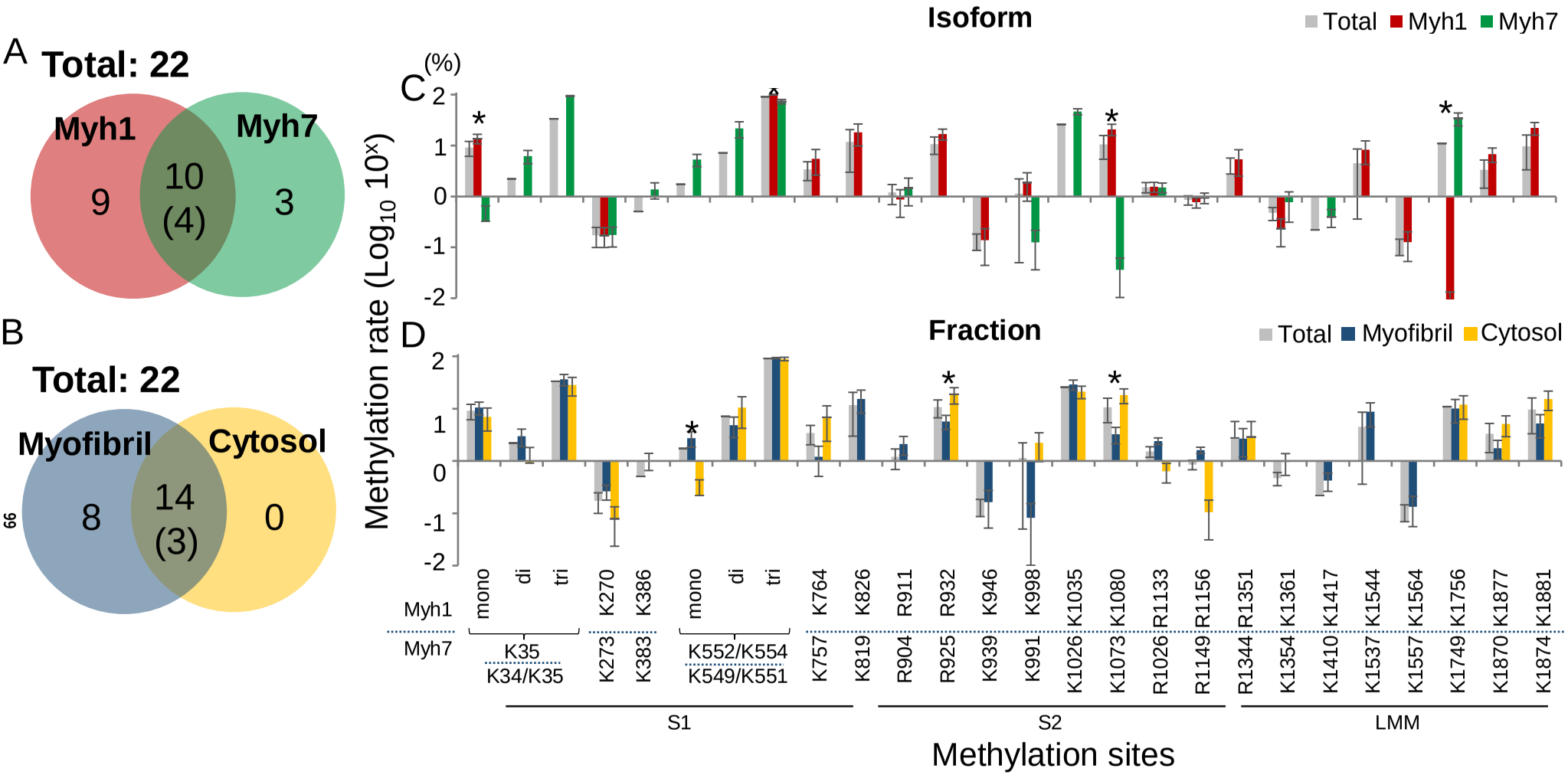

Fig. 35. The comparison of methylation rate between two categories

A, B. The Venn diagram shows the number of unique or common methylation sites in each category. The total number indicates the number of identified methylation sites in this category. The numbers in parentheses in the intersection show the number of sites with significant differences between the two groups in modification rates identified in both groups.

C, D. The y-axis of graphs is shown by Log (10), the label of the x-axis indicates methylation sites. Total indicates the average of all samples. Values represent the mean ± SE. * $p < 0.05$ between two comparison groups. Total, n = 96; The other groups, n = 48.

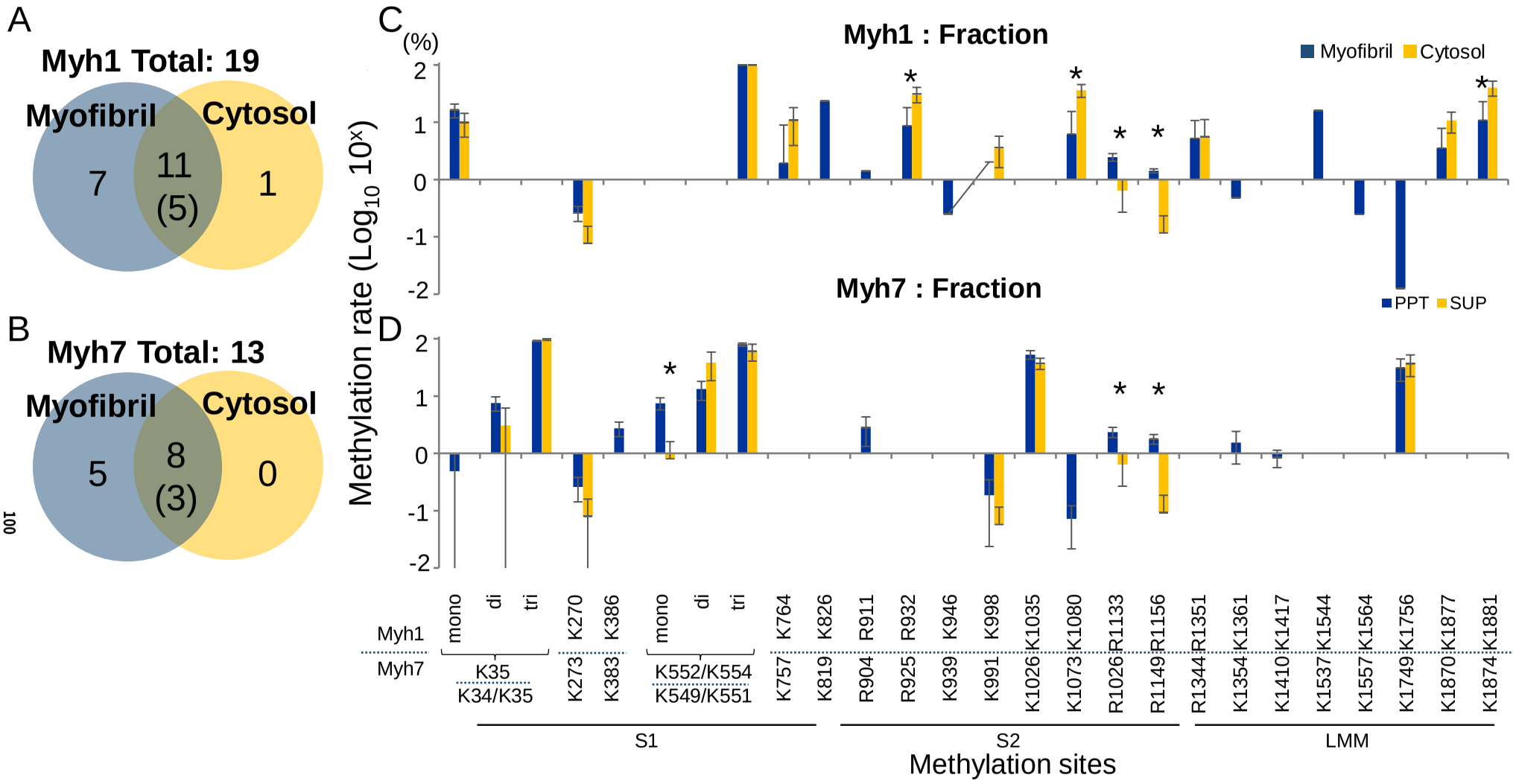

Fig. 36. The comparison of Myh1 or Myh7 methylation rate between two categories

A, B. The Venn diagram shows the number of unique or common methylation sites in each category. The total number indicates the number of identified methylation sites in this category. The numbers in parentheses in the intersection show the number of sites with significant differences between the two groups in modification rates identified in both groups.

C, D. The y-axis of graphs is shown by Log (10), the label of the x-axis indicates methylation sites. Values represent the mean ± SE. * $p < 0.05$ between two comparison groups. n = 24 for each group.

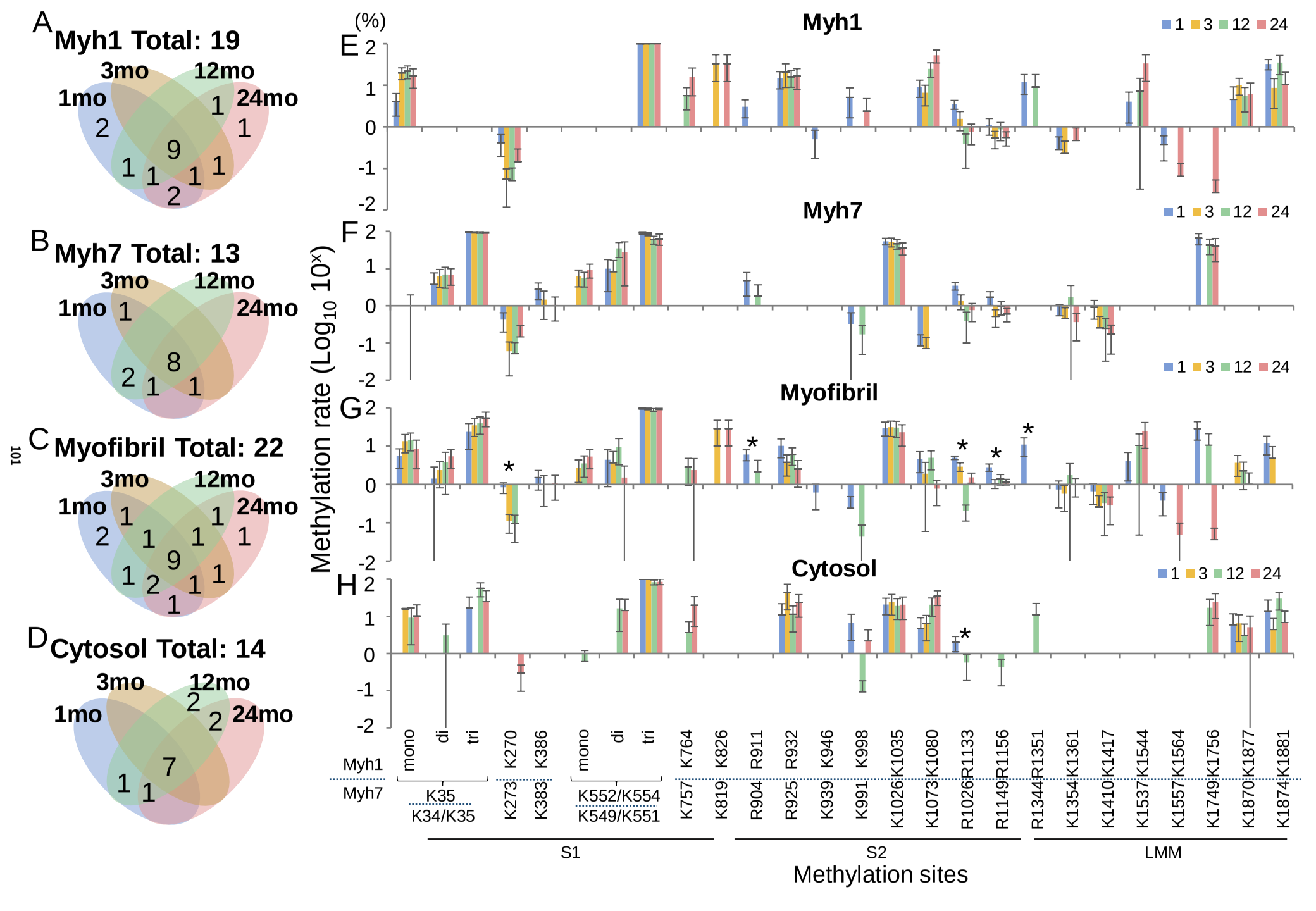
A
Myh1 Total: 19
3mo
12mo
1mo
24mo
2
1
9
1
1
1
1
2
1
B
Myh7 Total: 13
3mo
12mo
1mo
24mo
1
8
2
1
1
C
Myofibril Total: 22
3mo
12mo
1mo
24mo
2
1
1
1
1
9
1
2
1
1
1
D
Cytosol Total: 14
3mo
12mo
1mo
24mo
2
2
7
1
1
(%)
E
Myh1
F
Myh7
G
Myofibril
H
Cytosol
1 3 12 24
Methylation rate (Log10 10x)
mono
di
tri
K270
K386
K764
K826
R911
R932
K946
K998
K1035
K1080
R1133
R1156
R1351
K1361
K1417
K1544
K1564
K1756
K1877
K1881
Myh1
Myh7
K35
K34/K35
K552/K554
K549/K551
S1
S2
LMM
Methylation sites

Fig. 37. The comparison of methylation rate among mice ages

A–D The Venn diagram shows the number of unique or common methylation sites in each category. The total number indicates the number of identified methylation sites in this category. F–H. The y-axis of graphs is shown by Log (10), the label of the x-axis indicates methylation sites. Values represent the mean ± SE. * $p < 0.05$ comparison between 1-month-old and the others. $n = 12$ for each group.

aged mice at some amino acid residues located to the S2 and LMM (Fig. 37C, D, G, H). Then, clustering analysis was performed using data of methylation rate of sites in S2 and LMM domain. Each sample obtained from TA or SOL was classified into Myh1 and Myh7. The separation of cytosol and myofibril was unclear in Myh1 analysis, while the cytosolic group was separated from the myofibril group in Myh7 analysis. The samples derived from 1-month-old mice were gathered on the left side a sequence of a cluster in Myh1 analysis and was detected as a group separated from other ages in Myh7 analysis (blue dashed circle of Ages panel in Fig. 38A and B). These results suggested that the methylation pattern in the myosin rod was different between young mice and adult mice.

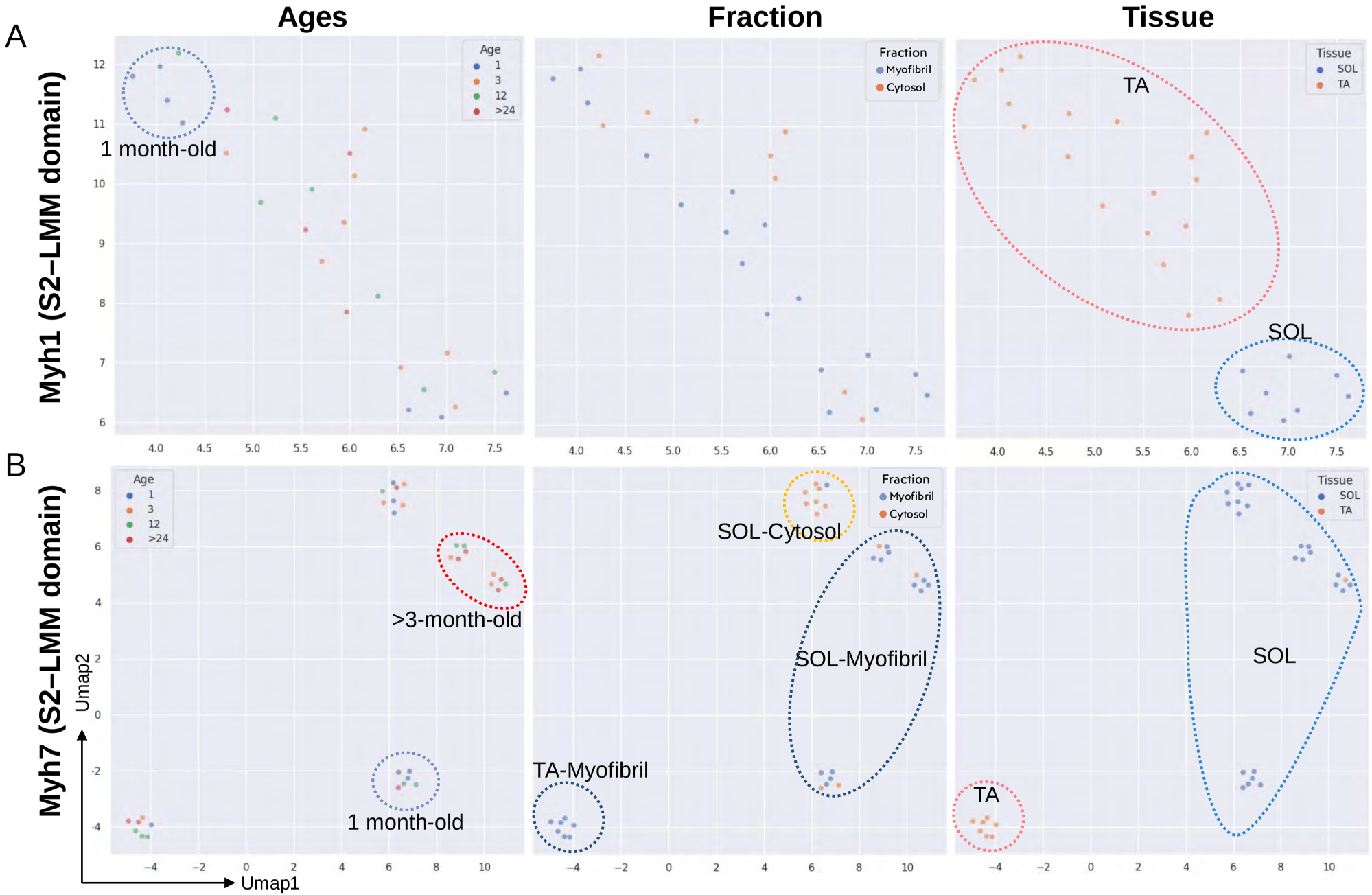

Fig. 38. Uniform Manifold Approximation and Projection (Umap) Plots using S2–LMM methylation data of Myh1 or Myh7
It is shown that Umap diagram using data of methylation rate of the sites located in S2–LMM from mice. The dot color in each panel reflects the categories shown as a legend. The circles show that clusters are separated from others in each panel.

Discussion

This chapter demonstrated that the myosin replacement rate was different between myosin isoforms in the same myotubes. Furthermore, myosin isoform-specific methylated amino acid residues were found in Myh1 and Myh7. Different replacement rates between Myh1 and Myh7 may be caused by PTM, which modifies the biochemical properties of Myhs. These results suggests that myosin replacement in the thick filament might be modulated by post-translational modification such as methylation.

The homology of the primary structure between Myh1 and Myh7 is 81.9%, and the difference of amino acid sequence exists uniformly in both head and rod. In fig. 28, it was observed KuO-Myh1 and eGFP-Myh7 were incorporated into the same thick filament and formed thick filament in cooperation. Although the mutation in LMM domain is one of the causes of myopathy, the sequence difference between Myh1 and Myh7 were not affect thick filament formation. However, the difference of myosin replacement rates was shown between myosin isoforms under identical intracellular conditions (Fig. 28). This result suggests that myosin isoform itself is one of the keys to decide on replacement rate.

In this chapter, I showed the myosin methylation as a potential involvement factor in myosin replacement. Identified methylated amino acid residues were different between the cytosolic and myofibril fractions. Approximately half of the methylation amino residues identified in this study were located in LMM in both tissue and cell (Fig. 29B), implying LMM is likely a domain with high methylation frequency. The LMM domain plays a critical role in myosin polymerization and thick filament formation. The LMM consists of the coiled-coil structure with a heptad repeat of amino acid residues to form Myh dimers. Defects of coiled-coil structures caused by a mutation(s) lead to the myosin aggregation and the reduction of myosin incorporation into the thick filament (Armel & Leinwand, 2009, 2010a, 2010b; Colegrave & Peckham, 2014; Parker et al., 2018;

Viswanathan et al., 2017; Wolny et al., 2013). As the amino acid residues distribution with positive and negative charges is critical in thick filament packing, alternation of distributed charged amino acid residues may disrupt myosin-myosin interaction to form the thick filament. Although methylated lysine and methylated arginine were identified in the LMM domain in this study, methylation does not shift lysine and arginine from positive charge to negative charge. On the other hand, methylation of lysine and arginine has the potential to decrease their hydrophilicity because the methyl group is hydrophobic (Luo et al., 2021). Increment of myosin hydrophobicity with methylation may enhance lateral interaction between myosins to form thick filaments.

In comparison to the difference in methylation rate among aging, the difference was detected between 1-month-old mouse and the other aged mouse in both Myh1 and Myh7 (Fig. 38 and 39). Immunoblot study in the myofibril fraction of TA also showed that methylation rate was higher in 1-month-old mouse than the other aged. In addition, a previous study shows that the replacement rate of eGFP-Myh7 is higher in 3-wk-old-mouse than in 12- and 24-old-mouse. These results suggest a potential that the difference of methylation site and/or methylation rate is involved in the myosin replacement at a younger age. In previously, a heart and skeletal muscle-specific methyltransferase, SMYD1, is shown that interact with myosin and plays an important role in sarcomere organization. In younger mice that is muscle forms actively, myosin accumulation to the myofibrils might be regulated by methyltransferase via methylation that has hydrophobicity enhance effect described above.

The previous studies show that DNA methylation changes during ages and modification effects, such as acetylation and arginylation, on contraction function (Cornachione et al., 2014; Samant et al., 2015). However, it has not been studied on PMT effect on myosin polymerization ability and myosin solubility in the cytosolic environment. In addition, because myofiber-specific methyltransferase function and myosin methylation function are known a little, it is needed more

Acknowledgements

I am grateful to Dr. Nishimura Takanori for accepting and teaching me in the laboratory.To Dr. Ojima Koichi, I would like to great thanks for your direction. I was taught everything about research (how to experiment, how to write a paper, way of think, etc.).

I am indebted to Dr. Kobayashi Ken, Dr. Kumura Haruto, Dr. Tkahashi Masashi, Dr. Suzuki Takahiro for critical reading this thesis and suggestions.

I gratefully acknowledge to Mr. Yasui Masanori, Mr. Ito Toshiaki, Mr. Oshima Eiki, Ms.Kuzuma Yukiko, Dr. Takasuka Taichi, Dr. Nishigami Yukinori for your support to research.

I would like to thank members in the Muscle Biology Research Unit of NARO for their advice and support of my research. Special thanks to Dr. Sei Muroya, Ms. Ikuyo Ikushima, Ms. Mika Oe, and Ms. Miho Ichimura.

I gratefully acknowledge past and present members of the Cell tissue biology laboratory. You made my research life very enjoyable.

Last but not least, I would like to thank my family and friends for their support.

General Discussion

In this thesis, three main results were found regarding myosin replacement: (1) myosin was the most frequently replaced at the tip of the thick filament using both newly synthesized and recycled myosin, (2) replacement rate of Myh3 was suppressed by Myh3 specific Ub ligase, Ozz, via Myh3 ubiquitination, (3) myosin replacement rate was different depending on myosin isoforms. Based on these results, our myosin replacement model was proposed (Fig. 39).

We have studied the myosin replacement in the thick filament using an imaging technique. In previously, it shows that eGFP-Myh3 in the thick filament is exchanged independently of MypbC and myomesin (Ojima et al., 2015). Myosin replacement is significantly reduced under treatment with de novo protein synthesis cycloheximide (Ojima et al., 2015), not at all, myosin replacement is remarkably suppressed with an inhibitor of a chaperone HSP90 which is important for the folding of Myh head domain (Ojima et al., 2018). In addition, an amount of cytosolic myosin affects myosin replacement rate in the thick filament (Ojima et al., 2017). These results suggest that both synthesized and cytosolic myosin are important for myosin replacement, and thick filament components are independently exchanged at appropriate timing. However, it had remained unclear whether thick filament associate-myosins are evenly replaced, whether the myosin dissociated from the thick filament is re-incorporated into the thick filament, and if so, how distinguish between the reused myosin and the degraded myosin. Although it has not been studied on PMT effect on myosin polymerization ability and myosin solubility in the cytosolic environment, the effect of modulation such as methylation on myosin replacement is expected.

In chapter 1, I showed that myosin is frequently exchanged at the tip of the thick filament and the thick filament-dissociated myosin is reused for myosin replacement. It is thought that the synthesized myosin molecule is inserted into the thick filament and re-insert another thick

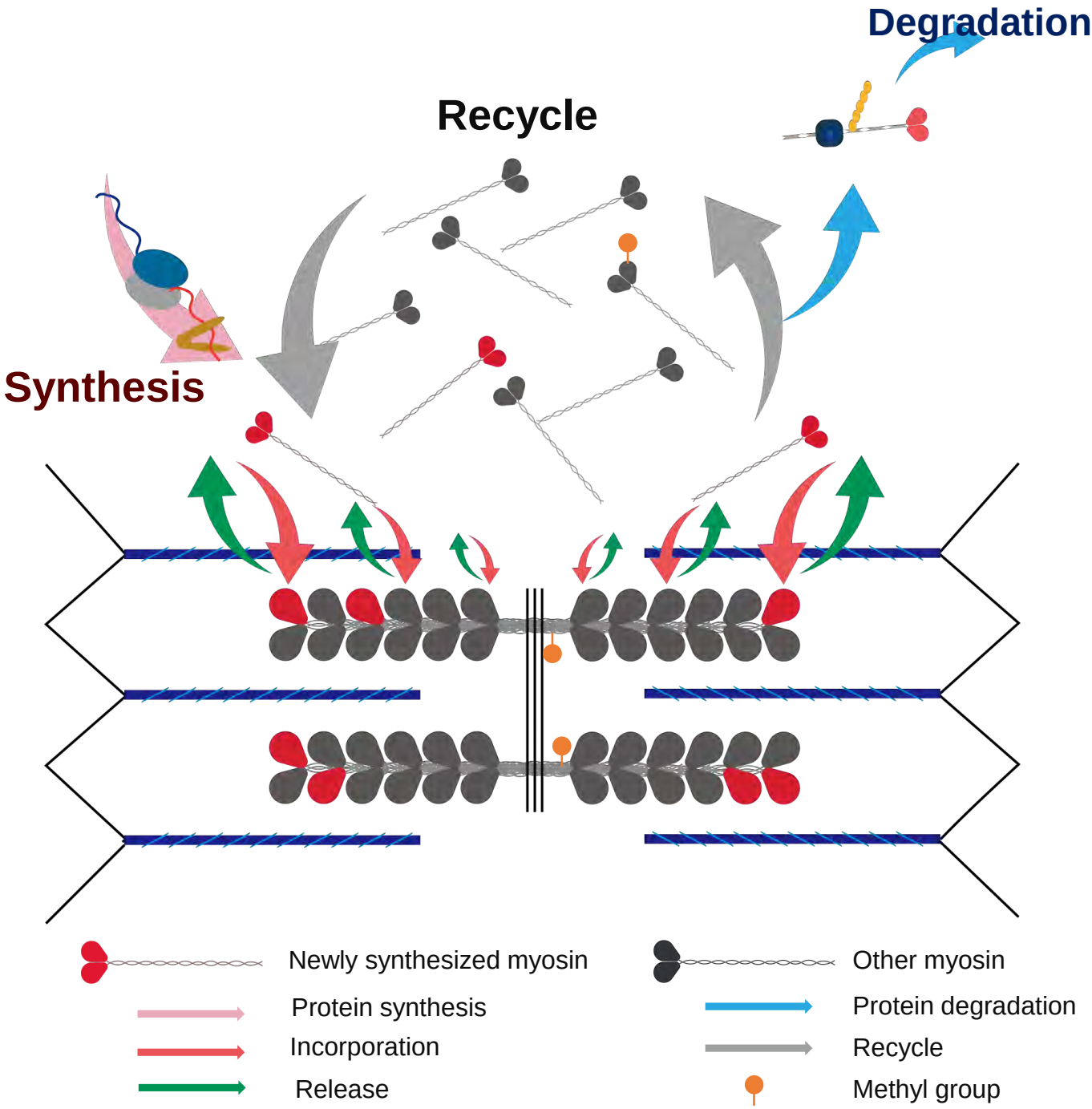

Fig.39 A model of myosin replacement in the thick filament
Thick filament–associated myosin is replaced with both newly synthesized and recycled myosin molecules. Myosin release and insertion occur concurrently. This occur more frequently at the edge of the filament, as indicated by the size of the green and red arrow. Newly synthesized myosins are relative readily incorporated into the thick filament, as shown by the pink arrow. The blue arrows show the flow of myosin degradation. A certain amount of released myosin from the thick filament is recognized and ubiquitinated by E3 ligase for degradation. The remaining myosins are recycled and re-incorporated into the thick filament. The difference of methylation among isoforms and aging might regulate myosin replacement rate in the thick filament.

filament via cytosol after release from the thick filament. Although the myosin exchange unit is unclear, I predict that the cytosol myosin exists primarily as a monomer or dimer and these units may also function as exchange units from previous study (Davis, 1993b).

It was partially indicated the involvement of E3 ligase in myosin replacement in how distinguish between the reused myosin and the degraded myosin. I showed that overexpression of Ozz and MG132 treatment suppressed eGFP-Myh3 replacement in the thick filament. However, it remained unclear involvement E3 ligase in replacement of other myosin isoforms. The effect of Murf1 overexpression differed among myosin isoforms (Fig. 12–15). Moreover, it is shown that the treatment of MG132 suppressed eGFP-Myh7 replacement in slow fiber but not KuO-Myh1 replacement in fast fiber (Kigaki, 2020). It is expected that the effect of E3 ligase and functional combinations of E3 ligase differ depending on Myh isoforms and intracellular environment.

Finally, I demonstrated that might be a factor for regulating myosin replacement rate was the state of the myosin molecule, as well as the intracellular environment and myosin associate protein. In chapter 3, I observed different replacement rates between KuO-Myh1 and eGFP-Myh7 in the same myotubes (Fig. 28). In addition, it was shown that the methylation rate and methylate amino residues of myosin were different among isoforms, fractions, and mice ages. These differences were validated in the myosin rod region that is important for myosin polymerization and insertion into the thick filament.

Collectively, myosin in the thick filament is frequently replaced especially in the tips of the thick filament using both synthesized and reused myosin molecules. E3 ligases participate in myosin replacement through the choice of myosin degradation. In addition to the intracellular environment such as protein synthesis and degradation activity, the difference of methylation among isoforms, fractions, and aging might regulate myosin replacement in the thick filament.

Acknowledgements

I am grateful to Dr. Nishimura Takanori for accepting and teaching me in the laboratory.To Dr. Ojima Koichi, I would like to great thanks for your direction. I was taught everything about research (how to experiment, how to write a paper, way of think, etc.).

I am indebted to Dr. Kobayashi Ken, Dr. Kumura Haruto, Dr. Tkahashi Masashi, Dr. Suzuki Takahiro for critical reading this thesis and suggestions.

I gratefully acknowledge to Mr. Yasui Masanori, Mr. Ito Toshiaki, Mr. Oshima Eiki, Ms.Kuzuma Yukiko, Dr. Takasuka Taichi, Dr. Nishigami Yukinori for your support to research.

I would like to thank members in the Muscle Biology Research Unit of NARO for their advice and support of my research. Special thanks to Dr. Sei Muroya, Ms. Ikuyo Ikushima, Ms. Mika Oe, and Ms. Miho Ichimura.

I gratefully acknowledge past and present members of the Cell tissue biology laboratory. You made my research life very enjoyable.

Last but not least, I would like to thank my family and friends for their support.

References

Agarwal, M., Sharma, A., Kumar, P., Kumar, A., Bharadwaj, A., Saini, M., Kardon, G., & Mathew, S. J. (2020). Myosin heavy chain-embryonic regulates skeletal muscle differentiation during mammalian development. *Development (Cambridge)*, *147*(7). https://doi.org/10.1242/dev.184507

Armel, T. Z., & Leinwand, L. A. (2009). Mutations in the β-myosin rod cause myosin storage myopathy via multiple mechanisms. *Proceedings of the National Academy of Sciences of the United States of America*, *106*(15), 6291–6296. https://doi.org/10.1073/pnas.0900107106

Armel, T. Z., & Leinwand, L. A. (2010a). A mutation in the β-myosin rod associated with hypertrophic cardiomyopathy has an unexpected molecular phenotype. *Biochemical and Biophysical Research Communications*, *391*(1), 352–356. https://doi.org/10.1016/j.bbrc.2009.11.062

Armel, T. Z., & Leinwand, L. A. (2010b). Mutations at the same amino acid in myosin that cause either skeletal or cardiac myopathy have distinct molecular phenotypes. *Journal of Molecular and Cellular Cardiology*, *48*(5), 1007–1013. https://doi.org/10.1016/j.yjmcc.2009.10.011

Atkinson, S. J., & Stewart, M. (1992). Molecular interactions in myosin assembly of the 28-residue charge repeat in the rod. *J. Mol. Biol*, *226*, 7–13.

Avram, H., & Aaron, C. (1998). The ubiquitin system. *Annual Review of Biochemistry*, *67*, 425–479. https://doi.org/10.1038/458421a

Azevedo, M., & Baylies, M. K. (2020). Getting into Position: Nuclear Movement in Muscle Cells. *Trends in Cell Biology*, *30*(4), 303–316. https://doi.org/10.1016/j.tcb.2020.01.002

Biggar, K. K., & Li, S. S. C. (2015). Non-histone protein methylation as a regulator of cellular signalling and function. *Nature Reviews Molecular Cell Biology*, *16*(1), 5–17. https://doi.org/10.1038/nrm3915

Blom, N., Sicheritz-Pontén, T., Gupta, R., Gammeltoft, S., & Brunak, S. (2004). Prediction of post-translational glycosylation and phosphorylation of proteins from the amino acid sequence. *Proteomics*, *4*(6), 1633–1649. https://doi.org/10.1002/pmic.200300771

Bodine, S. C., Latres, E., Baumhueter, S., Lai, V. K. M., Nunez, L., Clarke, B. A., Poueymirou, W. T., Panaro, F. J., Erqian Na, Dharmarajan, K., Pan, Z. Q., Valenzuela, D. M., Dechiara, T. M., Stitt, T. N., Yancopoulos, G. D., & Glass, D. J. (2001). Identification of ubiquitin ligases required for skeletal muscle atrophy. *Science*, *294*(5547), 1704–1708. https://doi.org/10.1126/science.1065874

Burbaum, L., Schneider, J., Scholze, S., Böttcher, R. T., Baumeister, W., Schwille, P., Plitzko, J. M., & Jasnin, M. (2021). Molecular-scale visualization of sarcomere contraction within native cardiomyocytes. *Nature Communications*, *12*(1), 1–20. https://doi.org/10.1038/s41467-021-24049-0

Campos, Y., Qiu, X., Zanoteli, E., Moshiach, S., Vergani, N., Bongiovanni, A., John Harris, A., & D'Azzo, A. (2010). Ozz-E3 ubiquitin ligase targets sarcomeric embryonic myosin heavy chain during muscle development. *PLoS ONE*, *5*(3), 1–14. https://doi.org/10.1371/journal.pone.0009866

Casella, J. F., Craig, S. W., Maack, D. J., & Brown, A. E. (1987). Cap Z(36/32), a barbed end actin-capping protein, is a component of the Z-line of skeletal muscle. *The Journal of Cell Biology*, *105*(1), 371–379. https://doi.org/10.1083/jcb.105.1.371

Chen, C. -n., Thompson, L. D. V., & Snow, L. A. (2017). Orthopaedic Physical Therapy Secrets (Third Edition)IIchi. In *Orthopaedic Physical Therapy Secrets (Third Edition)*. Elsevier.

https://doi.org/10.1016/B978-0-323-28683-1.00001-1

Chikuni, K., Muroya, S., & Nakajima, I. (2004). Myosin heavy chain isoforms expressed in bovine skeletal muscles. *Meat Science*, *67*(1), 87–94. https://doi.org/10.1016/j.meatsci.2003.09.011

Clark, K. A., McElhinny, A. S., Beckerle, M. C., & Gregorio, C. C. (2002). Striated muscle cytoarchitecture: An intricate web of form and function. *Annual Review of Cell and Developmental Biology*, *18*(1), 637–706. https://doi.org/10.1146/annurev.cellbio.18.012502.105840

Cohen, S., Brault, J. J., Gygi, S. P., Glass, D. J., Valenzuela, D. M., Gartner, C., Latres, E., & Goldberg, A. L. (2009). During muscle atrophy, thick, but not thin, filament components are degraded by MuRF1-dependent ubiquitylation. *Journal of Cell Biology*, *185*(6), 1083–1095. https://doi.org/10.1083/jcb.200901052

Colegrave, M., & Peckham, M. (2014). Structural implications of β-cardiac myosin heavy chain mutations in human disease. *Anatomical Record*, *297*(9), 1670–1680. https://doi.org/10.1002/ar.22973

Cornachione, A. S., Leite, F. S., Wang, J., Leu, N. A., Kalganov, A., Volgin, D., Han, X., Xu, T., Cheng, Y. S., Yates, J. R. R., Rassier, D. E., & Kashina, A. (2014). Arginylation of Myosin Heavy Chain Regulates Skeletal Muscle Strength. *Cell Reports*, *8*(2), 470–476. https://doi.org/10.1016/j.celrep.2014.06.019

Craig, R., & Woodhead, J. L. (2006). Structure and function of myosin filaments. *Current Opinion in Structural Biology*, *16*(2), 204–212. https://doi.org/10.1016/j.sbi.2006.03.006

Cripps, R. M. (1999). Assembly of thick filaments and myofibrils occurs in the absence of the myosin head. *The EMBO Journal*, *18*(7), 1793–1804. https://doi.org/10.1093/emboj/18.7.1793

da Silva Lopes, K., Pietas, A., Radke, M. H., & Gotthardt, M. (2011). Titin visualization in real time reveals an unexpected level of mobility within and between sarcomeres. *Journal of Cell Biology*, *193*(4), 785–798. https://doi.org/10.1083/jcb.201010099

Dao, T. P., Kolaitis, R. M., Kim, H. J., O'Donovan, K., Martyniak, B., Colicino, E., Hehnly, H., Taylor, J. P., & Castañeda, C. A. (2018). Ubiquitin modulates liquid-liquid phase separation of UBQLN2 via disruption of multivalent interactions. *Molecular Cell*, *69*(6), 965–978. https://doi.org/10.1016/j.molcel.2018.02.004

Davis, J. S. (1988). Assembly processes in vertebrate skeletal thick filament formation. *Annual Review of Biophysics and Biophysical Chemistry*, *17*, 217–239.

Davis, J. S. (1993a). Myosin Thick Filaments and Subunit Exchange: A Stochastic Simulation Based on the Kinetics of Assembly. *Biochemistry*, *32*(15), 4035–4042. https://doi.org/10.1021/bi00066a026

Davis, J. S. (1993b). Myosin Thick Filaments and Subunit Exchange: A Stochastic Simulation Based on the Kinetics of Assembly. *Biochemistry*, *32*(15), 4035–4042. https://doi.org/10.1021/bi00066a026

Dennis, J. E., Shimizu, T., Reinach, F. C., & Fischman, D. A. (1984a). Localization of C-protein isoforms in chicken skeletal muscle: Ultrastructural detection using monoclonal antibodies. *Journal of Cell Biology*, *98*(4), 1514–1522. https://doi.org/10.1083/jcb.98.4.1514

Dennis, J. E., Shimizu, T., Reinach, F. C., & Fischman, D. A. (1984b). Localization of C-protein isoforms in chicken skeletal muscle: Ultrastructural detection using monoclonal antibodies. In *Journal of Cell Biology* (Vol. 98, Issue 4, pp. 1514–1522). https://doi.org/10.1083/jcb.98.4.1514

Estrella, N. L., & Naya, F. J. (2014). Transcriptional networks regulating the costamere,

sarcomere, and other cytoskeletal structures in striated muscle. *Cell. Mol. Life Sci*, *71*, 1641–1656. https://doi.org/10.1007/s00018-013-1512-0

Fielitz, J., Kim, M. S., Shelton, J. M., Latif, S., Spencer, J. A., Glass, D. J., Richardson, J. A., Bassel-Duby, R., & Olson, E. N. (2007). Myosin accumulation and striated muscle myopathy result from the loss of muscle RING finger 1 and 3. *Journal of Clinical Investigation*, *117*(9), 2486–2495. https://doi.org/10.1172/JCI32827

Fowler, V. M., Sussmann, M. A., Miller, P. G., Flucher, B. E., & Daniels, M. P. (1993). Tropomodulin is associated with the free (pointed) ends of the thin filaments in rat skeletal muscle. *Journal of Cell Biology*, *120*(2), 411–420. https://doi.org/10.1083/jcb.120.2.411

Galler, S., Hilber, K., & Pette, D. (1997). Stretch activation and myosin heavy chain isoforms of rat, rabbit and human skeletal muscle fibres. *Journal of Muscle Research and Cell Motility*, *18*(4), 441–448. https://doi.org/10.1023/A:1018646814843

H.-W. Windhorst. (2014). 2021年までの世界の食肉生産とその世界貿易の推移予測 (前篇). *Animal-Husbandry*, *68*, 155–159.

Habets, P. E. M. H., Franco, D., Ruijter, J. M., Sargeant, A. J., Sant'Ana Pereira, J. A. A., & Moorman, A. F. M. (1999). RNA content differs in slow and fast muscle fibers: Implications for interpretation of changes in muscle gene expression. *Journal of Histochemistry and Cytochemistry*, *47*(8), 995–1004. https://doi.org/10.1177/002215549904700803

Hasebe-Kishi, F., & Shimada, Y. (2000). Dynamics of actin and a-actinin in nascent myofibrils and stress fibers. *Journal of Muscle Research and Cell Motility*, *21*, 717–724.

He, Z. H., Bottinelli, R., Pellegrino, M. A., Ferenczi, M. A., & Reggiani, C. (2000). ATP consumption and efficiency of human single muscle fibers with different myosin isoform

composition. *Biophysical Journal*, *79*(2), 945–961. https://doi.org/10.1016/S0006-3495(00)76349-1

Henderson, C. A., Gomez, C. G., Novak, S. M., Mi-Mi, L., & Gregorio, C. C. (2018). Overview of the muscle cytoskeleton. *Comprehensive Physiology*, *7*(3), 891–944. https://doi.org/10.1002/cphy.c160033

Higuchi, H., Funatsu, T., Ishijima, A., Okamura, N., & ISHIWATAt, I. (1986). Accumulated strain mechanism for length determination of thick filaments in skeletal muscle. I. Experimental bases. In *Journal of Muscle Research and Cell Motility* (Vol. 7).

Ho, G., & Chisholm, R. L. (1997). Substitution mutations in the myosin essential light chain lead to reduced actin-activated ATPase activity despite stoichiometric binding to the heavy chain. *Journal of Biological Chemistry*, *272*(7), 4522–4527. https://doi.org/10.1074/jbc.272.7.4522

Hoppeler, H., & Billeter, R. (1991). Conditions for oxygen and substrate transport in muscles in exercising mammals. *The Journal of Experimental Biology*, *160*, 263–283. https://doi.org/10.1242/jeb.160.1.263

Huang, Q., & Zhang, X. (2020). Emerging roles and research tools of atypical ubiquitination. *Proteomics*, *20*, 1900100. https://doi.org/10.1002/pmic.201900100

Humphrey, S. J., James, D. E., & Mann, M. (2015). Protein Phosphorylation: A Major Switch Mechanism for Metabolic Regulation. *Trends in Endocrinology and Metabolism*, *26*(12), 676–687. https://doi.org/10.1016/j.tem.2015.09.013

Huxley, H. E. (1963a). Electron microscope studies on the structure of natural and synthetic protein filaments from striated muscle. *Journal of Molecular Biology*, *7*(3), 281–308. https://doi.org/10.1016/S0022-2836(63)80008-X

Huxley, H. E. (1963b). Electron Microscope Studies on the Structure of Natural and Synthetic

Protein Filaments from Striated Muscle. In *J. Mol. Biol* (Vol. 7).

Huxley, H. E. (1969). The Mechanism of Muscular Contraction. *Science*, *164*(3886), 1356–1366. https://doi.org/DOI: 10.1126/science.164.3886.1356

Johnson, C. A., Walklate, J., Svicevic, M., Mijailovich, S. M., Vera, C., Karabina, A., Leinwand, L. A., & Geeves, M. A. (2019). The ATPase cycle of human muscle myosin II isoforms: Adaptation of a single mechanochemical cycle for different physiological roles. *Journal of Biological Chemistry*, *294*(39), 14267–14278. https://doi.org/10.1074/jbc.RA119.009825

Johnson, C. S., Mckenna, N. M., & Wang, Y.-L. (n.d.). *Association of Microinjected Myosin and Its Subfragments with Myofibrils in Living Muscle Cells*. http://rupress.org/jcb/article-pdf/107/6/2213/1057458/2213.pdf

Kaminer, B., & Bell, L. A. (1966). Myosin Filamentogenesis : Effects of pH and Ionic Concentration. *J. Mol. Biol*, *20*, 391–401.

Kigaki, S. (2020). The effect of myofibril type on the replacement of myosin molecules in myofibrils (筋原線維におけるミオシン分子の 置換に及ぼす筋線維型の影響). *Master's Thesis (Japanese).*

Kile, B. T., Schulman, B. A., Alexander, W. S., Nicola, N. A., Martin, H. M. E., Hilton, D. J., Kile, B. T., Alexander, W. S., Nicola, N. A., Martin, H. M. E., & Hilton, D. J. (2002). The SOCS box : a tale of destruction and degradation. *TRENS in Biochemical Sciences*, *27*(5), 235–241.

Kontrogianni-Konstantopoulos, A., Ackermann, M. A., Bowman, A. L., Yap, S. V., & Bloch, R. J. (2009). Muscle giants: Molecular scaffolds in sarcomerogenesis. *Physiological Reviews*, *89*(4), 1217–1267. https://doi.org/10.1152/physrev.00017.2009

Koyama, S., Hata, S., Witt, C. C., Ono, Y., Lerche, S., Ojima, K., Chiba, T., Doi, N., Kitamura,

F., Tanaka, K., Abe, K., Witt, S. H., Rybin, V., Gasch, A., Franz, T., Labeit, S., & Sorimachi, H. (2008). Muscle RING-Finger Protein-1 (MuRF1) as a Connector of Muscle Energy Metabolism and Protein Synthesis. *Journal of Molecular Biology*, *376*(5), 1224–1236. https://doi.org/10.1016/j.jmb.2007.11.049

Labeit, S., & Kolmerer, B. (1995). Titins: Giant proteins in charge of muscle ultrastructure and elasticity. *Science*, *270*(5234), 293–296. https://doi.org/10.1126/science.270.5234.293

Lagirand-cantaloube, J., Offner, N., Csibi, A., Leibovitch, M. P., Batonnet-pichon, S., Tintignac, L. A., Segura, C. T., & Leibovitch, S. A. (2008). The initiation factor eIF3-f is a major target for Atrogin1 / MAFbx function in skeletal muscle atrophy. *EMBO Journal*, *27*(8), 1266–1276. https://doi.org/10.1038/emboj.2008.52

Lecker, S. H., Goldberg, A. L., & Mitch, W. E. (2006). Protein degradation by the ubiquitin-proteasome pathway in normal and disease states. *Journal of the American Society of Nephrology*, *17*(7), 1807–1819. https://doi.org/10.1681/ASN.2006010083

Liberti, M. V., & Locasale, J. W. (2020). Histone Lactylation: A New Role for Glucose Metabolism. *Trends in Biochemical Sciences*, *45*(3), 179–182. https://doi.org/10.1016/j.tibs.2019.12.004

Lodka, D., Pahuja, A., Geers-Knörr, C., Scheibe, R. J., Nowak, M., Hamati, J., Köhncke, C., Purfürst, B., Kanashova, T., Schmidt, S., Glass, D. J., Morano, I., Heuser, A., Kraft, T., Bassel-Duby, R., Olson, E. N., Dittmar, G., Sommer, T., & Fielitz, J. (2016). Muscle RING-finger 2 and 3 maintain striated-muscle structure and function. *Journal of Cachexia, Sarcopenia and Muscle*, *7*(2), 165–180. https://doi.org/10.1002/jcsm.12057

Lokireddy, S., McFarlane, C., Ge, X., Zhang, H., Sze, S. K., Sharma, M., & Kambadur, R. (2011). Myostatin induces degradation of sarcomeric proteins through a Smad3 signaling mechanism during skeletal muscle wasting. *Molecular Endocrinology*, *25*(11), 1936–1949.

https://doi.org/10.1210/me.2011-1124

Lokireddy, S., Wijesoma, I. W., Sze, S. K., McFarlane, C., Kambadur, R., & Sharma, M. (2012). Identification of atrogin-1-targeted proteins during the myostatin-induced skeletal muscle wasting. *American Journal of Physiology - Cell Physiology*, *303*(5), 512–529. https://doi.org/10.1152/ajpcell.00402.2011

Lowey, S., Slayter, H. S., Weeds, A. G., & Baker, H. (1969). Substructure of the myosin molecule. I. Subfragments of myosin by enzymic degradation. *Journal of Molecular Biology*, *42*, 1–29. https://doi.org/10.1146/annurev.biochem.53.1.35

Luo, Y.-Y., Wu, J.-J., & Li, Y.-M. (2021). Regulation of liquid–liquid phase separation with focus on post-translational modifications. *Chemical Communications*, *57*(98), 13275–13287. https://doi.org/10.1039/d1cc05266g

Luther, P. K., Bennett, P. M., Knupp, C., Craig, R., Padrón, R., Harris, S. P., Patel, J., & Moss, R. L. (2008). Understanding the Organisation and Role of Myosin Binding Protein C in Normal Striated Muscle by Comparison with MyBP-C Knockout Cardiac Muscle. *Journal of Molecular Biology*, *384*(1), 60–72. https://doi.org/10.1016/j.jmb.2008.09.013

Luther, P. K., & Vydyanath, A. (2011). Myosin binding protein-C: An essential protein in skeletal and cardiac muscle. *Journal of Muscle Research and Cell Motility*, *31*(5–6), 303–305. https://doi.org/10.1007/s10974-010-9235-4

Mejuch, T., & Waldmann, H. (2016). *Synthesis of Lipidated Proteins*. https://doi.org/10.1021/acs.bioconjchem.6b00261

Moriscot, A. S., Baptista, I. L., Bogomolovas, J., Witt, C., Hirner, S., Granzier, H., & Labeit, S. (2010). MuRF1 is a muscle fiber-type II associated factor and together with MuRF2 regulates type-II fiber trophicity and maintenance. *Journal of Structural Biology*, *170*(2), 344–353. https://doi.org/10.1016/j.jsb.2010.02.001

Moyle, L. A., Jacques, E., & Gilbert, P. M. (2020). Engineering the next generation of human skeletal muscle models: From cellular complexity to disease modeling. *Current Opinion in Biomedical Engineering*, *16*, 9–18. https://doi.org/10.1016/j.cobme.2020.05.006

Narita, T., Weinert, B. T., & Choudhary, C. (2019). Functions and mechanisms of non-histone protein acetylation. *Nature Reviews Molecular Cell Biology*, *20*(3), 156–174. https://doi.org/10.1038/s41580-018-0081-3

Nastasi, T., Bongiovanni, A., Campos, Y., Mann, L., Toy, J. N., Bostrom, J., Rottier, R., Hahn, C., Conaway, J. W., Harris, A. J., & d'Azzo, A. (2004). Ozz-E3, a muscle-specific ubiquitin ligase, regulates β-catenin degradation during myogenesis. *Developmental Cell*, *6*(2), 269–282. https://doi.org/10.1016/S1534-5807(04)00020-6

Nury, D., Doucet, C., & Coux, O. (2007). Roles and potential therapeutic targets of the ubiquitin proteasome system in muscle wasting. *BMC Biochemistry*, *8*(SUPPL. 1), 1–10. https://doi.org/10.1186/1471-2091-8-S1-S7

Obermann, W. M. J., Gautel, M., Weber, K., & Fu, D. O. (1997). *Molecular structure of the sarcomeric M band : mapping of titin and myosin binding domains in myomesin and the identification of a potential regulatory phosphorylation site in myomesin*. *16*(2), 211–220.

Oe, M., Ojima, K., & Muroya, S. (2021). Difference in potential DNA methylation impact on gene expression between fast- and slow-type myofibers. *Physiological Genomics*, *53*(2), 69–83. https://doi.org/10.1152/PHYSIOLGENOMICS.00099.2020

OECD-FAO. (2021). OECD-FAO Agricultural Outlook 2021–2030. In *OECD-FAO Agricultural Outlook 2021–2030*. http://dx.doi.org/10.1787/agr-outl-data-%0Ahttp://www.fao.org/documents/card/en/c/cb5332en

Ojima, K., Ichimura, E., Suzuki, T., Oe, M., Muroya, S., & Nishimura, T. (2018). HSP90 modulates the myosin replacement rate in myofibrils. *American Journal of Physiology -*

Cell Physiology, *315*(1), C104–C114. https://doi.org/10.1152/ajpcell.00245.2017

Ojima, K., Ichimura, E., Yasukawa, Y., Oe, M., Muroya, S., Suzuki, T., Wakamatsu, J. I., & Nishimura, T. (2017). Myosin substitution rate is affected by the amount of cytosolic myosin in cultured muscle cells. *Animal Science Journal*, *88*(11), 1788–1793. https://doi.org/10.1111/asj.12826

Ojima, K., Ichimura, E., Yasukawa, Y., Wakamatsu, J. I., & Nishimura, T. (2015). Dynamics of myosin replacement in skeletal muscle cells. *American Journal of Physiology - Cell Physiology*, *309*(10), 669–679. https://doi.org/10.1152/ajpcell.00170.2015

Parker, F., Batchelor, M., Wolny, M., Hughes, R., Knight, P. J., & Peckham, M. (2018). A1603P and K1617del, Mutations in β-Cardiac Myosin Heavy Chain that Cause Laing Early-Onset Distal Myopathy, Affect Secondary Structure and Filament Formation In Vitro and In Vivo. *Journal of Molecular Biology*, *430*(10), 1459–1478. https://doi.org/10.1016/j.jmb.2018.04.006

Passmore, L. A., & Barford, D. (2004). *Getting into position : the catalytic mechanisms of protein ubiquitylation*. *525*, 513–525.

Perera, S., Mankoo, B., & Gautel, M. (2012). Developmental regulation of MURF E3 ubiquitin ligases in skeletal muscle. *Journal of Muscle Research and Cell Motility*, *33*(2), 107–122. https://doi.org/10.1007/s10974-012-9288-7

Pizon, V., Iakovenko, A., van der Ven, P. F. M., Kelly, R., Fatu, C., Fürst, D. O., Karsenti, E., & Gautel, M. (2002). Transient association of titin and myosin with microtubules in nascent myofibrils directed by the MURF2 RING-finger protein. *Journal of Cell Science*, *115*(23), 4469–4482. https://doi.org/10.1242/jcs.00131

Prill, K., & Dawson, J. F. (2020). Assembly and maintenance of sarcomere thin filaments and associated diseases. *International Journal of Molecular Science*, *21*(542), 1–20.

Rall, J. A. (2021). Investigation of the molecular motor of muscle: from generating life in a test tube to myosin structure over beers. *Advances in Physiology Education*, *45*(4), 730–743. https://doi.org/10.1152/advan.00077.2021

Rayment, I., Rypniewski, W. R., Schmidt-Bäse, K., Smith, R., Tomchick, D. R., Benning, M. M., Winkelmann, D. A., Wesenberg, G., & Holden, H. M. (1993). Three-dimensional structure of myosin subfragment-1: A molecular motor. *Science*, *261*(5117), 50–58. https://doi.org/10.1126/science.8316857

Reggiani, C., Bottinelli, R., & Stienen, G. J. M. (2000). Sarcomeric myosin isoforms: Fine tuning of a molecular motor. *News in Physiological Sciences*, *15*(1), 26–33. https://doi.org/10.1152/physiologyonline.2000.15.1.26

Resnicow, D. I., Deacon, J. C., Warrick, H. M., Spudich, J. A., & Leinwand, L. A. (2010). Functional diversity among a family of human skeletal muscle myosin motors. *Proceedings of the National Academy of Sciences of the United States of America*, *107*(3), 1053–1058. https://doi.org/10.1073/pnas.0913527107

Rubinstein, N., Chi, J., & Holtzer, H. (1976). Coordinated synthesis and degradation of actin and myosin in a variety of myogenic and non-myogenic cells. *Experimental Cell Research*, *97*, 387–393.

Rudolph, F., Hüttemeister, J., da Silva Lopes, K., Jüttner, R., Yu, L., Bergmann, N., Friedrich, D., Preibisch, S., Wagner, E., Lehnart, S. E., Gregorio, C. C., & Gotthardt, M. (2019). Resolving titin's lifecycle and the spatial organization of protein turnover in mouse cardiomyocytes. *Proceedings of the National Academy of Sciences of the United States of America*, *116*(50), 25126–25136. https://doi.org/10.1073/pnas.1904385116

Saad, A. D., Dennis, J. E., Tan, I. P., & Fischman, D. A. (1991). Visualization of myosin exchange between synthetic thick filaments. *Journal of Muscle Research and Cell*

Motility, *12*(3), 225–234. https://doi.org/10.1007/BF01745111

Saad, A. D., Pardee, J. D., & Fischman, D. A. (1986). Dynamic exchange of myosin molecules between thick filaments. *Proceedings of the National Academy of Sciences of the United States of America*, *83*(24), 9483–9487. https://doi.org/10.1073/pnas.83.24.9483

Samant, S. A., Pillai, V. B., Sundaresan, N. R., Shroff, S. G., & Gupta, M. P. (2015). Histone deacetylase 3 (HDAC3)-dependent reversible lysine acetylation of cardiac myosin heavy chain isoforms modulates their enzymatic and motor activity. *Journal of Biological Chemistry*, *290*(25), 15559–15569. https://doi.org/10.1074/jbc.M115.653048

Schiaffino, S, & Reggiani, C. (2011). Fiber Types In Mammalian Skeletal Muscles. *Physiol Rev*, *91*, 1447–1531. https://doi.org/10.1152/physrev.00031.2010.-Mammalian

Schiaffino, Stefano, & Reggiani, C. (2011). Fiber types in Mammalian skeletal muscles. *Physiological Reviews*, *91*(4), 1447–1531. https://doi.org/10.1152/physrev.00031.2010

Schiaffino, Stefano, Rossi, A. C., Smerdu, V., Leinwand, L. A., & Reggiani, C. (2015). Developmental myosins: Expression patterns and functional significance. *Skeletal Muscle*, *5*(1), 1–14. https://doi.org/10.1186/s13395-015-0046-6

Service, K. (1982). Native Bare Zone Assemblage Nucleates Myosin Filament Assembly. In *J. Mol. Bi01* (Vol. 161).

Sharkey, L. M., Safren, N., Pithadia, A. S., Gerson, J. E., Dulchavsky, M., Fischer, S., Patel, R., Lantis, G., Ashraf, N., Kim, J. H., Meliki, A., Minakawa, E. N., Barmada, S. J., Ivanova, M. I., & Paulson, H. L. (2018). Mutant UBQLN2 promotes toxicity by modulating intrinsic self-assembly. *Proceedings of the National Academy of Sciences of the United States of America*, *115*(44), E10495–E10504. https://doi.org/10.1073/pnas.1810522115

Sitbon, Y. H., Yadav, S., Kazmierczak, K., & Szczesna-Cordary, D. (2020). Insights into myosin regulatory and essential light chains: a focus on their roles in cardiac and skeletal

muscle function, development and disease. *Journal of Muscle Research and Cell Motility*, *41*(4), 313–327. https://doi.org/10.1007/s10974-019-09517-x

Skubiszak, L., & Kowalczyk, L. (2002). Myosin molecule packing within the vertebrate skeletal muscle thick filaments. A complete bipolar model. *Acta Biochimica Polonica*, *49*(4), 829–840. https://doi.org/10.18388/abp.2002_3743

Sohn, R. L., Vikstrom, K. L., Strauss, M., Cohen, C., Szent-Gyogyi, A. G., & Leinwand, L. A. (1997). A 29 residue region of the sarcomeric myosin rod is necessary for filament formation. *Journal of Molecular Biology*, *266*, 317–330.

Solomon, V., & Goldberg, A. L. (1996). Importance of the ATP-ubiquitin-proteasome pathway in the degradation of soluble and myofibrillar proteins in rabbit muscle extracts. *Journal of Biological Chemistry*, *271*(43), 26690–26697. https://doi.org/10.1074/jbc.271.43.26690

Swist, S., Unger, A., Li, Y., Vöge, A., von Frieling-Salewsky, M., Skärlén, Å., Cacciani, N., Braun, T., Larsson, L., & Linke, W. A. (2020). Maintenance of sarcomeric integrity in adult muscle cells crucially depends on Z-disc anchored titin. *Nature Communications*, *11*(1). https://doi.org/10.1038/s41467-020-18131-2

Szczesna, D. (2003). Regulatory light chains of striated muscle myosin. Structure, function and malfunction. *Current Drug Targets - Cardiovascular and Haematological Disorders*, *3*(2), 187–197. https://doi.org/10.2174/1568006033481474

Thompson, R. C., Buvoli, M., Buvoli, A., & Leinwand, L. A. (2012). Myosin filament assembly requires a cluster of four positive residues located in the rod domain. *FEBS Letters*, *586*(19), 3008–3012. https://doi.org/10.1016/j.febslet.2012.06.019

Tintignac, L. A., Lagirand, J., Batonnet, S., Sirri, V., Leibovitch, M. P., & Leibovitch, S. A. (2005). Degradation of MyoD mediated by the SCF (MAFbx) ubiquitin ligase. *The Journal of Biological Chemistry*, *280*(4), 2847–2856.

https://doi.org/10.1074/jbc.M411346200

Tonino, P., Kiss, B., Gohlke, J., Smith, J. E., & Granzier, H. (2019a). Fine mapping titin's C-zone: Matching cardiac myosin-binding protein C stripes with titin's super-repeats. *Journal of Molecular and Cellular Cardiology*, *133*(May), 47–56. https://doi.org/10.1016/j.yjmcc.2019.05.026

Tonino, P., Kiss, B., Gohlke, J., Smith, J. E., & Granzier, H. (2019b). Fine mapping titin's C-zone: Matching cardiac myosin-binding protein C stripes with titin's super-repeats. *Journal of Molecular and Cellular Cardiology*, *133*(April), 47–56. https://doi.org/10.1016/j.yjmcc.2019.05.026

Tsutsui, H., Karasawa, S., Shimizu, H., Nukina, N., & Miyawaki, A. (2005). Semi-rational engineering of a coral fluorescent protein into an efficient highlighter. *EMBO Reports*, *6*(3), 233–238. https://doi.org/10.1038/sj.embor.7400361

Van Wessel, T., De Haan, A., Van Der Laarse, W. J., & Jaspers, R. T. (2010). The muscle fiber type-fiber size paradox: Hypertrophy or oxidative metabolism? *European Journal of Applied Physiology*, *110*(4), 665–694. https://doi.org/10.1007/s00421-010-1545-0

Viswanathan, M. C., Tham, R. C., Kronert, W. A., Sarsoza, F., Trujillo, A. S., Cammarato, A., & Bernstein, S. I. (2017). Myosin storage myopathy mutations yield defective myosin filament assembly in vitro and disrupted myofibrillar structure and function in vivo. *Human Molecular Genetics*, *26*(24), 4799–4813. https://doi.org/10.1093/hmg/ddx359

Walklate, J., Ujfalusi, Z., & Geeves, M. A. (2016). Myosin isoforms and the mechanochemical cross-bridge cycle. *Journal of Experimental Biology*, *219*(2), 168–174. https://doi.org/10.1242/jeb.124594

Wang, J., Shaner, N., Mittal, B., Zhou, Q., Chen, J., Sanger, J. M., & Sanger, J. W. (2005). Dynamics of Z-band based proteins in developing skeletal muscle cells. *Cell Motility and*

the Cytoskeleton, *61*(1), 34–48. https://doi.org/10.1002/cm.20063

Weeds, A. G., & Lowey, S. (1971). Substructure of the myosin molecule. II. The light chains of myosin. *Journal of Molecular Biology*, *61*(3), 701–725. https://doi.org/10.1016/0022-2836(71)90074-X

Wenderoth, M. P., & Eisenberg, B. R. (1987). Incorporation of nascent myosin heavy chains into thick filaments of cardiac myocytes in thyroid-treated rabbits. *Journal of Cell Biology*, *105*(6 I), 2771–2780. https://doi.org/10.1083/jcb.105.6.2771

William F. Harrington, M. E. R. (1984). Myosin. *Annual Review of Biochemistry*, *53*, 35–73. https://www.annualreviews.org/doi/abs/10.1146/annurev.bi.53.070184.000343

Wolny, M., Colegrave, M., Colman, L., White, E., Knight, P. J., & Peckham, M. (2013). Cardiomyopathy mutations in the tail of β-cardiac myosin modify the coiled-coil structure and affect integration into thick filaments in muscle sarcomeres in adult cardiomyocytes. *Journal of Biological Chemistry*, *288*(44), 31952–31962. https://doi.org/10.1074/jbc.M113.513291

Zak, R., Martin, A. F., Prior, G., & Rabinowitz, M. (1977). Comparison of turnover of several myofibrillar proteins and critical evaluation of double isotope method. *Journal of Biological Chemistry*, *252*(10), 3430–3435.

Zhang, D., Tang, Z., Huang, H., Zhou, G., Cui, C., Weng, Y., Liu, W., Kim, S., Lee, S., Perez-Neut, M., Ding, J., Czyz, D., Hu, R., Ye, Z., He, M., Zheng, Y. G., Shuman, H. A., Dai, L., Ren, B., … Zhao, Y. (2019). Metabolic regulation of gene expression by histone lactylation. *Nature*, *574*(7779), 575–580. https://doi.org/10.1038/s41586-019-1678-1

Zhang, X., Huang, Y., & Shi, X. (2015). Emerging roles of lysine methylation on non-histone proteins. In *Cellular and Molecular Life Sciences* (Vol. 72, Issue 22, pp. 4257–4272). Birkhauser Verlag AG. https://doi.org/10.1007/s00018-015-2001-4